PRACTICAL PERFORMANCE AND SYSTEM CAPACITY OF LIGHTWAVE AM SCM VIDEO SYSTEMS

by

Chul-Jong Chung

Dissertation submitted to the Faculty of the

Virginia Polytechnic Institute and State University

in partial fulfillment of the requirements for the degree of

DOCTOR OF PHILOSOPHY

in

Electrical Engineering

APPROVED:

Ira Jacobs, Chairman

Charles W. Bostian

Richard O. Claus

Yuriko Renardy

Ahmad Safaai-Jazi

April, 1992

Blacksburg, VA 24061

PRACTICAL PERFORMANCE AND SYSTEM CAPACITY OF LIGHTWAVE AM SCM VIDEO SYSTEMS

by

Chul-Jong Chung

Ira Jacobs, Chairman

Electrical Engineering

(ABSTRACT)

Subcarrier multiplexing (SCM) on lightwave systems is an important technique for the near term implementation of *broadband services*† by both telecommunication and cable TV companies. With advance in opto-electronics technology in the mid-1980s, lightwave SCM systems can now be practically implemented to provide a carrier platform for both digital and analog signals and (for short distance applications) are presently more cost effective than time division multiplexed systems.

AM SCM systems are particularly attractive for multichannel video signal transmission due to their compatibility with the *National Television Systems Committee Amplitude Modulated Vestigial Sideband* (NTSC AM-VSB) TV format. However, AM SCM systems are generally recognized to have a limited system capacity due to large *carrier-to-noise ratio* (CNR) and low *nonlinear distortion* requirements. This research dissertation contains a comprehensive study of the system capacity of such systems based on theoretical analysis, experiment, and simulation.

---

† A glossary of italicized terms is provided at the end of dissertation.

The practical performance of lightwave AM SCM systems are limited by the *laser diode threshold-nonlinearity* and *laser relative intensity noise*, the *photodiode shot noise*, and the *receiver thermal noise*. The practical system performance is evaluated and compared with that of the theoretical performance limit. The analysis indicates that AM SCM systems have sufficient system capacity for typical CATV *loop distribution* and *supertrunking* systems. It is shown that previous reported limits are generally overly conservative. A sensitivity analysis identifies the critical performance limiting parameters and provides system designers with achievable system performance as device characteristics improve.

For *1550 nm AM SCM systems* employing *erbium-doped fiber amplifiers* (EDFA) operating on the *1300 nm single-mode-fiber* of telephone networks, there are additional sources of nonlinear distortion and noise to be considered. The nonlinear distortion produced by *laser-chirp* and *fiber-induced-dispersion* and the noise produced by the EDFA can significantly degrade the system performance. The analysis shows that the maximum link distance is limited by the *composite-second-order (CSO) distortion*, and the maximum number of subscribers is limited by the EDFA excess fluctuation noise.

This dissertation is dedicated

to my parents

ACKNOWLEDGEMENTS

I would like to express my deepest gratitude to Prof. Ira Jacobs, Ph.D. supervisor and committee chairman, for his technical guidance and support throughout my studies. Also, encouragement not only from Prof. Ira Jacobs but also from his wife Irene Jacobs are greatly appreciated. Without them, this dissertation could have never materialized.

I thank all of my Ph.D advisory committee members; Prof. Charles W. Bostian, Prof. Richard. O. Claus, Prof. Yuriko Renardy, and Prof. Ahmad Safaai-Jazi for their time and effort throughout the course of the dissertation study. Special thanks go to Prof. Safaai-Jazi and Prof. Claus for their continuous encouragement and technical advice.

I would like to acknowledge my gratitude for the managers and technical members of staff at Bell Communication Research; Dr. Carl W. Lundgren, Jr., Paul Spencer (who now is at Eastman Kodak, Rochester, NY), Dr. Winston I. Way, Perry Venkatesan, Beth Koelbl, Dr. Aly Elrefaie, Dr. Richard S. Vodhanel, Dr. Chinlon Lin, David Burpee, Dr. Peter Kaiser, for their technical guidance, financial support, and for providing the facilities for the experimental results reported in this dissertation.

I am also grateful for my friends whom I met at Virginia Tech: Prof. B.H. Cho, C.H. Cho, T.H. Cho, B.J. Choi, J.Y. Choi, Prof. D.S. Ha, Dr. B.T. Han, Prof. Y.H. Han, Mike Gunther, C.H. Kim, Prof. H.J. Kim, Dr. K.H. Kim, Prof. J.W. Kim, Dr. S.J. Kim, Y.S. Kim, Dr. C. Lee, E.J. Lee, H.K. Lee, S.Y. Lee,

Kent Murphy, Prof. J.K Paek, Prof. J.W. Park, Dr. G.H. Rhim, Prof. Y.S. Shin, Dr. Y.S. Won, for their continuous support and encouragement.

My special thanks go to Dr. C.K. Jen of the National Research Council of Canada and Prof. I. Shi of McGill University for their initial encouragement and technical guidance through M.Eng studies, and the suggestion to pursue a Ph.D. degree. In particular, continuous encouragement from Dr. Jen is greatly appreciated.

I am extremely grateful to my brother W.J. Chung for his encouragement and support in many ways during my Ph.D. study. Lastly, my greatest appreciation goes to my parents who provided me to the utmost of their support, guidance, and encouragement through all these years, and I dedicate this dissertation to them.

TABLE OF CONTENTS

LIST OF FIGURES

Figures

CHAPTER 1.

INTRODUCTION

Fiber optic multichannel video signal transmission is a subject of intense interest in both the telecommunication and cable TV (CATV) industries as they prepare their network infrastructure for future *broadband services*†. Both these industries anticipate that the entertainment segment, namely interactive and enhanced multichannel video services such as *pay-per-view* and *switched-video-libraries*, will be the foremost attraction of broadband services and may be the impetus for its growth. Realizing the significance of video services for the future broadband networks, both the telecommunication and CATV industries have been engaged in active research on lightwave multichannel video systems over the past few years. This dissertation is an integral part of this effort.

In this introduction, first, the importance of video services to the telecommunication and CATV industries is discussed. This is followed by a review of the current status of multichannel video systems on fibers. Previous research in this area is discussed, and open research topics are identified. Finally, research objectives and organization of the dissertation are presented.

---

† A glossary of italicized terms is provided at the end of the dissertation. The terms are italicized the first time they appear.

1.1. Video Service Perspective of the Telecommunication Industry

Since C.K. Kao and G.A. Hockham's [1] prediction in 1966 of the ability of glass fibers to carry optical signals with intrinsic loss lower than 4.0 dB/Km and the subsequent experimental verification by researchers at Corning [2], research in fiber optics has progressed rapidly toward its application in telecommunications. The first system experiments and trials were held in 1976 [3], and deployment of commercial systems began in 1979 [4]. As a consequence of research and development efforts spanning the past three decades, much of today's voice long-distance interoffice/intercity *trunking* signals are carried by optical fibers, providing increased transmission capacity and reliability compared to both copper-based and microwave radio transmission systems. At present, the use of optical fibers is both technically and economically justified, not only in long-distance transport of telephonic signals, but also in medium-distance loop carriers connecting central switching office to local *loop distribution* units. The deployment of optical fibers is now expanding to the last mile of telephone networks as telephone operating companies are planing *Fiber In the Loop* (FITL) systems in the *distribution plant* and with their final goal of *Fiber-to-the-Home* (FTTH) systems. The FTTH systems will then be able to provide full fiber optic network infrastructures that will support the envisioned broadband services [5].

With relatively low growth in voice networks, and thus low growth in revenues from voice services, local telecommunication service operators (such as regional Bell operating companies) are now actively seeking out new opportunities. (In contrast to this, CATV networks have been growing at a much faster rate than those of the telecommunication networks. Furthermore, currently envisioned enhanced video services such as *pay-per-view* and *switched-video-libraries* promise an even higher growth rate of video service networks as well as increases in operating revenues.) With FITL on the way, the telecommunication service operators will be well positioned to provide video services in their networks. The total fiber network would be able to deliver better video picture quality and higher system reliability

than present coaxial based CATV networks. Furthermore, integration of video services into their present voice and data networks would eventually allow telecommunication companies to provide fully integrated broadband services to subscribers. At present, however, due to economics and government regulations [6,7], the telecommunication service operators' activity on the integration of video service into their network is limited primarily to field trials [8] and research activities [9-12]. Bell Communications Research (Bellcore), which is a research organization funded by the seven regional Bell Operating Companies, has been extremely active in research in this area and has provided support for the research reported in this dissertation.

1.2. Video Service Perspective of the CATV Industry

The situation is quite different for CATV service operators. The CATV operators' main business has always been in video services and their business has been protected from telecommunications service providers by government regulations. However, this may soon change with further deregulation of information service businesses. CATV service operators would then face competition from telecommunication service operators in providing video services to residential subscribers. Traditionally, despite the explosive growth of CATV networks over the last four decades [6], CATV companies have been conservative in exploring or developing new technologies . However, this is starting to change. With new business opportunities provided by fiber optics technology, CATV service operators and their equipment suppliers are now actively taking part in the research and development of lightwave technology for the transport and distribution of multi-channel CATV video signals [13-17].

Cable TV companies are quickly realizing that the initial cost of installing fiber is offset by reductions in capital, operating, and maintenance costs of video signal trunking. At the same time, optical fibers in

their network provide improved reliability and better quality signals to customers. Furthermore, optical fibers are considered the most economical way of increasing channel capacity for future revenue growth. The first deployment of optical fibers in CATV networks started with *supertrunking* of CATV signals [13] in 1987, and CATV application is currently one of the fastest growing areas of fiber optics. Although present application of fiber optics is limited primarily to the *supertrunking/trunking* part of their network, there are extensive research efforts by CATV companies and associated research laboratories not only in the area of CATV signal transport/distribution but also in many aspects of video services (such as on-line pay-per-view and switched video services) [13-17].

1.3 Current Status of Multi-Channel CATV Signal Transmission

Most of current multichannel CATV signals are transmitted over coaxial cables. In these systems, due to high signal loss of coaxial cables, as well as the splitting losses in branching networks, electronic amplifiers/repeaters are employed to maintain sufficient signal power levels from head-end stations to the subscribers. Although today's coaxial CATV systems are generally cost effective, there are inherent performance problems and limitations due to repeater amplifiers. These amplifiers add noise and nonlinear distortion, thus degrading the signal quality. Also, since the amplifiers contain active components which must withstand the harsh outside plant environment and must be provided with electrical power, system reliability is an important issue. Furthermore, cascaded amplifiers impose stringent operating tolerances making system installation and maintenance difficult. In contrast to these impairments associated with coaxial systems, low signal loss fiber optic systems can provide repeaterless transmission, thus providing higher picture quality and improved system reliability. At present, high capacity trunking fiber optic video systems can be built at lower cost than coaxial systems and are becoming the technology of choice. In

addition, deployment of optical fibers will provide CATV networks with high capacity network infrastructures which will be needed for the future broadband services.

For fiber optic multichannel video systems, analog *subcarrier multiplexing* (SCM) technique is presently considered the most promising multiplexing technique [9-12]. In a SCM system, a number of baseband electronic signals are first frequency division multiplexed, and this electronic signal is then used to intensity modulate the laser diode. Because of the versatility of being able to carry a variety of signal formats (such as amplitude-modulated (AM), frequency-modulated (FM), and even digital formats) simultaneously and its lower cost than time domain multiplexing, SCM systems can provide an ideal carrier platform for the near term implementation of broadband service networks.

In particular, the *amplitude-modulated* (AM) SCM technique is the simplest in terms of its compatible electrical interface to the North American *National Television Systems Committee Amplitude Modulated Vestigial Sideband* (NTSC AM-VSB) TV format. In this technique, the NTSC AM-VSB signal directly intensity modulates a laser without need for any signal conversion as would be necessary in FM and digital systems. Consequently, the AM SCM technique provides reduced system cost and complexity over other types of modulation and multiplexing. However, AM SCM systems have in the past been limited to a small number of channels and limited optical power margins due to high dispersion and loss of optical fibers; and due to electrical bandwidth, *nonlinear distortion*, and *relative intensity noise* (RIN) limitations of lasers [18-22]. Since the late-1980s rapid advancement of the 1300/1550 nm *distributed feedback* (DFB) lasers with high output power, high linearity and low RIN, as well as high-speed low-noise receiver modules, have permitted the implementation of practical AM SCM systems with more than 40 channels and 10 km link distance [23-25]. However, owing to large *carrier-to-noise ratio* (CNR) and signal nonlinear distortion requirements, AM SCM systems have a limited *system capacity* compared to other modulation techniques such as frequency modulated (FM) SCM or digital systems.

1.4 Previous Research and Potential Research Areas

1.4.1 Review of Lightwave Multichannel AM SCM System Research

SCM video systems first appeared in 1977 [18,19]. At that time, SCM systems had a limited number of channels and limited optical power margins, and thus were not adequate for transport of multichannel CATV signals. High performance SCM systems reappeared in 1986-7 when several groups of researchers reported experiments. T.E. Darcie et al. of AT&T Bell Laboratories reported a demonstration of subcarrier multiplexing for an optical multiple-access-network [26]. R. Olshansky and V.A. Lanzisera of GTE Laboratories reported a 60-channel FM video SCM transmission system [27]. W.I. Way et al. of Bell Communications Research reported a SCM system for a microwave multicarrier transmission link [28]. These experiments became possible with the advent of extremely low noise, high linearity and high speed DFB lasers [29-31], and low noise and high speed detectors/receivers [32-34]. Since then, there have been continuing improvements in opto-electronics device performance for SCM systems particularly in the area of high linearity, high power, and low noise laser diodes [23-25, 35,36].

Following earlier experimental work, recent papers have appeared that consider system design issues, performance, and limitations of multichannel SCM video systems [9,10,13,23-25]. Of these, review articles by T.E. Darcie [9] and W.I. Way [10] give a general overview of the AM SCM video systems describing the system performance, requirements, and impairments. Lightwave AM SCM video transmission systems and distribution network design issues, from the perspective of CATV companies also appeared in the literature [13-17].

1.4.2 Study of Practical AM SCM System Performance and Capacity

Although there have been many papers analyzing the performance of AM SCM systems, it was not until 1989 that A. Saleh of AT&T Bell Laboratories identified the threshold nonlinearity of laser diodes as a fundamental limit on channel capacity. In this paper, the nonlinear distortion power due to the laser threshold characteristic is estimated, and the channel capacity is calculated based on the CNR degradation due to the nonlinear distortion power and photodetector shot noise. Although this contribution of identifying the laser threshold nonlinearity as the fundamental limiting factor of the channel capacity is generally accepted, there was skepticism that the numerical results were overly conservative. Supporting this skepticism, experimental results showing higher channel capacity were reported by M. Tanabe et al. [25]. Theoretical analysis showing Saleh's conservative estimate of the nonlinear distortion power has also been recently reported by Alameh and Minasian [38].

In addition to the conservative estimate of the nonlinear distortion, there appears to be yet another reason which leads to under-estimating the channel capacity. In order to calculate the channel capacity, Saleh considered the nonlinear distortion as a noise power which degrades the system noise performance. Alameh and Minasian [38] also continued to use the same approach for the channel capacity calculation. However, in normal CATV practice, the performance requirements are given separately for noise and nonlinear distortion. (The noise performance is specified by the *carrier-to-noise ratio* (CNR), and nonlinear distortion performance is specified by the *Composite-Second-Order* (CSO) and the *Composite-Triple-Beat* (CTB).) Thus, consideration of nonlinear distortion as noise which degrades the system CNR seems to be inappropriate.

Furthermore, channel capacity reported by Saleh [37] and Minasian and Alameh [38] are given in terms of the number of channels per milliwatt of the received optical power. As will be shown later, the number of channels per milliwatt of the received optical power is a valid measure of system capacity only when the photodetector shot noise is the dominant noise in the CNR analysis. When additional system noise is considered, namely the laser RIN and receiver thermal noise, the channel capacity is no longer linearly dependent on the received optical power. Thus, use of number of channels per milliwatt of the received optical power is an inappropriate parameter for describing the system capacity of a practical system. Thus, both the methodology and assumptions of prior theory do not adequately describe the capacity of "practical" CATV systems.

1.4.3 Study of 1550 nm AM SCM Systems on 1300 nm Single-Mode Fiber Platform of Telecommunication Networks

Although AM SCM systems are generally recognized to have limited power margins, recent successful development of *erbium-doped fiber amplifiers* (EDFA) have alleviated the power margin limitation by means of optical signal amplification [16,39-41]. However, in order to benefit from EDFA technology, AM SCM systems must operate with 1550 nm sources since the EDFA gain profile lies in the 1550 nm region. 1550 nm AM SCM systems can also potentially be used simultaneously to deliver both analog voice and video services when multiplexed together with 1300 nm using *wavelength division multiplexing* (WDM) in telecommunication networks. However, because most of the optical fibers in telecommunication networks are *dispersion* optimized for 1300 nm sources, 1550 nm AM SCM systems will suffer from increased fiber dispersion by operating away from the dispersion minimum. Correspondingly, the *chirp* of the laser diode and dispersion of the fiber together will produce additional nonlinear distortion further degrading the nonlinear distortion performance.

The phenomenon of dispersion-induced distortion due to laser chirp at 1550 nm operation was first observed by M. Shiegematsu and co-workers [42] from their experiments in 1990. Soon after this, M.R. Phillips et al. [43] presented an analytical method to predict the CSO and CTB using solutions to the wave-equation. E.E. Bergmann et al. [44] also reported an analytical method to interpret the CSO nonlinear distortion in their experiment. The results of experiments [43,44] indicate that the CSO could reach unacceptable levels even for a fiber length less than 10 km. Since presently envisioned telecommunication local distribution loops may approach 10 km, this imposes significant restriction in designing AM SCM systems on a standard 1300 nm single-mode fiber platform.

The study of dispersion-induced distortion due to laser chirp is the subject of on-going research. The analytical method [43] reported by Phillips et al. requires numerical solution of the wave-equations and provides no insight into the nonlinear generation mechanism. The analysis reported by Bergmann et al. [44] does not appear sufficiently accurate to predict the behavior of nonlinear distortion for distances less than 5 Km. Accordingly, there is need for more research in this area for better understanding of the mechanisms causing nonlinear distortion and the resulting system capacity limitations.

1.5. Research Objectives

As discussed in the previous section, although extensive research efforts have improved the system performance and brought better understanding of system limitations and impairments, there are still many unresolved issues regarding the system performance limits and capacity. Based on a review and assessment of the current state of fiber optic AM SCM systems, the following major research objectives are established.

(1) Study of the nonlinear distortion resulting from the threshold nonlinearity of the laser diode and its impact on the system channel capacity,

(2) Study of the nonlinear distortion produced by the combined effects of laser chirp and fiber dispersion and its impact on the maximum link distance of the 1550 nm AM SCM video systems, and

(3) Study of fiber optic AM SCM video system performance and capacity.

The first objective is to improve previously reported estimates of the nonlinear distortion and to present a proper method, based on conventional CATV measurement practice, for the calculation of channel capacity. It also includes the channel capacity comparison between theoretical shot noise limited and practical systems. The second objective is to study the nonlinear distortion causing mechanisms due to laser diode chirp and fiber dispersion, and to deduce the maximum subscriber loop distance for 1550 nm video services arising from this limitation. The third objective is to study practical fiber optic AM SCM system performance and capacity. It includes (1) system performance sensitivity analyses, (2) system capacity in terms of channel capacity and system power margins, (3) practical limit of the channel capacity, and (4) specific performance limitations associated with 1550 nm AM SCM systems when integrated into telecommunication networks.

1.6 Organization of Dissertation

The dissertation is organized in the following manner. First, in Chapter 1 a perspective of the telecommunication and CATV industry on video services, a review of the current status of multichannel

AM SCM video systems, a review of previous research in AM SCM systems, and research objectives are presented. In Chapter 2, the AM SCM lightwave system is described along with a discussion of system impairments, limitations, and typical performance requirements. The study of the nonlinear distortion produced by the threshold nonlinearity of the laser diode in multichannel AM-VSB video systems and its impact on system channel capacity is presented in Chapter 3. The study of the nonlinear distortion produced by the combined effects of laser chirp and the fiber-induced dispersion, and the maximum link distance limitation due to this effect is presented in Chapter 4. In Chapter 5, a comprehensive study of AM SCM system performance and capacity is presented. Finally, summary and conclusions are given in Chapter 6. A glossary of the technical terms (italicized when they appear for the first time) is provided for readers who are not generally familiar with the topic. A description of the BOSS simulation tool [45] used for the simulations is included in an appendix.

CHAPTER 2.

LIGHTWAVE MULTICHANNEL AM SCM VIDEO SYSTEMS

An overall description of lightwave multichannel AM SCM video systems is presented in this chapter. Prior to describing the lightwave AM SCM video system, a brief review of current CATV systems in terms of the CATV network architecture, channel frequency allocation, TV spectrum, performance parameters, and performance testing technique is presented. Basic lightwave AM SCM system configuration, system performance, impairments, and limitations are then discussed in that order.

2.1 Review of CATV Systems

CATV systems in the Unites States began in 1952 [6,7] to deliver off-the-air broadcast signals in areas where TV signal reception was inadequate with conventional TV antennas. For those areas, large community antennas were set up to share the received broadcast signals among many TV sets. Typical areas needing community antenna services were rural areas far away from TV broadcast antennas and metropolitan areas subject to multi-path reflections from large buildings. CATV was originally an acronym standing for *Community Antenna TeleVision*, but now has come to more broadly mean cable television.

By the end of 1960, nearly all areas of the United States that could benefit from CATV systems had been served. The next evolution in CATV networks took place in the mid-1970s when satellite delivery of TV programs became wide spread allowing viewing of TV programs other than locally generated ones. Thus, mini-networks such as Turner Broadcast Services (TBS) and FOX were started. These mini-networks offered not only a variety of programmed channels similar to the major broadcast networks (ABC, CBS, NBC, PBS) but also offered specialized channels such as news, sports, weather, shopping, etc.. Increases in the number of channels with added variety of programs attracted subscribers and resulted in a major expansion of CATV networks even into areas which did not require the traditional community antenna services. Today, CATV services are available to 80 percent of the U.S. households, and of that more than 60 percent are active subscribers representing approximately 50 million households [46]. Accordingly, the term CATV came to mean more than just community antenna service; and nowadays is more often referred to as *CAble TeleVision* to distinguish it from over-the-air broadcasting.

2.1.1 Current CATV Network Architecture

The architecture of current CATV networks is basically a tree-and-branch type. As shown in Figure 2.1, source signals, which include satellite received programs and locally generated programs, at the *headend* (central distribution site) are branched out to local distribution sites called *hubs*. The connection between the headend and hubs is referred to as *supertrunking*. At the hubs, the CATV signals are distributed to subscribers via trunk/bridge amplifiers and taps. Trunk/bridge amplifiers compensate for the distribution and propagation losses in coaxial cables. The taps provide power splitting functions from main coaxial cables to drop cables. The drop cables are then connected to the subscriber TV sets via service-access-control units. The service-access-control units are physical switches that provide control of the subscriber connection to the CATV network.

Current CATV networks are extremely cost effective in providing broadband multichannel CATV signals to subscribers. However, performance limitations of the RF components, mainly due to noise and distortion accumulation across the cascaded amplifiers, and signal reflections within the discrete components in the distribution sites, cause degradation in TV image quality. In addition, reliability of cascaded trunk/bridge amplifiers under the harsh field environment and the supply of electrical power to these components have resulted in relatively poor overall system reliability. At present, fiber optic supertrunking systems are at cost parity with their coaxial counterparts and are being extensively deployed in CATV networks [14,46]. At the same time, applications of optical fibers in CATV networks are now extending closer to the CATV feeder/distribution networks not only to further enhance TV signal quality and system reliability but also to prepare the network infrastructure for future switched broadband services. One of the popular approaches of optical fiber deployment in the feeder/distribution parts of CATV networks is the fiber-backbone technique proposed by American Television and Communications [14, 47]. In this technique, fiber is used from the headend to conversion nodes (see Figure 2.2), and the existing coaxial cable and amplifiers are then used from the conversion point to the feeders. This reuses the existing coaxial cable and amplifiers, but avoids the reliability and performance problems of a large number of amplifiers in tandem.

2.1.2 TV Channel Spectrum and CATV Channel Frequency Allocation

Coaxial cable systems can provide approximately 400 MHz of usable spectrum for typical lengths of 1000 to 2000 ft [13]. Transmission of signals having a bandwidth greater than 500 MHz is generally impractical due to transmission loss and signal dispersion associated with the coaxial cable. Accordingly, for the 6 MHz bandwidth of NTSC AM-VSB TV channels, the number of channels that can be carried is limited to about 50-60 channels [48,49]. Figure 2.3.a shows the CATV frequency allocation plan for 52

channel CATV systems. Five "low-band" channels and seven "high-band" channels, corresponding to broadcast channels 2 – 6 and 7 – 13, are assigned within the 54 MHz – 88 MHz and 174 MHz – 216 MHz bands, respectively, to be compatible with conventional TV sets which are not equipped with CATV converters. The spectrum between 120 – 174 MHz (above the FM band), which is not used for broadcasting owing to intermodulation considerations, is used in coaxial systems to obtain an additional nine "mid-band" channels. The remaining 31 channels are allocated at spectrum above 216 MHz.

The AM VSB TV channel spectrum is illustrated in Figure 2.3.b. showing the location of major frequency components, namely the video carrier, color subcarrier, and audio carrier. As can be seen in the figure, the video carrier is located 1.25 MHz above the low frequency cut-off of the channel. This provides a vestigial lower sideband which is necessary since sharp cut-off filters cannot be used with video signals. For example, for Channel 2 whose spectrum is assigned between 54 MHz and 60 MHz, the video carrier is located at 55.25 MHz. Within a TV spectrum, the video carrier is the most dominant frequency component, and performance testing of the CATV signal is carried out mainly using the video carrier only. More details on performance measurements are provided in the following section.

2.1.3 CATV Signal Performance Parameters and Measurements

Performance of multichannel AM-VSB CATV signals is specified by the noise and nonlinear distortion associated with the video carrier. The noise performance is specified by the *carrier-to-noise ratio* (CNR). The CNR is the ratio of the carrier power to the noise power within a 4 MHz video signal bandwidth. (Note that there is a difference between the 4 MHz effective video signal bandwidth and the 6 MHz physical channel bandwidth.) The nonlinear distortion performance is specified by the *composite-second-order* (CSO) and the *composite-triple-beat* (CTB) which are the intermodulation distortion products resulting from frequency beating of subcarriers. The CSO and CTB are the strongest accumulated sum of the second (A±B)

order and the third (A±B–C) order products within the 6 MHz channel bandwidth. The CSO and CTB are the most dominant distortion products in multichannel AM SCM systems. Although other types of nonlinear distortion exist such as cross-modulation distortion and harmonic distortion products, they are relatively small compared to the CSO and CTB and usually ignored in system performance measurements.

In the standard CATV channel allocations, the CSO products fall 1.25 MHz above or below the video carriers because they are generated by sums and differences of two carriers whose frequencies are located at 1.25 MHz above the integer multiples of 6 MHz. For 42 channel systems, there are more CSO products 1.25 MHz below the video carrier than 1.25 MHz above due to the unequal distribution of the second-order intermodulation products within the CATV channel band. Therefore, CSO is measured at 1.25 MHz below the video carrier. Similarly, the third-order intermodulation products fall on the video carrier frequencies themselves, and therefore CTB is measured at the video carrier frequency with the video carrier of the desired channel turned off. CSO and CTB are measured relative to that of the carrier power level and specified in terms of dBc.

Performance measurements of the composite CATV signal are conventionally done with unmodulated multiple carriers [24, 48, 49]. These unmodulated carrier based measurements give 3 dB, 6 dB, and 9 dB better results on the CNR, CSO, and CTB, respectively, as compared to the ones using live-video CATV signals. Requirements are specified in terms of unmodulated carriers since these measurements are simpler to make.

2.1.4 CATV Signal Performance Requirements

Present coaxial systems are designed to deliver a CNR of about 45 dB to 48 dB, and a CTB and CSO of about -55 dBc to subscriber TV units. The requirements for supertrunking systems are about 10 dB more

stringent for both the CNR requirement and the CSO and CTB requirements. In this dissertation, the following performance requirements will be used: for trunking/feeder distribution systems, CNR=48 dB, CSO and CTB <-60 dBc; for supertrunking systems, CNR=55 dB, CSO<-65 dBc and CTB<-65 dBc. These requirements will then be used to evaluate the channel capacity and system power margins. These results will be shown to depend strongly on the specified requirements.

2.2 Lightwave Multichannel AM SCM Video Systems

As mentioned in Section 2.1, coaxial CATV systems are limited in terms of channel carrying capacity due to high signal loss in coaxial cables and noise and nonlinear distortion accumulation in supertrunking-repeater and trunk/bridge amplifiers. In comparison, fiber optic CATV systems can provide higher channel capacity and can be built without repeater amplifiers, thus, improving overall signal quality. In this section, basic fiber optic AM SCM CATV system configuration, impairments, performance, and limitations are discussed.

2.2.1 Basic Lightwave Multichannel AM SCM Video System Configuration

A basic configuration of fiber optic multichannel AM SCM systems is shown in Figure 2.4. In these systems, a number of baseband AM-VSB TV signals are first frequency division multiplexed using local oscillators of different frequencies (subcarriers). This combined VHF signal is then used to intensity modulate the laser diode. (For this reason, SCM systems are also known as frequency-division-multiplexed intensity-modulated (FDM-IM) systems.) The generated light output of the laser diode is carried by single-mode optical fibers. At the receiving end of the fiber link, a high speed photodetector generates a photo-current proportional to the received light intensity. This photo-current contains the sum of all the

transmitted subcarrier channels. From these, the desired TV channel signal is extracted by tuning a local oscillator to the desired channel and down-converting the VHF signal to the original baseband amplitude modulated signal. In this respect, each receiver in SCM systems need have only the bandwidth of the desired channel. This permits use of low bandwidth electronic receivers as compared to the high bandwidth electronic receivers in digital systems. This also means the AM SCM technique is currently the most cost effective fiber optic multichannel CATV systems due to use of existing CATV electronics.

2.2.2 AM SCM System Impairments

Many factors may degrade the noise and nonlinear distortion performance of multichannel lightwave AM SCM systems [9,24]. Of these, the noise performance is affected by; (1) phase-to-intensity converted noise due to optical reflections generated from discontinuities in the fiber link [10,50, 51], (2) intrinsic relative intensity noise (RIN) of laser diodes [9,52], (3) thermal noise of the receivers [9,10], and (4) shot noise of the photodetectors. In practical systems, the phase-to-intensity converted noise from optical reflections can be sufficiently suppressed using optical isolators, low return loss connectors, or fusion splices. On the other hand, the intrinsic RIN of laser diodes and thermal noise of receivers cannot be reduced beyond a certain level. Therefore, in studying the noise performance of the system, laser diode RIN and receiver thermal noise should be considered together with photodetector shot noise.

The nonlinear distortion performance is generally affected by: (1) intrinsic nonlinearity from laser diodes [53-57], (2) the threshold nonlinearity of laser diode [25,35,37,38], (3) the nonlinear response of photodiodes [10], and (4) the nonlinear distortion produced by the laser diode chirp and fiber dispersion [42-44]. Of these, with current device technology the intrinsic nonlinear distortion of a laser diode is sufficiently low such that it is not a performance limiting factor. Current laser diodes exhibits CSO and CTB of about -65 dBc to -70 dBc under typical multichannel CATV signal modulation, and ideal device

performance studies indicate that CSO and CTB distortion levels lower than -70 dBc [55, 57] can be obtained. The nonlinear distortion contribution from the photodetector is relatively small compared to that produced by other terms [10]. The nonlinear distortion produced by laser diode chirp and fiber dispersion can be reduced to a negligible level by minimizing the dispersion of the fiber or minimizing the laser chirp. The nonlinear distortion produced by signal clipping due to threshold nonlinearity of the laser diode can be avoided by not over-modulating the laser diode with the composite AM SCM signal. However, because the intrinsic nonlinearity of laser diodes is sufficiently low, the laser diode is over-modulated to a certain extent to get higher CNR, higher channel capacity, and higher power margins in typical systems. Detailed study of the nonlinear distortion produced by the over-modulation of laser diodes and the nonlinear distortion performance limitation due to this effect are presented in Chapter 3.

2.2.3 AM SCM System Noise and Nonlinear Distortion Performance and Limitations

As stated in the Section 2.2.2, for the practical AM SCM system noise performance analysis, laser diode RIN, receiver thermal noise, and photodetector shot noise are included in the CNR equation. Eq. (2.1) represents the CNR of a given channel.

$$CNR = \frac{\frac{1}{2} m^2 \Re^2 P_O^2}{RIN \cdot \Re^2 P_O^2 \cdot B + 2q\Re P_O \cdot B + \langle i_{th}^2 \rangle \cdot B} \tag{2.1}$$

where $\Re$ is the photodiode responsivity, P_O is the average received optical power, B is the effective noise bandwidth (4 MHz for a video channel), q is the electron charge, and $\langle i_{th}^2 \rangle$ is the receiver thermal noise spectral density. (Each of the terms in Eq. (2.1) has the unit of current squared.) The first term in the denominator represents the RIN contribution, the second term represents the shot noise contribution, and the third term represents the receiver thermal noise contribution. By preventing optical reflections into the

laser diode cavity using high performance isolators and fusion splicing, the RIN contribution to the CNR can be limited to intrinsic RIN of laser diodes.

To compare the CNR performance prediction based on Eq. (2.1) with that of the actual system CNR, the system CNR was measured. The experimental setup is as indicated in the block diagram in Figure 2.5. A forty-two TV channel Matrix Signal Generator (MSG) is used as the multiple carrier signal source. The per-channel modulation index m=0.054 is used. Its composite SCM output is used to intensity modulate a highly linear InGaAsP 1550 nm Fujitsu DFB laser transmitter with a -50 dB isolator built into its package. The transmitter is connected to an InGaAsP *pin*-FET receiver module from ORTEL (Model 2610B) via 5 meters of 1310 nm dispersion-minimized single-mode optical fiber. The laser diode exhibits a RIN of -155 dB/Hz when measured at a bias current of 30 mA. The ORTEL pin-FET receiver module has a responsivity of 0.93 A/W and a thermal noise current density of 7 pA/$\sqrt{\text{Hz}}$.

The experimentally measured CNR with respect to various received optical power levels is plotted in Fig. 2.6 along with that calculated from Eq.(2.1). Also plotted separately in Figure 2.6 are the individual noise contributions of the laser diode RIN, the photodetector shot noise, and the receiver thermal noise. As can be seen in Figure 2.6, in general there is close agreement between the measured and the calculated CNR indicating that Eq. (2.1) can indeed predict the CNR performance of the system. The CNR difference for low received optical power levels may be attributable to measurement errors and discrepancy between the actual receiver thermal noise and that provided by the device specification. Comparisons of the system CNR with noise contributions from the individual RIN, shot noise, and thermal noise illustrate that there are three noise limited regimes for different received optical power levels; (1) a RIN noise limited region, which limits the maximum attainable CNR at high received optical power levels; (2) a thermal noise limited region, which limits the maximum attainable CNR at low received optical power levels; and (3) a shot noise limited region, which limits the maximum attainable CNR at intermediate power levels.

Its was mentioned earlier that the nonlinear distortion performance of the system is mainly dictated by the nonlinear distortion performance of the laser diode. Accordingly, the linearity of the laser diode is checked by measuring the CSO at Channel 2 using the same experimental setup shown in Figure 2.5. (Channel 2 typically exhibits the worst CSO performance over all channels. Also, the CSO of Channel 2 is always higher than the CTB of any other channel. Thus, the CSO measurement at Channel 2 represents the worst nonlinear distortion in our system.) Figure 2.7 shows the CSO measurement results as a function of the laser diode bias current. As can be seen in the figure, the optimum linearity is obtained for a bias current of approximately 30 mA. At high bias current, the increase in the CSO is due to the gain compression (saturation) phenomenon. At low bias current, the increase in the CSO is attributed to the additional CSO produced by the signal clipping due to the threshold nonlinearity of laser diode.

2.3 Summary and Discussion

In this chapter, review of coaxial CATV systems and fiber optic AM SCM CATV system is presented. In particular, basic noise and nonlinear distortion performance of the multichannel fiber optic AM SCM system is described in detail to illustrate the basic limitations of the system. These performance limitations will impose limitations in overall system capacity given in terms of channel carrying capacity and system power margins. The remainder of this dissertation will present a detailed study of how these limitations influence the overall system capacity. Specifically, the channel capacity limitation due to the threshold nonlinearity of laser diode is studied in Chapter 3. The nonlinear distortion produced by the laser diode chirp and fiber dispersion and system limitation due to this effect are discussed in Chapter 4. This study of nonlinear distortion produced by the laser diode chirp and fiber dispersion bears particular importance in understanding 1550 nm EDFA amplified multichannel AM SCM video system performance limitations

when the system is being incorporated into the standard 1310 nm single-mode fiber platform of the telecommunication network. In Chapter 5, a comprehensive study of overall AM SCM system performance and capacity and their limits are described.

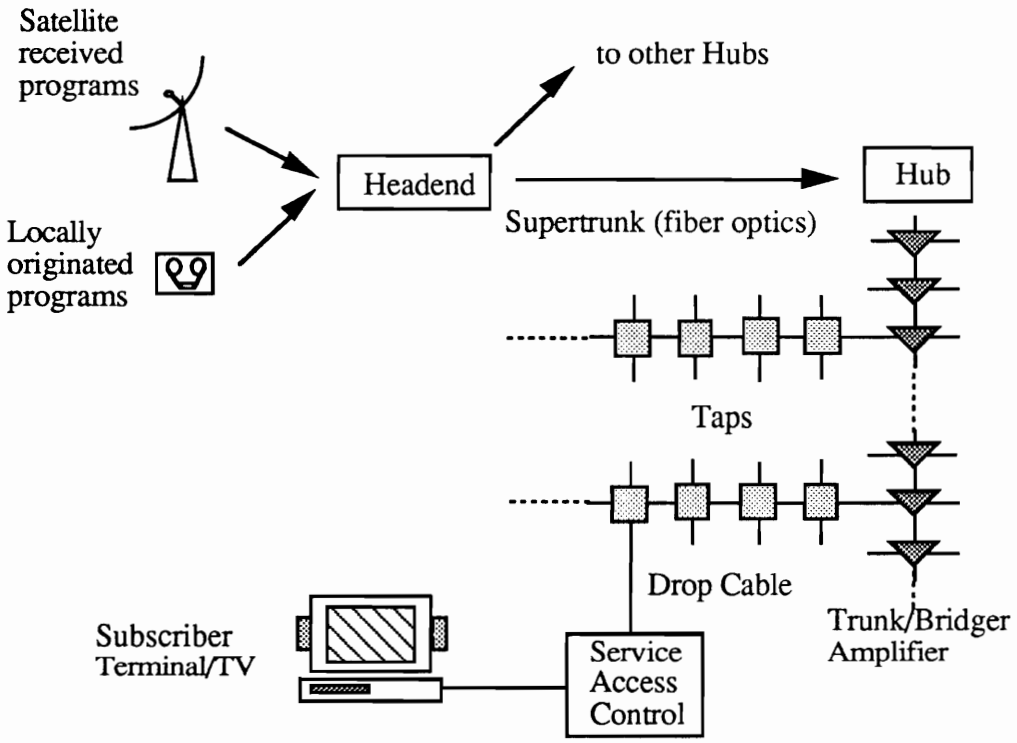

Figure 2.1 Tree-and-branch architecture of CATV networks.

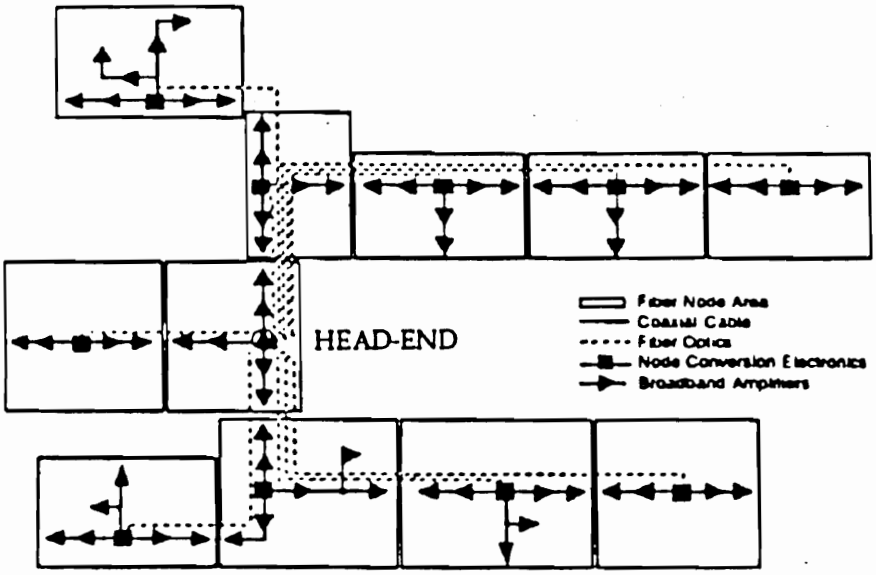

Figure 2.2 Fiber backbone trunking/feeder networks (from ref. [47]).

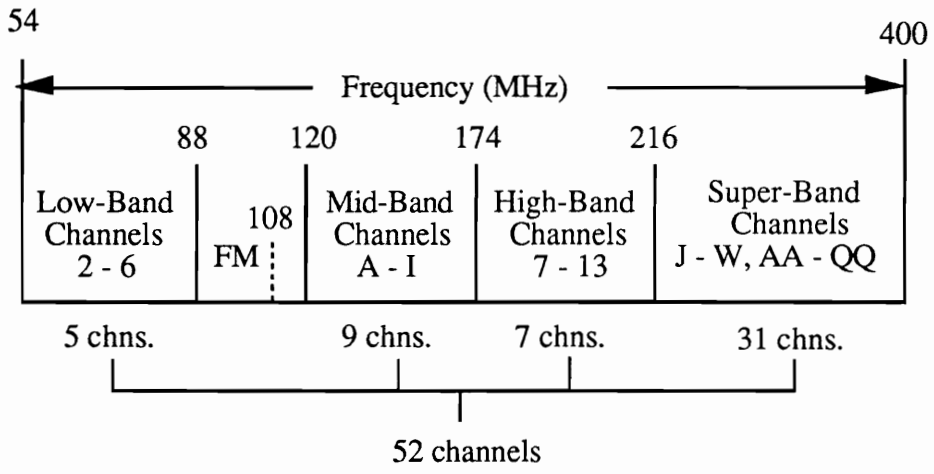

Figure 2.3.a CATV frequency allocation plan.

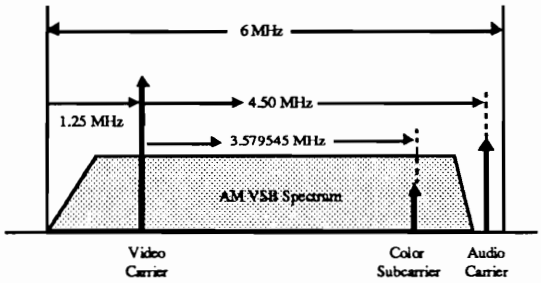

Figure 2.3.b TV spectrum showing main frequency components.

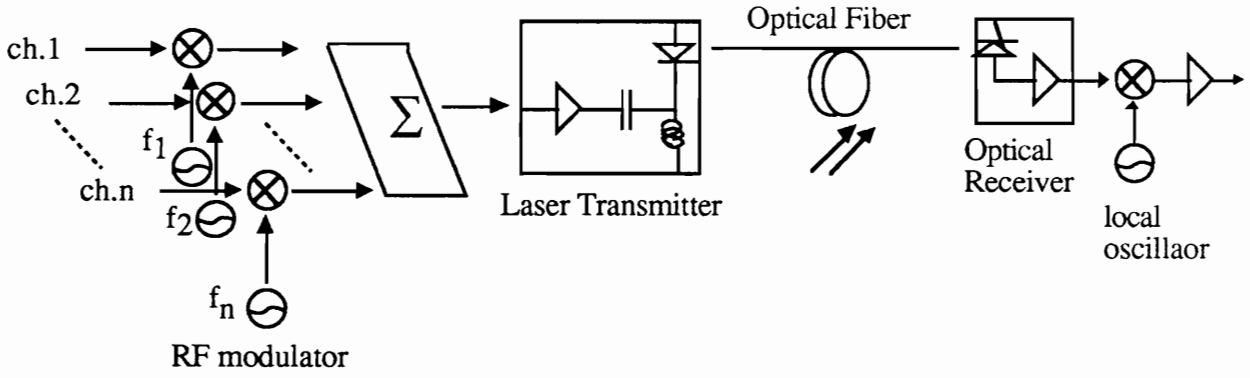

Figure 2.4 A basic configuration of the lightwave multichannel AM SCM system.

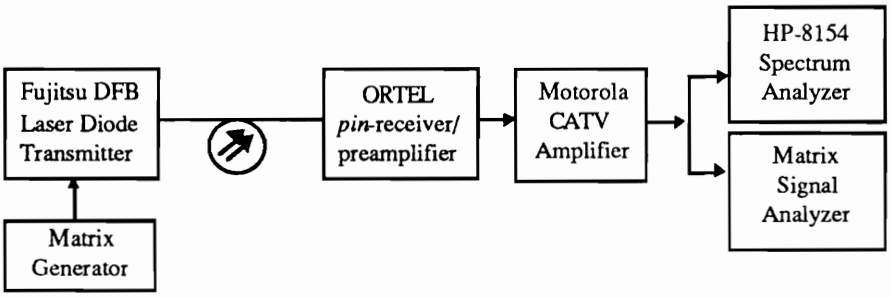

Figure 2.5 Block diagram of fiber optic multichannel AM SCM video system experiments.

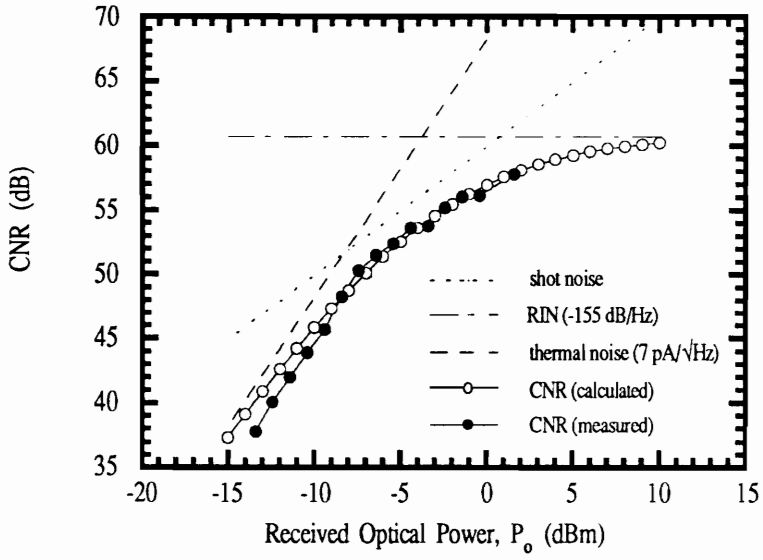

Figure 2.6 AM SCM system CNR as a function of the received optical power.

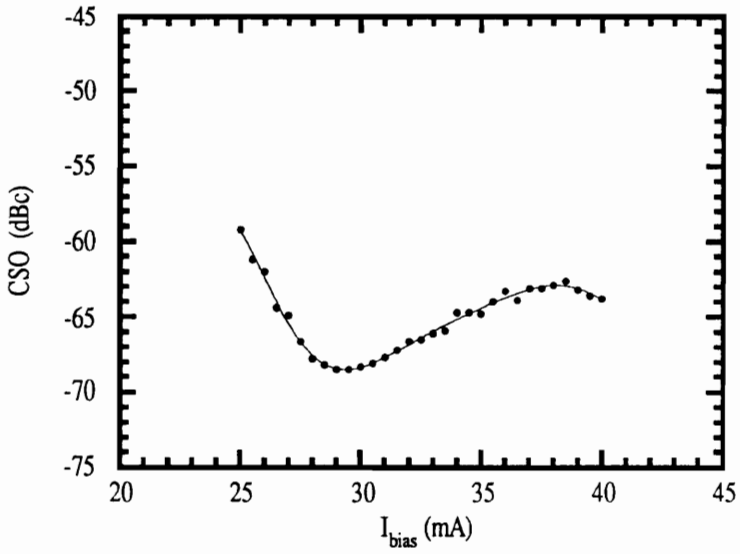

Figure 2.7 Linearity of the Fujitsu DFB laser as a function of bias current.

CHAPTER 3.

THRESHOLD NONLINEARITY OF LASER DIODES AND CHANNEL CAPACITY LIMITATION DUE TO THIS EFFECT

In multichannel AM SCM systems, the nonlinear distortion performance is basically limited by the nonlinear distortion from laser diodes. However, because laser diodes are available with intrinsic nonlinear distortion that exceed system requirements, typical systems are designed to operate where nonlinear distortion performance is limited by over-modulation of laser diodes to obtain higher system power margins or channel capacity. When laser diodes are over-modulated, their threshold characteristic generates nonlinear distortion due to clipping of the intensity modulated signal when the modulating current falls below the threshold current. (Owing to the near Gaussian distribution of a multichannel CATV signal, some over-modulation always exists.) This signal clipping induced nonlinear distortion is generally higher than that produced by the intrinsic device nonlinearities, and, as the rms modulation index increases, it quickly becomes the dominant nonlinear distortion producing mechanism in the system. The threshold nonlinearity is a device independent characteristic and fundamentally limits the nonlinear distortion performance of the system. In this chapter, we describe how the nonlinear threshold characteristic degrades the nonlinear distortion performance and thus how it eventually limits the system channel capacity.

3.1 Motivation and Approach

In a multichannel AM SCM system, when the number of channels or the per-channel modulation is increased beyond a certain level, the modulating current may fall below the laser threshold, due to the negative tail of the near Gaussian distribution of the amplitude of the composite multichannel signal. This results in the negative-peak-clipping of the intensity modulated laser output, as shown in Figure 3.1. In 1989, A. Saleh of AT&T Bell Laboratories was the first to identify that this threshold nonlinearity of the laser diode is the fundamental factor which limits the channel capacity of fiber optic multichannel AM SCM video systems [37]. Saleh then calculated the signal clipping induced nonlinear distortion power (NLD) and the corresponding channel capacity of AM SCM systems by considering the NLD as noise which degrades the system CNR. In calculating the NLD, Saleh assumed that all of the clipped portion of the signal comes back into the signal bandwidth as NLD and is distributed uniformly over the channels. Also, in calculating the channel capacity, he considered a theoretical CNR performance limit imposed by the NLD and photodetector shot noise. His calculation, for example, gave a maximum of 50 channels that could be accommodated with a CNR requirement of 55 dB. However, although Saleh's contribution in identifying the laser threshold characteristic as the fundamental channel capacity limiting factor is generally recognized, there was skepticism that his NLD estimates and consequently his channel capacity estimates were too conservative. Supporting this skepticism, 80 channel AM SCM experiments by Tanabe et al. [25] demonstrated higher channel capacity than Saleh's limit, and the NLD calculation by Alameh and Minasian [38] also indicated that Saleh's estimate of the NLD may be overly conservative. Alameh and Minasian calculated the spectrum of the clipped signal using a transform method and showed that not all of the clipped portion of the signal falls within the CATV channel bandwidth as NLD.

Alameh and Minasian [38] provided an estimate of the channel capacity based on their calculation of NLD. In this calculation, they also considered the NLD as noise as did Saleh. However, according to conventional CATV performance specifications, as mentioned in Chapter 2, the nonlinear distortion performance (CSO and CTB) requirements are separate from the noise (CNR) performance requirement. Therefore, a more appropriate approach to determine the channel capacity should be based on the specified CNR, CSO and CTB performance requirements. In addition, for practical systems, rather than theoretical systems, laser diode RIN and receiver thermal noise cannot be ignored and must be included in the CNR analysis in addition to photodetector shot noise.

On the basis of the discussion given above, research needs in the following areas have been identified: (1) study of nonlinear distortion produced by the laser threshold nonlinearity to further verify that Saleh's NLD is indeed overly conservative, (2) study of channel capacity limitation based on separate noise (CNR) and nonlinear distortion (CSO and CTB) performance, and (3) comparative study of the channel capacity of theoretical systems, considering only photodetector shot noise, with practical systems considering laser RIN and receiver thermal noise in addition to the photodetector shot noise.

The nonlinear distortion produced by the laser threshold nonlinearity is investigated using simulation and experiments. The NLD obtained from the simulation of signal-clipping due to the laser threshold nonlinearity is compared with that obtained from our experiments and previously published results. The laser threshold limited channel capacity is then determined based on the experimentally measured CSO and CTB results and the CNR performance analysis, considering both practical and shot noise limited theoretical systems. Also presented is a methodology of channel capacity calculation based on conventional CATV performance measurement practice.

3.2 Simulation of Laser Threshold Nonlinear Distortion

In this section, the NLD produced by the laser threshold nonlinearity is determined from simulation and compared with previously reported ones. Modeling of the composite multichannel CATV signal, threshold characteristics of laser diodes, description of the simulation, and NLD measurement results are presented in that order. The simulation is carried out using the Block Oriented System Simulator™ (BOSS) [45] which is a time-domain simulation tool which allows one to "build" and test systems on the basis of user-specified functional blocks. Details of BOSS are presented in the Appendix.

3.2.1 Composite Multichannel CATV Signal Model

The composite multichannel signal current I(t) which modulates the laser diode in an AM SCM system can be represented as

$$I(t) = I_{bias} \left[1 + \sum_{i=1}^{N} m_i \cos (\omega_i t + \phi_i) \right] \tag{3.1}$$

where I_{bias} is the bias current, N is the number of video carriers (TV channels), m_i, ω_i, and ϕ_i are the per-channel modulation index, angular video carrier frequency, and phase of channel i, respectively. In the following, we assume a constant per-channel modulation index, viz., m_i=m. For random phases and with N larger than 10, I(t) can be modeled as a Gaussian random process with a mean value of I_{bias} and a variance of $\sigma^2=I_{bias}^2Nm^2/2$ [58]. When this I(t) is used to intensity modulate the laser diode, as shown in Figure 3.1, the generated optical signal P(t) has an average power of P_o and variance of $\sigma_{opt}^2=P_o^2Nm^2/2$. We can then define an rms optical modulation index of the optical signal as

$$\mu = \sqrt{\sigma_{opt}^2/P_0^2} = \sqrt{Nm^2/2} \tag{3.2}$$

which represents the ratio of the rms level of the composite multichannel signal with respect to the mean power level and is the parameter that determines the nonlinear distortion.

A BOSS functional block called Video Channel Generator (VCG), which generates 42 channel composite signal, is created to generate the composite multichannel signal. The VCG produces unmodulated tones for 5 "low-band" channels (Channels 2 to 6, from 55.25 MHz to 83.25 MHz), 9 "mid-band" channels (Channels A to I, from 121.25 MHz to 169.25 MHz), 7 "high-band" channels (Channels 7 to 13, from 175.25 MHz to 211.25 MHz), and 21 "super-band" channels (Channels J to GG, from 216.25 MHz to 337.25 MHz) according to the U.S. CATV channel frequency allocation as shown in Figure 2.3.a. Figure 3.2 shows the spectrum of 42 channel composite signal generated by the VCG.

3.2.2 Description of Simulation

For the NLD simulation measurements, a noise-loading technique is used [59]. The noise-loading technique is a method of measuring the distortion signals. First, a particular frequency band of interest, where the NLD is to be measured, is notch-filtered out from an input signal. This is then passed through the distortion generating component, and the NLD falling into the notched-out frequency band is measured at the output. (In our simulation, since a multichannel composite signal is used as input instead of wide-band noise, the term channel-loading technique seems more appropriate.) In our simulation, the distortion generating component is the laser diode with the threshold characteristic.

Figure 3.3 gives the block diagram of the simulation system for the NLD determination. First, the desired channel, at which the NLD is to be measured, is notched-out from the composite multichannel signal of the VCG using the notch-filter. The notch filter is an IIR filter with a 6 MHz bandwidth that may be centered at any of the channels. The notched-out signal is then fed into the laser diode which is modeled by an ideal linear characteristic above a threshold current I_{th} as shown in Figure 3.1. By appropriately lowering the I_{bias} level of the VCG signal, the signal clipping can be gradually introduced. The NLD falling in the notched-out frequency band is then determined from the spectrum display. A raised-cosine window is applied at the output of the laser diode prior to the calculation of the frequency spectrum to avoid spurious responses. The measurement of nonlinear distortion (NLD) is obtained by calculating the total power of NLD components (including CSO and CTB) falling within the 4 MHz video bandwidth.

Simulations are performed by successively notching out each channel for various levels of signal clipping, determining the distortion products that fall within that channel, and normalizing by the channel signal (corresponding to the unmodulated video carrier) power. The NLD is obtained by averaging 45 measurements using different input data sequences (different sets of random phases for each carrier) and evaluated at different time intervals. Each input data sequence consists of 2^{15} samples at 1 ns intervals. This gives an effective frequency resolution of 30 kHz which is the IEEE recommended resolution bandwidth of the spectrum analyzer for the measurement of CATV nonlinear distortion [60]. An example of the spectrum of the clipped-signal for μ=0.35 is shown in the Figure 3.4. In Figure 3.5, the NLD across the 42 channel signal band is shown for an 8.5 percent modulation index per channel, which corresponds to μ=0.389. As can be in this figure, the NLD is nearly uniform across the channels.

3.2.3 NLD Simulation Results

In Figure 3.6, the C/NLD for Channel 11 is shown as a function of rms modulation index μ, and compared with the results calculated by Saleh [37] and Alameh and Minasian [38]. It is seen that the simulation gives at least 10 dB better C/NLD than is obtained with Saleh's estimate [37] and is generally consistent with Alameh and Minasian's calculation [38]. The difference with Saleh's results may be attributed to the fact that a significant portion of the NLD resides outside of the signal band, contrary to Saleh's original assumption. Furthermore, the CSO and CTB calculation by A. Angenent [61] also indicates that the total NLD, which mainly consists of the CSO and CTB, within a video channel bandwidth is much less than Saleh's prediction, thus, supporting our simulation results. Apparently, Saleh attempted to improve his NLD estimates [9] by including a higher order expansion term and considering that only half of the clipped-signal energy falls within band. (The basis of this modification does not appear to have been published.) Nevertheless, as can be seen from Figure 3.6, there are still substantial differences for small values of μ although the difference in C/NLD obtained from the simulation and the modified expression is reduced, particularly for large values of μ.

3.3 Measurement of Laser Threshold Nonlinear Distortion

Objectives of the nonlinear distortion experiments are (1) to measure the spectral distribution of NLD to show that a significant portion of the nonlinear distortion resides outside the signal bandwidth, (2) to measure the composite-second-order (CSO) and the composite-triple-beat (CTB) due to the laser threshold characteristic, and (3) to show that the effect of the NLD on the CNR degradation is negligible for the range of μ of interest. The CSO and CTB measurements along with other nonlinear distortion products will also

allow assessment of the NLD power within a 4 MHz video bandwidth and enable us to compare with simulation and previously reported results.

3.3.1 Experimental Setup and Procedure

For the measurement of the NLD due to laser diode threshold nonlinearity, the same experimental set-up shown in Figure 2.5 is used. The output of a highly linear InGaAsP 1550 nm Fujitsu DFB laser diode is connected by a short fiber pigtail to an ORTEL (model 2610B) *pin* photodiode module. The laser diode has intrinsic CSO and CTB that are lower than -65 dBc, when measured with 42 channels and with per-channel modulation index of 0.05, and has a RIN lower than -155 dB/Hz, when measured with a bias current of 30 mA. The photodiode module has a responsivity of 0.93 A/W and a thermal noise current density of 7 pA/$\sqrt{\text{Hz}}$. The matrix generator (MG) Model SX-16 from Matrix Test Equipment, Inc., produces a composite 42 carrier CATV multichannel signal that is used to intensity modulate the laser diode. A Motorola MHW6182 CATV amplifier is used to obtain additional signal gain at the output of the photodiode module. The amplified signal is then connected either to the HP 8154 spectrum analyzer to observe the NLD spectrum or to the matrix signal analyzer (MSA) Model R-75 from Matrix Test Equipment, Inc., to make CSO and CTB measurements. The MSA is a composite multi-channel signal analyzer and is used to make the calibrated measurements of CSO, CTB, and CNR.

The NLD measurement is performed by setting the bias current at a fixed value and varying the modulation index per channel m, thus, effectively varying the rms optical modulation index $\mu=m\sqrt{(N/2)}$, where N is the number of channels. The bias current is set at 30 mA, at which the lowest intrinsic CSO and CTB is obtained. When μ exceeds a certain level, the modulation current may fall below the laser threshold, which results in the clipping of the negative-peaks of the intensity modulated signal, thereby producing the NLD. The NLD is measured over a range of μ from 0.2, for which there is essentially no

clipping induced NLD, to μ=0.5, for which there is significant clipping induced NLD. For all cases, the NLD of Channel 2 (center frequency of 55.25 MHz) was measured. (The NLD of Channel 2 is generally the poorest of all channels, and the variation in NLD across the channels is within a few decibels.) The NLD is obtained by measuring the peak power of all of NLD products within the 4 MHz video bandwidth, and then summing all of the distortion products. It is found that the clipped NLD is essentially uniformly distributed across the channel band, which is in agreement with our simulation results.

3.3.2 NLD Measurement Results

The measured NLD are plotted in Figure 3.7 along with the NLD obtained by our simulations. Also plotted in Figure 3.7 are the results of the Alameh and Minasian [38], and Saleh [9,37] analyses. The flattening of the experimental results, when μ<0.29, is a result of intrinsic device dependent nonlinearities resulting in a minimum level of NLD. As can be seen in Figure 3.7, as the rms modulation index μ is increased, the output of the intensity modulated signal begins to produce additional NLD, and it quickly dominates over the intrinsic NLD for μ>0.29.

Experimental, simulation, and Alameh and Minasian's [38] results, in Figure 3.7, are also shown to be in close agreement and are significantly better than Saleh's estimates [9,37]. In fact, the comparison even with the modified NLD estimate [9] shows that there is approximately a 10 dB difference for μ<0.3, which is the low nonlinear distortion region of interest. As mentioned previously, this difference is attributed to Saleh's assumption that all of the clipped portion of the signal comes back as distortion. The measurement of a clipped signal spectrum at μ=0.27 shown in Figure 3.8.a illustrates that a major portion of the NLD resides as out-of-signal band components. The shape of the NLD spectrum shown in Figure 3.8.a is also consistent with the shape of the calculated spectrum of Alameh and Minasian [38], thus, further verifying that Saleh's assumption leads to an over estimate of NLD.

3.3.3 CSO and CTB Measurement Results

In the above comparison, all nonlinear distortion products were treated as noise to allow a comparison among the simulation, prior analyses, and measurements. However, as noted previously, conventional CATV signal nonlinear distortion performance is specified in terms of CSO and CTB requirements. Looking into the nonlinear distortion within the 4 MHz video channel bandwidth of Channel 2, shown in Figure 3.8.b, indicates that nonlinear distortion appears as discrete products and not as wide-band noise. Therefore, it is more appropriate to consider how the nonlinear distortion produced by the laser threshold characteristic degrades the overall CSO and CTB performance of the system, rather than by treating it as noise.

Figure 3.9 shows the measured CSO and CTB of Channel 2 and Channel 11. To measure the CSO and CTB degradation due to signal clipping, the modulation index per channel m is initially set to a small value such that the resulting total current level does not fall below the laser threshold. (The total current is the sum of a zero-mean signal current plus a constant bias current.) Then, the modulation index per channel m is gradually increased by increasing the signal current, thereby increasing μ and causing signal clipping. As can be seen in Figure 3.9, as the rms modulation index is increased, the output of the intensity modulated signal begins to produce additional CSO and CTB owing to signal clipping, and they quickly dominate over the intrinsic CSO and CTB for $\mu>0.29$. Comparison of the measured CSO and CTB due to signal clipping with that of the calculated values reported by Angenent [61] shows good agreement. Also included in the figure is the measured CNR for Channel 2. From this we can see that the CNR continues to increase although the clipped-signal induced nonlinear distortion degrades the CSO and CTB. This shows that the noise contribution from the nonlinear distortion is not significant, at least for the μ range

that is of interest, namely $\mu \approx 0.3$. This verifies that considering the NLD as a noise degrading factor is indeed inappropriate.

3.4. Lightwave multichannel AM SCM video channel capacity

In this section, the channel capacity of multichannel AM SCM systems is studied based on the separate noise (CNR) and nonlinear distortion (CSO, and CTB) performance requirements. Also presented is a comparative study of the channel capacity of photodetector shot noise limited theoretical systems and practical systems which include additional laser RIN and receiver thermal noise.

3.4.1 Channel Capacity Calculations

In prior papers by Saleh [37] and Alameh and Minasian [38], channel capacity was calculated by assuming that the CNR is degraded equally by the shot noise ShN and NLD , i.e., $CNR \equiv C/(ShN+NLD)$. However, as discussed in the previous section, in actual systems the NLD appears as discrete intermodulation products, and thus it is more reasonable to consider whether the clipped composite signal meet the CSO and CTB requirements. Therefore, our approach is first to determine the maximum μ which satisfies a given CSO and CTB requirement, and then use that μ to calculate the corresponding number of channels at a specified CNR. Combining the CNR Eq. (2.1) with the $\mu = m\sqrt{(N/2)}$ the following equation for channel capacity N is obtained,

$$N = \frac{\Re^2 P_o^2}{CNR\,(RIN \cdot B \cdot \Re^2 P_o^2 + 2q \cdot B \cdot \Re P_o + \langle i_{th}^2 \rangle \cdot B)}\,\mu^2 \qquad (3.3)$$

where $\Re$ is the responsivity of the photodetector, P_0 is the optical power at the photodetector, RIN is the laser relative intensity noise, B is the 4 MHz video bandwidth, q is the electron charge, and $\langle i_{th}^2 \rangle$ is the receiver thermal noise spectral density.

In Figure 3.10, the number of channels N are plotted versus the rms modulation index μ for CNR of 55 dB and P_0 of 0 dBm. The values of RIN= -155 dB/Hz and $\sqrt{\langle i_{th}^2 \rangle}$= 7 pA/$\sqrt{\text{Hz}}$ are used here as representative of the performance achievable with a good device technology. Also plotted on the same figure are the experimentally measured CSO and CTB at Channel 2 to indicate increases in the CSO and CTB as clipping increases. (The CSO at Channel 2 is generally the worst CSO/CTB over all the channels.) The channel capacity can be obtained from Figure 3.10 in the following manner. First determine μ corresponding to given system CSO and CTB requirements from the right ordinate. Then for that value of μ read out the number of channels from the left ordinate of the graph. For example, with CSO and CTB requirements of -60 dBc, the corresponding μ is $\approx$ 0.31. At this μ, the channel capacity is about 115. This is higher than previous reported values [37, 38]. The main reason for this difference is due to not considering the NLD as a CNR degradation mechanism in our analysis.

The calculation of the channel capacity in this section is based on the CSO and CTB performance obtained from experiments using 42 channels. This assumes that the CSO and CTB are not significantly affected when the number of channels is increased. This is supported by observations made from our experiments and simulations and prior theory [10]. Also, it may be noted from Figure 3.10, the value of μ, and consequently the maximum number of channels, are not sensitive to small variations in the CSO and CTB levels.

3.4.2 Channel Capacity of Theoretical and Practical Systems

It is important to note that the number of channels depends on the received optical power, and this dependence is not linear when the laser diode RIN and receiver thermal noise are included in the analysis. As seen from Eq. (3.3), only when photodetector shot noise is dominant is the number of channels linear with the received optical power. Therefore, it is not generally valid to extrapolate shot noise limited results to lower receiver power levels. To illustrate this nonlinear dependence, the channel capacity is calculated as a function of received power and plotted in Figure 3.11 with CNR requirements of 50 and 55 dB for both fundamental and practical limits. The fundamental limit case corresponds to the shot noise limit, and the practical limit corresponds to the performance limit imposed by the laser RIN and the receiver thermal noise in addition to the shot noise. A linear power scale is used for the abscissa to show the nonlinear functional relationship when the laser RIN and the receiver thermal noise are included. In these plots, we have again used RIN=-155 dB/Hz, $\sqrt{\langle i_{th}^2 \rangle}$=7 pA/$\sqrt{\text{Hz}}$, corresponding to good device technology, and μ=0.31, which is the maximum value consistent with CSO and CTB requirements of -60 dBc. As can be seen from the curves in Figure 3.11, only in the fundamental limit is the channel capacity linearly dependent on P_O. In the practical limit, the channel capacity shows a nonlinear dependence on P_O. Thus, in practice, both the received power and the desired CNR must be specified to determined the capacity. Furthermore, it is not generally appropriate to express the channel capacity in terms of the number of channels per milliwatt of received power. Also shown in Figure 3.11 is the channel capacity for CNR requirements of 50 and 55 dB. The comparison of the two shows that the channel capacity is extremely sensitive to the CNR requirement.

3.5 Summary

Simulation and experimental measurements of the NLD due to over-modulation of laser diodes in multichannel AM-VSB system are presented. The experimentally measured NLD are lower than previous

estimates but consistent with more recent results. Using the CSO and CTB measurements, the practical channel capacity is calculated on the basis of conventional CATV signal performance requirements and is shown to be higher than previously reported ones. It is also shown that when laser diode RIN and receiver thermal noise are included in the analysis of channel capacity, the relationship between the number of channels and the received optical power is not simply linear, and thus the channel capacity must be specified with the received optical power level. More details on the relationship between channel capacity and received optical power are presented in Chapter 5 where overall system capacity of fiber optic AM SCM systems is discussed.

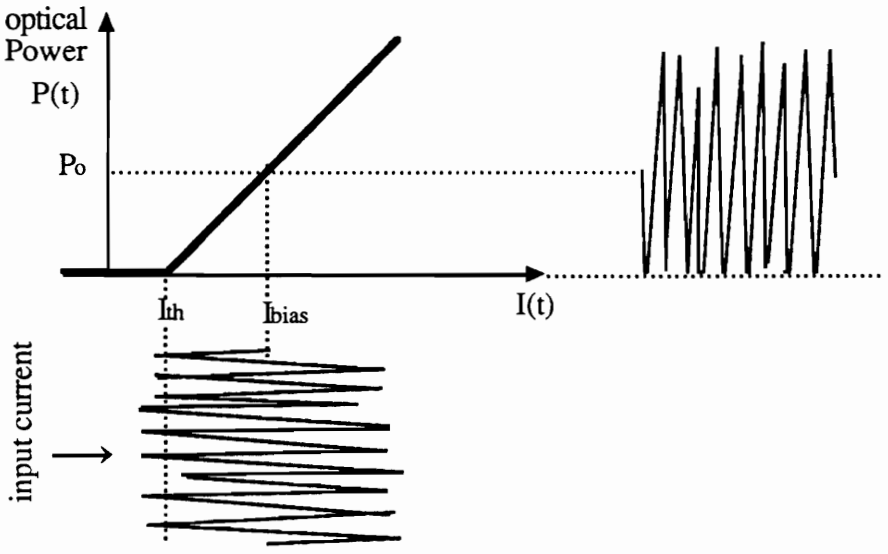

Figure 3.1 Intensity clipped signal due to the laser diode threshold nonlinear characterisitic.

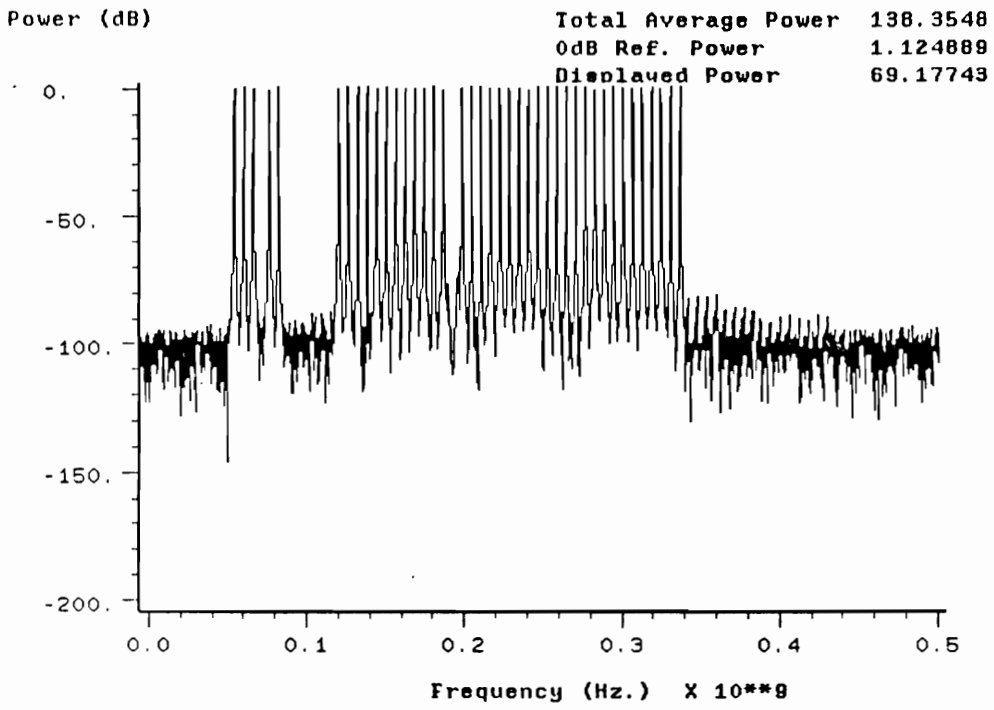

Figure 3.2 Spectrum of the 42 channel composite CATV simulation signal according to the U.S. CATV channel allocation. Channel 10 is notched-out to make the nonlinear distortion measurement.

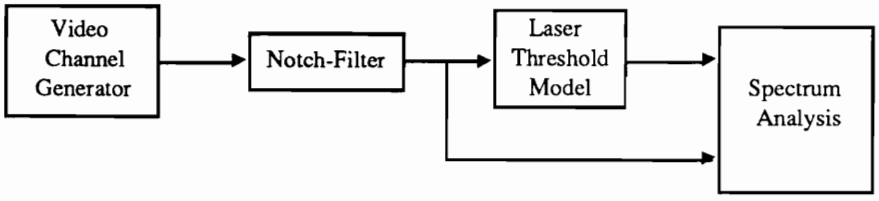

Figure 3.3 Block diagram representation of the noise-loading simulation system for the clipped-signal NLD determination.

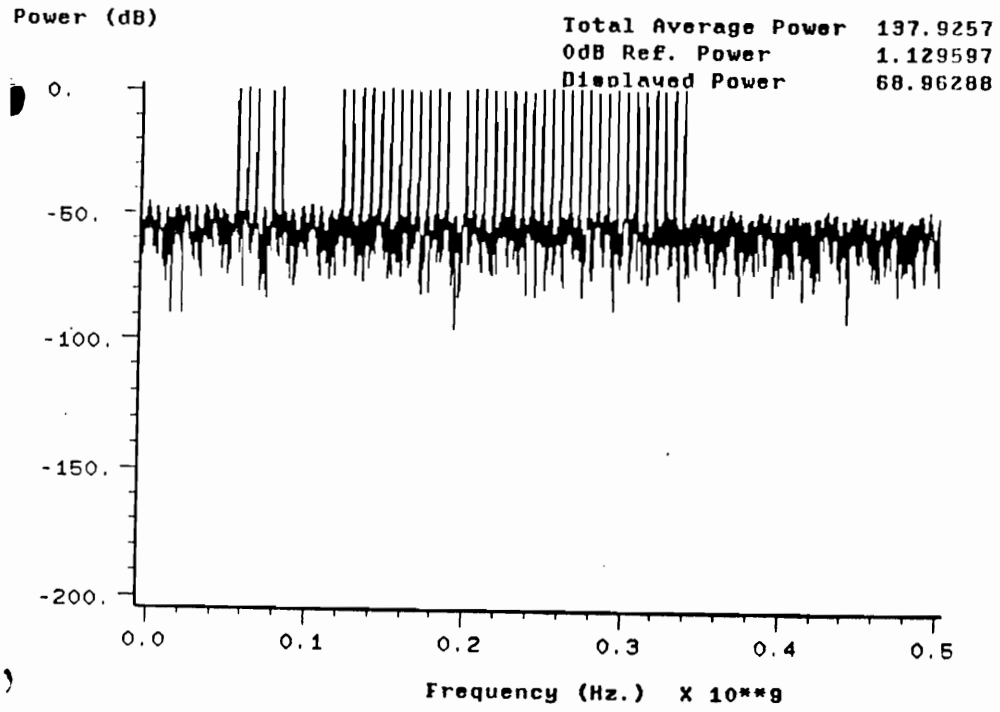

Figure 3.4 Spectrum of the clipped 42 channel composite CATV simulation signal for μ=0.35.

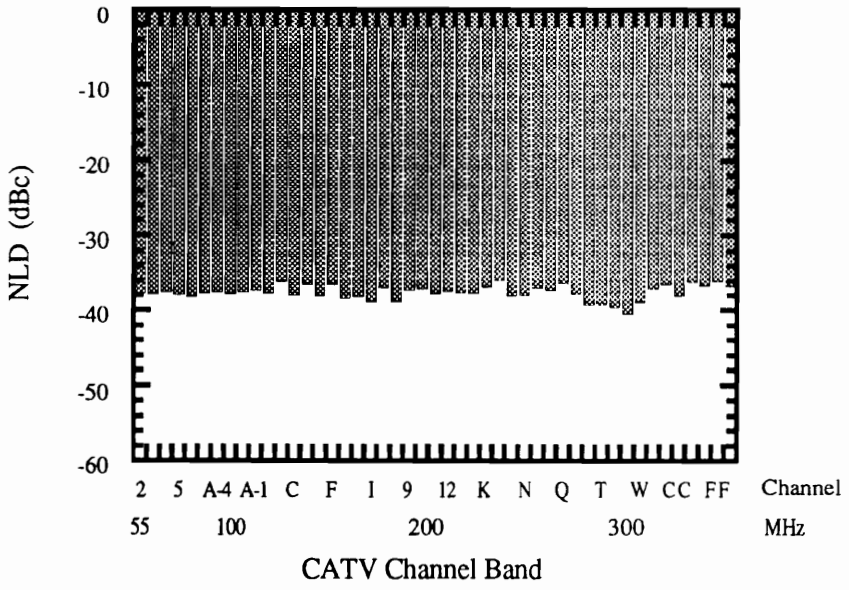

Figure 3.5 NLD across the 42 channel band with modulation index per channel of 8.5 %.

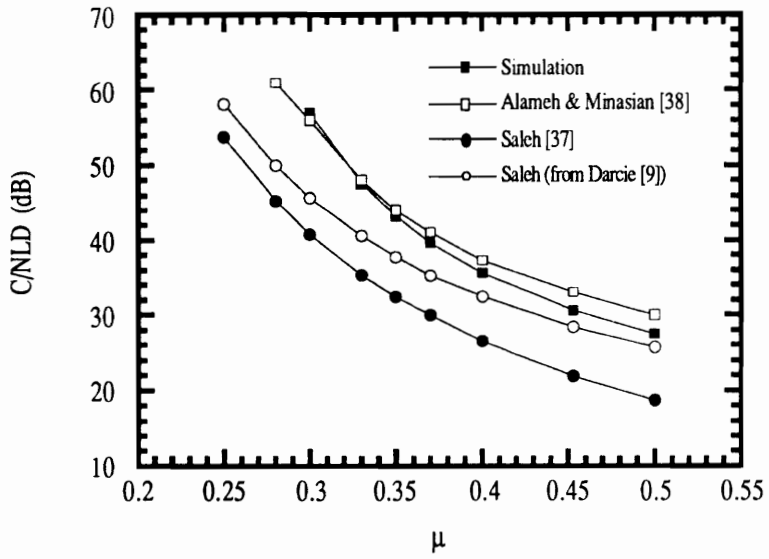

Figure 3.6 Comparison of the simulation results with prior approximations.

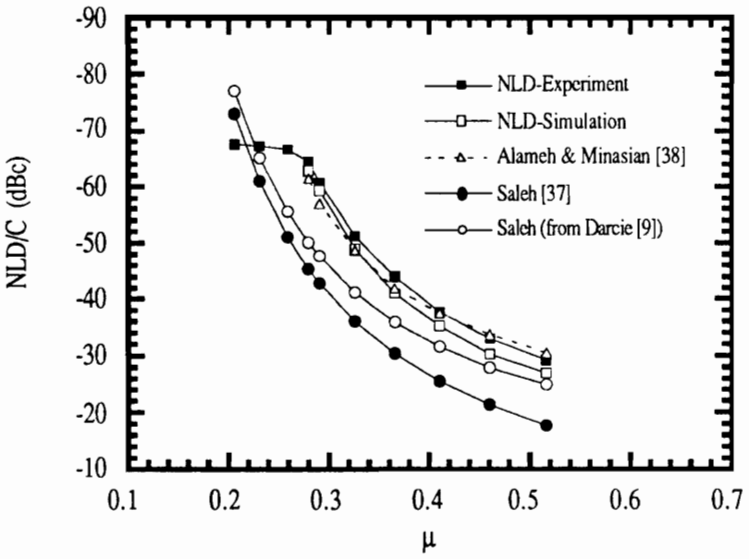

Figure 3.7 Comparison of the NLD results from experiments with prior theory and simulations.

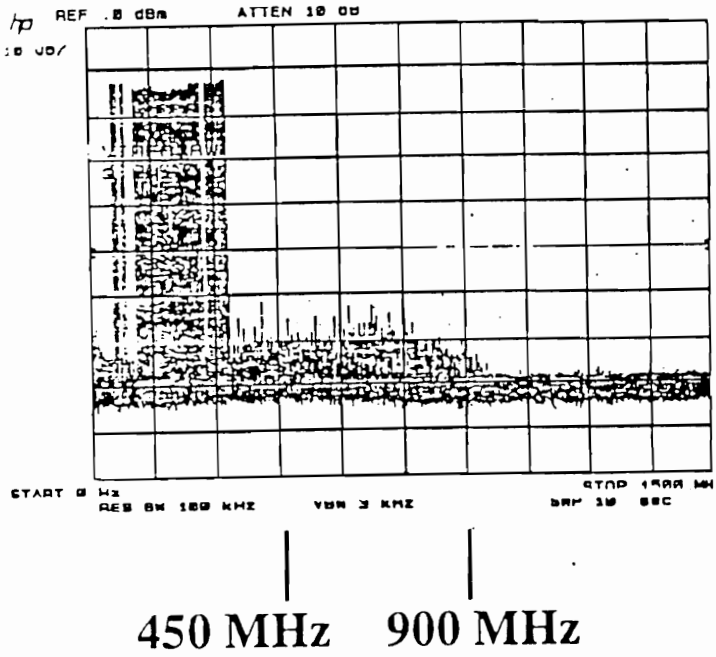

Figure 3.8.a Experimentally measured clipped-signal spectrum

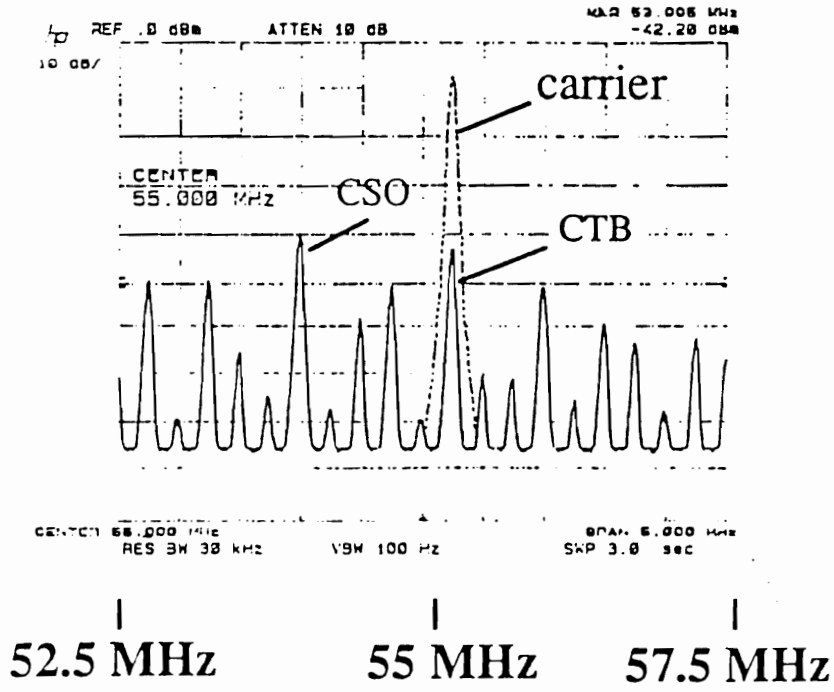

Figure 3.8.b Experimentally measured clipped-signal nonlinear distortion products at Channel 2 (carrier frequency at 55.25 MHz) showing the CSO (at 1.25 MHz below the carrier) and CTB (at the video carrier) with respect to the video carrier (shown with dotted line).

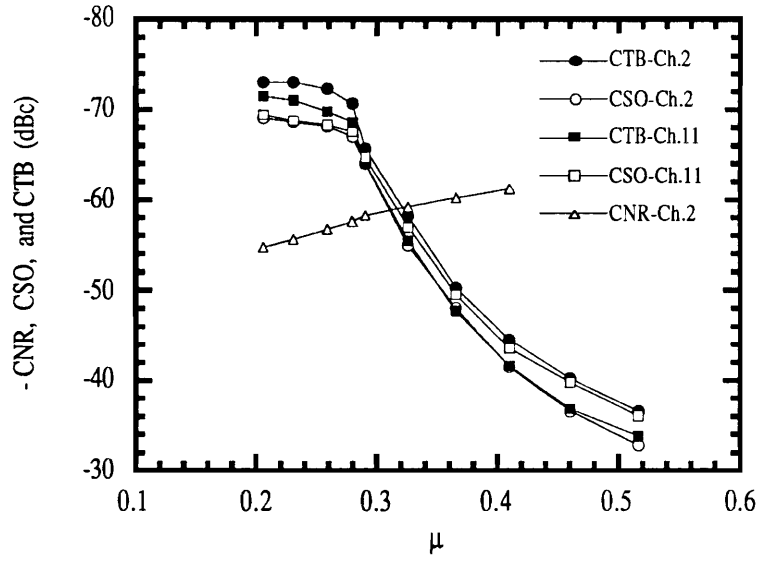

Figure 3.9 Experimentallty measured clipping induced CSO and CTB for Channel 2 and Channel 11 as a function of μ and the CNR of Channel 2.

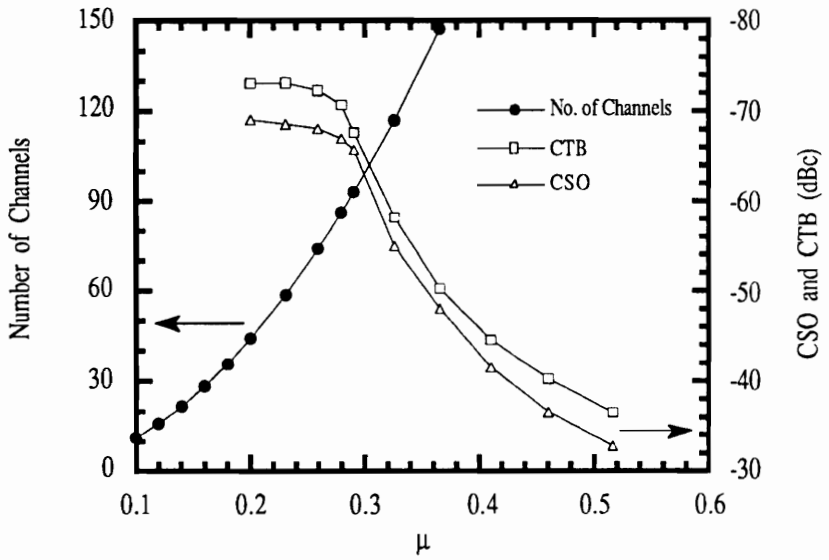

Figure 3.10 Number of channels and the clipping induced CSO and CTB versus μ with CNR of 55 dB, $\Re$=0.93 A/W, B=4 MHz, P_O= 0 dBm, RIN=-155 dB/Hz, and $\sqrt{<i_{th}^2>}$=7 pA/$\sqrt{Hz}$.

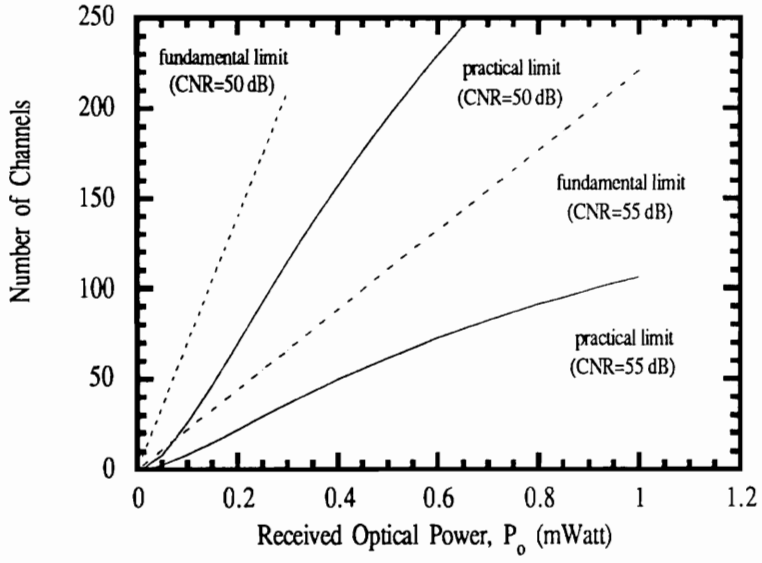

Figure 3.11 Number of channels versus the received optical power for practical and fundamental limits with CNR of 50 dB and 55 dB, $\Re$=0.93 A/W, B=4 MHz for RIN=-155 dB/Hz and $\sqrt{<i_{th}^2>}$=7 pA/$\sqrt{Hz}$.

CHAPTER 4.

NONLINEAR DISTORTION DUE TO LASER DIODE CHIRP AND OPTICAL FIBER DISPERSION

In a proposed *Fiber-In-The-Loop* (FITL) architecture of the telecommunication network [62, 63], 1550 nm multichannel AM SCM video distribution systems are to be *wavelength division multiplexed* (WDM) with the 1310 nm telephone systems to provide near term fiber optic delivery of voice and multichannel video services. With recent advances in erbium-doped fiber amplifiers (EDFAs), whose gain spectrum lies in the 1550 nm region, AM SCM systems now have sufficient power margins [39-41] to deliver video signals to many subscribers in the local *distribution plant*. However, because presently deployed optical fibers in the telecommunication networks are standard 1310 nm dispersion minimized single-mode fibers, 1550 nm systems will suffer from the increased fiber dispersion caused by operating away from the minimum dispersion wavelength. This added fiber dispersion and laser diode frequency chirp produces a second order type nonlinear distortion which degrades the CSO performance of 1550 nm systems. In this chapter, the mechanisms which produce this second order type nonlinear distortion are described and evaluated. The effects of this distortion on the overall system performance are studied using theoretical analysis, simulation, and experiment.

4.1 Motivation and Approach

The CSO degradation due to fiber dispersion and laser diode chirp in multichannel AM SCM systems was first reported in 1990 by M. Shiegematsu and co-workers [42] for their 1550 nm optically amplified systems with EDFAs using 1310 nm single-mode fibers. Following this, M.R. Phillips et al. [43] and E.E. Bergmann et al. [44] reported analytical methods to predict the CSO and CTB degradation. The analytical method presented by Phillips et al. [43] relies on numerical solution of the wave-equations. The analysis reported by Bergmann et al. [44] is based on the harmonic analysis from a series expansion of the fiber dispersion and laser phase nonlinearities. These results [42-44] indicate that the CSO distortion could reach -45 dBc with a nominal fiber dispersion of 17 ps/Km/nm at a fiber length of 10 Km for typical DFB lasers. This is above the -50 dBc minimum CSO requirement of AM SCM systems. Since some local distribution loops could approach 10 Km, the CSO degradation by laser chirp and fiber dispersion will significantly restrict the maximum link distance of the system.

Although the results of M. Phillips [42] and E. Bergmann [43] agree reasonably well with experimental measurements, neither analysis explains details of the nonlinear distortion generation mechanism. There had been earlier theoretical analysis of the fiber dispersion induced distortion due to the laser chirp, but these efforts were limited to single frequency analysis. In 1984, G. Meslener [64] studied the signal distortion due to the harmonics generated by using Fourier series expansions to numerically evaluate the signal distortion. In 1985, F. Koyoma and Y. Suematsu [65] analyzed the same effect using the first order exponential expansion and gave an analytic expression for the distortion of the intensity modulated signal. However, both of these results [64, 65] are based on a single frequency analysis, and thus no intermodulation distortion can be explained. More recently, C. Ih and Y. Gu [66] studied the intermodulation distortion based on a common frequency concept and Fourier series expansion, but only

numerical results are reported. Therefore, an analytic expression of the intermodulation distortion is highly desired for better understanding of the CSO degradation in multichannel systems.

In this chapter, we derive an analytic expression which describes the intermodulation distortion due to fiber dispersion and laser chirp. For this purpose, a model for laser diode chirp under the typical modulation frequency of a CATV signal is first derived. Based on this model, a small-signal two-tone analysis is carried out to derive an analytic expression for the distortion. A two-tone simulation is performed to check the results of the analysis. Experiments and simulation are used to extend the results to the multichannel case to evaluate the CSO degradation in AM SCM video systems. Maximum link distance limitations for local loop distribution due to the CSO degradation is presented.

4.2 Laser Diode Chirp Model

When laser diodes are intensity modulated by varying the modulation current, the optical frequency of the output is also changed. This accompanying frequency variation is referred as frequency-chirping (or simply chirp). This is caused by the modulation induced refractive index variation of the active region of the laser diode. Study of the laser diode chirp is based on the following single-mode laser rate-equations. The laser rate-equations describe the dynamics of photons generated in the active region of the laser [67].

$$\frac{dN}{dt} = \frac{I}{qV} - g_o (N - N_t)(1 - \varepsilon S) S - \frac{N}{\tau_n} \tag{4.1.a}$$

$$\frac{dS}{dt} = \Gamma g_o (N - N_t)(1 - \varepsilon S) S - \frac{S}{\tau_p} + \frac{\beta \Gamma N}{\tau_n} \tag{4.1.b}$$

$$\frac{d\phi}{dt} = \frac{\alpha}{2} \{\Gamma g_o (N - N_t) - \frac{1}{\tau_p}\} \tag{4.1.c}$$

where N (t) is the electron carrier density, S(t) is the photon density in the active region, $\phi(t)$ is the optical phase , I(t) is the injection current, V is the volume of the active laser cavity, ε is the gain compression factor, g_o is the gain constant, N_t is the electron carrier density at which the net gain in the active medium is zero, τ_n is the spontaneous recombination lifetime of the carriers, τ_p is the photon lifetime in the active cavity, q is the electron charge, Γ is the optical confinement factor specified by the ratio of the active region volume to the modal volume [68], β is the spontaneous emission factor given by the fraction of spontaneous emission coupled into the laser mode, and α is the laser linewidth enhancement factor [69]. Each of the terms in Eqs. (4.1.a) and (4.1.b) is simply book-keeping of the creation and annihilation of carriers and photons for a given supply of injection current. Therefore, Eqs. (4.1.a) and (4.1.b) represent the time variation of the electron carriers N(t) in the cavity and generated photons S(t) with respect to the injection current I(t). Eq. (4.1.c) represents instantaneous optical phase change (frequency) relative to that at the on-set of laser threshold, i.e., $\Gamma g_o(N - N_t) = 1/\tau_p$.

By applying a small signal analysis [30] (i.e., $I(t)=I_o+ie^{j\omega t}$, $N(t)=N_o+ne^{j\omega t}$, and $S(t)=S_o+se^{j\omega t}$, where I_o, N_o, and S_o are the steady state values), to Eqs. (4.1.a) and (4.1.b), neglecting second order terms, and solving for n (jω) in terms of s (jω) gives,

$$n(j\omega) = \frac{1}{\Gamma\tau_p\omega_r^2}(j\omega + \gamma_d)\, s(j\omega) \tag{4.2}$$

where ω_r is the resonant frequency and γ_d is the inverse of the damping time constant which are given by $\omega_r = \sqrt{g_o S_o/\tau_p}$ and $\gamma_d = \varepsilon S_o/\tau_p$. Also, from Eq. (4.1.c) the resulting optical frequency shift $\Delta\nu$ under sinusoidal signal modulation is given by

$$\Delta\nu(j\omega) = \frac{1}{2\pi}\frac{d\phi(j\omega)}{dt} = \frac{\alpha\Gamma g_o}{4\pi} n(j\omega) \tag{4.3}$$

Substituting Eq. (4.2) into Eq. (4.3) gives, the relationship between the optical frequency shift and the photon density is [70],

$$\Delta\nu\ (j\omega) = \frac{\alpha}{4\pi S_o}\ (j\omega + \gamma_d)\ s\ (j\omega) \tag{4.4}$$

Since the modulation frequencies corresponding to a composite multichannel CATV signal are less than 500 MHz, ω is much less than γ_d for typical DFB laser values of $\varepsilon=2.5\text{x}10^{-23}$ m^3, $S_o=10^{-21}$ m^3, and $\tau_p=1$ ps. Therefore, the optical frequency excursion $\Delta\nu$ under a typical CATV signal modulation of laser diode simplifies to

$$\Delta\nu\ (j\omega) = \frac{\alpha}{4\pi S_o}\ \gamma_d\ s\ (j\omega) = \frac{\alpha}{4\pi}\ \frac{\varepsilon}{\tau_p}\ s\ (j\omega) \tag{4.5}$$

Now, as can be seen from Eq. (4.5), the ω dependency of $\Delta\nu$ is limited only to the photon density variations and is proportional to the constants $\alpha\varepsilon/4\pi\tau_p$. Thus, the time dependence of $\Delta\nu(t)$ is proportional to the time dependence of S, S(t). Using the relation between the photon density and optical power P(t),

$$S(t) = \frac{2\Gamma\tau_p}{V\eta h\nu}\ P(t) \tag{4.6}$$

where η is the internal quantum efficiency of the laser, h is Planck's constant, and ν is the optical frequency, the following relation between $\Delta\nu$ and the optical intensity output P(t) of the laser diode under CATV signal modulation can be established

$$\Delta\nu(t) = \frac{\alpha}{4\pi}\ \frac{2\Gamma\varepsilon}{V\eta h\nu}\ P(t) = \frac{\alpha}{4\pi}\ \kappa\ P(t) \tag{4.7}$$

where $\kappa=2\Gamma\varepsilon/V\eta h\nu$ is a laser structure dependent constant having the unit of Hz/watt. (A representative value of κ is 10^{13} Hz/watt.) As shown in Eq.(4.7), the chirp is dependent on the linewidth enhancement α, laser diode physical constants κ, and output power P(t). One important thing to recognize from Eq.(4.7) is that $\Delta\nu$ is in-phase with the intensity modulated signal.

4.3 Two-Tone Analysis

In this section, a small-signal two-tone analysis of the nonlinear distortion, namely the second-harmonic distortion and the second-order intermodulation distortion, is carried out to study how laser chirp and fiber dispersion lead to this type of distortion

For the purpose of analysis, the optical field $E_S(t)$ at the output of the laser diode is approximated as

$$E_S(t) = \sqrt{P(t)} \cdot e^{-j(\omega_o t - \phi(t))} \tag{4.8}$$

where P(t) is the output intensity, ω_0 is the angular optical frequency, and $\phi(t)$ is the time varying phase related to the chirp in Eq. (4.7). For the two-tone (ω_1 and ω_2) intensity modulated laser, the optical output P(t) can be written as

$$P(t) = P_o\left[1+\sum_{i=1}^{2} m_i \cos\omega_i t\right] = P_o\left[1 + m_1 \cos\omega_1 t + m_2 \cos\omega_2 t\right] \quad , \tag{4.9}$$

and the corresponding field amplitude $\sqrt{P(t)}$ for small signals (m_1 and $m_2 << 1$) can be approximated by

$$\sqrt{P(t)} \approx \sqrt{P_o}\left[\, 1 + \frac{1}{2}\sum_{i=1}^{2} m_i \cos\omega_i t \;-\; \frac{1}{8}\left(\sum_{i=1}^{2} m_i \cos\omega_i t\right)^2 \right] \tag{4.10}$$

Also, using Eq. (4.7) and the small signal constraint $\alpha\kappa P_O m_i/2\omega_i << 1$, $e^{j\phi(t)}$ can be expanded as

$$e^{j\phi(t)} = e^{j\frac{\alpha\kappa P_o}{2}\sum_{i=1}^{2}\frac{m_i}{\omega_i}\sin\omega_i t} = 1 + j\frac{\alpha\kappa P_O}{2}\sum_{i=1}^{2}\frac{m_i}{\omega_i}\sin\omega_i t - \frac{1}{2}\left(\frac{\alpha\kappa P_O}{2}\sum_{i=1}^{2}\frac{m_i}{\omega_i}\sin\omega_i t\right)^2 \tag{4.11}$$

where terms higher than the second-order are ignored. Substituting Eqs. (4.10) and (4.11) into Eq. (4.8), multiplying-out, and ignoring the d.c. terms and terms higher than the second-order gives $E_S(t)$

$$\begin{aligned} E_s(t) = e^{-j\omega_o t}\Bigg\{ & 1 + \sum_{i=1}^{2}\frac{m_i}{2}\cos\omega_i t + j\frac{\alpha\kappa P_O}{2}\sum_{i=1}^{2}\frac{m_i}{\omega_i}\sin\omega_i t \\ & - \sum_{i=1}^{2}\frac{m_i^2}{16}\left[1 - \left(\frac{\alpha\kappa P_o}{\omega_i}\right)^2\right]\cos 2\omega_i t + j\frac{\alpha\kappa P_O}{8}\sum_{i=1}^{2}\frac{m_i^2}{\omega_i}\sin 2\omega_i t \\ & + \frac{m_1 m_2}{4}\left(1 + \frac{\alpha^2\kappa^2 P_o^2}{\omega_1\omega_2}\right)\cos(\omega_1 - \omega_2)t + \frac{m_1 m_2}{4}\left(1 - \frac{\alpha^2\kappa^2 P_o^2}{\omega_1\omega_2}\right)\cos(\omega_1 + \omega_2)t \\ & - j\frac{m_1 m_2}{8}\alpha\kappa P_o\left(\frac{1}{\omega_1} - \frac{1}{\omega_2}\right)\sin(\omega_1 - \omega_2)t + j\frac{m_1 m_2}{8}\alpha\kappa P_o\left(\frac{1}{\omega_1} + \frac{1}{\omega_2}\right)\sin(\omega_1 + \omega_2)t \Bigg\} \end{aligned} \tag{4.12}$$

The optical field $E_{out}(L,t)$ at the end of fiber of length L can be obtained from the inverse Fourier transform

$$E_{out}(L,t) = \frac{1}{2\pi}\int_{-\infty}^{\infty} d\omega E_S(\omega)\, H(\omega)\, e^{j\omega t} = \frac{1}{2\pi}\int_{-\infty}^{\infty} d\omega\, E_S(\omega)\, e^{j\beta(\omega)L}\, e^{j\omega t} \tag{4.13}$$

where $E_S(\omega)$ is the Fourier transform of $E_S(t)$. $H(\omega)$ is the transfer function of the optical fiber, and (neglecting attenuation) is given by $e^{j\beta(\omega)L}$ [71-73]. Expanding $\beta(\omega)$ in a Taylor series gives

$$\beta(\omega)L = \beta_0 L - \dot{\beta}(\omega - \omega_0)L - \ddot{\beta}(\omega - \omega_0)^2 L/2 \tag{4.14}$$

The first two terms in Eq. (4.14) can be ignored in our a.c. analysis since they represent constant phase and pure delay terms, respectively. The third term represents dispersion in the fiber which is related to the fiber dispersion coefficient D (typically expressed in units of ps/Km/nm) as

$$\ddot{\beta}(\omega_0) = -\frac{D\lambda^2}{2\pi c} \tag{4.15}$$

where λ is the source wavelength and c is the speed of the light. The evaluated $E_{out}(t)$ based on Eq. (4.13) is

$$E_{out}(L,t) = e^{-j\omega_0 t}\left\{1 + \sum_{i=1}^{2}\frac{m_i}{2}e^{-j\ddot{\beta}\frac{L}{2}\omega_i^2}\cos\omega_i t + j\frac{\alpha\kappa P_0}{2}\sum_{i=1}^{2}\frac{m_i}{\omega_i}e^{-j\ddot{\beta}\frac{L}{2}\omega_i^2}\sin\omega_i t\right.$$

$$- \sum_{i=1}^{2}\frac{m_i^2}{16}\left[1 - \left(\frac{\alpha\kappa P_o}{\omega_i}\right)^2\right]e^{-j\ddot{\beta}\frac{L}{2}4\omega_i^2}\cos 2\omega_i t + j\frac{\alpha\kappa P_0}{8}\sum_{i=1}^{2}\frac{m_i^2}{\omega_i}e^{-j\ddot{\beta}\frac{L}{2}4\omega_i^2}\sin 2\omega_i t$$

$$+ \frac{m_1 m_2}{4}\left(1 + \frac{\alpha^2\kappa^2 P_o^2}{\omega_1\omega_2}\right)e^{-j\ddot{\beta}\frac{L}{2}(\omega_1 - \omega_2)^2}\cos(\omega_1 - \omega_2)t$$

$$+ \frac{m_1 m_2}{4}\left(1 - \frac{\alpha^2\kappa^2 P_o^2}{\omega_1\omega_2}\right)e^{-j\ddot{\beta}\frac{L}{2}(\omega_1 + \omega_2)^2}\cos(\omega_1 + \omega_2)t$$

$$\left. - j\frac{m_1 m_2}{8}\alpha\kappa P_o\left(\frac{1}{\omega_1} - \frac{1}{\omega_2}\right)e^{-j\ddot{\beta}\frac{L}{2}(\omega_1 - \omega_2)^2}\sin(\omega_1 - \omega_2)t\right.$$

$$+ j\frac{m_1 m_2}{8}\alpha\kappa P_o\left(\frac{1}{\omega_1}+\frac{1}{\omega_2}\right)e^{-j\beta\frac{\ddot{L}}{2}(\omega_1+\omega_2)^2}\sin(\omega_1+\omega_2)t \qquad (4.16)$$

Then, the output intensity of the signal $P_{out}(t)$ is given by

$$P_{out}(L,t) = \left| E_{out}(L,t) \cdot E^{*}_{out}(L,t) \right|$$

$$= 1 + \sum_{i=1}^{2} m_i \cos\beta\frac{\ddot{L}}{2}\omega_i^2 \cos\omega_i t + \alpha\kappa P_O \sum_{i=1}^{2}\frac{m_i}{\omega_i}\sin\beta\frac{\ddot{L}}{2}\omega_i^2 \sin\omega_i t$$

$$+ \sum_{i=1}^{2}\frac{m_i^2}{8}\left[1-\left(\frac{\alpha\kappa P_o}{\omega_i}\right)^2\right]\cos\beta\frac{\ddot{L}}{2}2\omega_i^2\cos 2\omega_i t + \frac{\alpha\kappa P_O}{4}\sum_{i=1}^{2}\frac{m_i^2}{\omega_i}\sin\beta\frac{\ddot{L}}{2}2\omega_i^2\sin 2\omega_i t$$

$$+ \frac{m_1 m_2}{4}\left(1+\frac{\alpha^2\kappa^2 P_o^2}{\omega_1\omega_2}\right)\left[\cos\beta\frac{\ddot{L}}{2}(\omega_1^2-\omega_2^2)-\cos\beta\frac{\ddot{L}}{2}(\omega_1-\omega_2)^2\right]\cos(\omega_1-\omega_2)t$$

$$+ \frac{m_1 m_2}{4}\left(1-\frac{\alpha^2\kappa^2 P_o^2}{\omega_1\omega_2}\right)\left[\cos\beta\frac{\ddot{L}}{2}(\omega_1^2-\omega_1^2)-\cos\beta\frac{\ddot{L}}{2}(\omega_1+\omega_2)^2\right]\cos(\omega_1+\omega_2)t$$

$$+ \frac{m_1 m_2}{4}\alpha\kappa P_o\left[\left(\frac{1}{\omega_1}+\frac{1}{\omega_2}\right)\sin\beta\frac{\ddot{L}}{2}(\omega_1^2-\omega_1^2)+\left(\frac{1}{\omega_1}-\frac{1}{\omega_2}\right)\sin\beta\frac{\ddot{L}}{2}(\omega_1-\omega_2)^2\right]\sin(\omega_1-\omega_2)t$$

$$+ \frac{m_1 m_2}{4}\alpha\kappa P_o\left[\left(\frac{1}{\omega_1}+\frac{1}{\omega_2}\right)\sin\beta\frac{\ddot{L}}{2}(\omega_1+\omega_2)^2+\left(\frac{1}{\omega_1}-\frac{1}{\omega_2}\right)\sin\beta\frac{\ddot{L}}{2}(\omega_1^2-\omega_1^2)\right]\sin(\omega_1+\omega_2)t$$

(4.17)

As can be seen from Eq. (4.17), in addition to the fundamental frequency terms ω_1 and ω_2, harmonic distortion, $2\omega_1$ and $2\omega_2$ terms, and intermodulation distortion , $\omega_1 + \omega_2$ and $\omega_1 - \omega_2$ terms have been generated. Coefficients of these terms are dependent on modulation indices, the linewidth enhancement factor α, a constant related to physical structure of the laser cavity κ, average light output of the laser diode

P_0, angular frequency of each tone ω_i, fiber dispersion $\ddot{\beta}$, and fiber length L. The coefficients of nonlinear distortion terms (harmonic and intermodulation frequencies) are dependent on the frequencies ω_1 and ω_2 as well as on the above paramters. Details on these distortion terms are discussed in the next section.

To check for the correctness of Eq. (4.17), in the absence of fiber dispersion, set $\ddot{\beta}=0$. This makes all the terms in Eq. (4.17) zero except for the fundamental cosine terms and the second-order harmonic terms,

$$P_{out}(L,t) = 1 + \sum_{i=1}^{2} m_i \cos\omega_i t + \sum_{i=1}^{2} \frac{m_i^2}{8}\left[1 - \left(\frac{\alpha\kappa P_o}{\omega_i}\right)^2\right] \cos 2\omega_i t \tag{4.18}$$

Ideally, this equation should be the same as the P(t) of Eq. (4.9) consisting only of the fundamental terms. However, due to the series expansion of the $\sqrt{P(t)}$ there still exist the second order harmonic terms. Similarly, in the absence of laser chirp, $\alpha=0$, $P_{out}(t)$ should become P(t) of Eq. (4.9). However, due to the same reason as above we have both harmonic and intermodulation terms,

$$\begin{aligned} P_{out}(L,t) = {} & 1 + \sum_{i=1}^{2} m_i \cos\frac{\ddot{\beta}L}{2}\omega_i^2 \cos\omega_i t + \sum_{i=1}^{2} \frac{m_i^2}{8} \cos\frac{\ddot{\beta}L}{2}4\omega_i^2 \cos 2\omega_i t \\ & + \frac{m_1 m_2}{4}\left[\cos\frac{\ddot{\beta}L}{2}(\omega_1^2 - \omega_2^2) - \cos\frac{\ddot{\beta}L}{2}(\omega_1 - \omega_2)^2\right] \cos(\omega_1 - \omega_2)t \\ & + \frac{m_1 m_2}{4}\left[\cos\frac{\ddot{\beta}L}{2}(\omega_1^2 - \omega_1^2) - \cos\frac{\ddot{\beta}L}{2}(\omega_1 + \omega_2)^2\right] \cos(\omega_1 + \omega_2)t \end{aligned} \tag{4.19}$$

The distortion calculated from Eqs. (4.18) and (4.19), which is a result of the series expansion, is negligible compared to the distortion resulting from Eq. (4.17) where the dominant distortion term is the sin $2\omega_i t$ term.

4.4 Two-Tone Simulations

The two-tone simulation is based on the same mathematical formulation given in Section 4.3 without imposing the small-signal constraint. The simulation system block diagram for evaluating of the nonlinear distortion produced by the fiber dispersion and laser chirp is shown in Figure 4.1.a. Using the intensity modulated signal P(t), the chirped optical field $E_S(t)$ is obtained from the laser diode chirp model described in Section 4.2. $E_S(t)$ is then convolved with the time-domain dispersive response of the optical fiber to obtain the optical field $E_{out}(t)$ at the end of the fiber. The convolution operation is done in the frequency domain to speed up the calculation. (BOSS takes care of this process automatically.) The resulting output is then squared (multiplied by its complex conjugate) to obtain the output power $P_{out}(t)$. The frequency response of the fiber $H(\omega)$ is taken to be a unit (constant) amplitude response and $\beta(\omega)L$ phase response as specified in Eqs. (4.14) and (4.15). If the constant phase and pure delay term are ignored, $H(\omega)$ has simple quadratic phase response. Figure 4.1.b shows the fiber dispersion induced quadratic phase response $H(\omega) = e^{-j\ddot{\beta}(\omega - \omega_0)^2 L/2}$ where $\ddot{\beta} = -D\lambda^2/2\pi c$ as in Eq. (4.15), and λ=1550 nm, D= 20 ps/Km/nm, and $L=10^4$ Km. Such long fiber lengths are necessary to produce significant levels of harmonic and intermodulation products for comparison with the results obtained from the two-tone small signal analysis.

Figure 4.2.a shows the BOSS implementation of the two-tone simulation. In the simulation, the amplitudes of the two tones (given by cosine terms in the figure) having frequency of f_1=60 MHz and f_2=100 MHz are multiplied with their phase terms (give by sine terms in the figure). The power spectrum of the two-tone signal is shown in Figure 4.3.a. This signal is fed into the unit amplitude quadratic phase filter representing a fiber dispersion characteristic. The output at the end of the fiber is multiplied by its complex conjugate to obtain the optical intensity of the signal. Figure 4.2.b shows the simulation

parameters as well as the ith channel modulation index m_i, and the chirp parameter $\alpha\kappa P_0/4\pi$ of Eq. (4.15). Small values of m_1=0.005, m_2=0.005, $\alpha\kappa P_0 m_1/4\pi f_1$=0.035, and $\alpha\kappa P_0 m_2/4\pi f_2$=0.020 are chosen in order to compare with the results from the two-tone small signal analysis.

Table 5.1 Comparison between two-tone analysis and simulation results

Distortion Products	analysis $\alpha = 5$	simulation $\alpha = 5$	analysis $\alpha = 6$	simulation $\alpha = 6$
Harmonic Distortion				
$2HD(\omega_1)/\omega_1$	- 57.05 dBc	- 56.67 dBc	- 55.31 dBc	- 55.61 dBc
$2HD(\omega_2)/\omega_2$	- 52.21 dBc	- 53.49 dBc	- 50.41 dBc	- 51.55 dBc
Intermodulation Distortion				
$IMD(\omega_2-\omega_1)/\omega_1$	- 61.82 dBc	- 61.60 dBc	- 60.28 dBc	- 59.51 dBc
$IMD(\omega_2+\omega_1)/\omega_2$	- 48.61 dBc	- 49.59 dBc	- 46.89 dBc	- 47.91 dBc

The output spectrum of the two-tone simulation is shown in Figure 4.3.b. It shows two harmonic products at 120 MHz and 200 MHz and two intermodulation products at 40 MHz and 160 MHz, in addition to the two fundamental tones. Table 5.1 summarizes the simulation results as well as the numerical results obtained from Eq. (4.17) of the two-tone analysis. As can be seen in the table, there is good agreement between the simulation results and analytical results. Calculations and simulations are carried out for α=5 and 6 to study how the linewidth enhancement factor affect these distortion products. As seen in Table 5.1, by increasing α from 5 to 6 the harmonic and intermodulation distortion terms are increased as predicted by Eq. (4.17). The same applies to κ, P_0, m_i . (Note that their increase is proportional to m_i^2.) Calculations also show that the sin $(\omega_1\pm\omega_2)t$ terms are an order of magnitude larger than the cos $(\omega_1\pm\omega_2)t$ terms for the intermodulation distortion products. Of the sin $(\omega_1\pm\omega_2)t$ terms, calculations also show that the

$(\frac{1}{\omega_1}+\frac{1}{\omega_2})\sin\beta\frac{L}{2}(\omega_1+\omega_2)^2$ coefficient in $\sin(\omega_1+\omega_2)t$ is the largest and thus the leading coefficient. This makes the sum $(\omega_1+\omega_2)$ terms larger than the difference $(\omega_1-\omega_2)$ terms. Consequently, we can expect that the CSO will be higher at higher frequency channels than at lower frequency channels for multichannel systems. In the next section, this is verified experimentally.

4.5 CSO Degradation in Multichannel AM-SCM Systems

In this section experimental measurement results of the CSO degradation in multichannel systems is discussed. Also presented is the multichannel simulation results and a discussion of how close the simulation can predict the CSO performance of the multichannel system and how the CSO degradation limits the maximum link distance for the 1550 nm systems using the standard 1310 nm single-mode fibers.

4.5.1 Experiments

For experimental measurements of the nonlinear distortion produced by laser chirp and fiber dispersion, the setup shown in Figure 4.4 is used. This is basically the same setup as that of the system CNR measurements shown in Figure 2.1 except that the short fiber link is replaced by 1310 nm single-mode optical fibers of greater length. The fiber exhibited signal dispersion D of approximately 17 ps/Km/nm for 1550 nm sources. The chirp of our 1550 nm DFB laser was approximately 400 MHz/mA at I_{bias}=42 mA which is measured with the method described in [70].

Both the CSO and CTB were measured setting the per-channel modulation index constant and varying the fiber length from 1 Km to 37 Km. Up to 32 Km, for m=0.04, the CTB degradation was not significant and was less than - 60 dBc for all channels. However, the CSO increased sharply within 5 Km

and soon reached the - 60 dBc level for some channels. The CSO measurement results are plotted for fiber lengths from 1 Km to 37 Km in Figure 4.5.a. The dotted lines are logarithmic-curve-fitted lines to the measurement data. These measurement results are in reasonable agreement with previous experimental results of E. Bergmann [44] and numerical results of M. Phillips et al. [43] considering that their lasers exhibited higher chirp of 720 MHz/mA and 590 MHz/mA, respectively.

As shown in Figure 4.5.a, the CSO increases as the fiber length increases. This increase is particularly sharp for higher frequency channels. For example, the CSO at Channel 42 approaches - 60 dBc for a 5 Km length of fiber whereas the CSO of Channel 2 remains lower than - 65 dBc. This is because the contribution from the sum $(\omega_1+\omega_2)$ intermodulation product is larger than the difference $(\omega_1-\omega_2)$ intermodulation product as discussed in the preceding section. In Figure 4.5.b, the CSO is plotted together with the CNR for fiber lengths from 1 Km to 15.5 Km for the same setup. Per-channel modulation index m=0.058 is used to obtain the maximum CNR. One important thing to recognize in this figure is that the CSO degradation is faster than the CNR degradation. With typical CATV distribution system performance requirements, namely CSO < -55 dBc and CNR > 50 dB, the CSO of Channel 42 increases to -55 dBc at a fiber length of 9 Km whereas the CNR remains above 50 dB. This means that the maximum link distance is limited by the CSO performance and not by the CNR performance for 1550 nm systems utilizing standard 1310 nm single-mode fibers.

4.5.2 Multichannel CSO Simulations

We have extended the simulation to a 42 channel system and measured the CSO performance. In this simulation, actual laser diode physical parameters and bias conditions are required to make the absolute CSO measurement. However, actual physical parameters of laser diodes were not available to us. Thus, we had to resort published values of typical DFB lasers [70]. They are: the optical confinement factor Γ=0.5, the

quantum efficiency of intrinsic laser η=0.4, the linewidth enhancement factor α=5, the gain compression factor ε=2.5x10^{-23} m^3, the active volume of laser cavity V=4.5x10^{-16} m^3. In addition to these, the speed of light c=3x10^8 m/s, optical source wavelength λ=1.55x10^{-6} m, photon energy hf=1.32x10^{-19} J, fiber dispersion D=17 ps/Km/nm are used in the calculation. The unmodulated laser output power was P_o=2.5 mWatts at I_{bias}=45 mA (27 mA above the laser threshold current I_{th}=18 mA). The coefficient $\alpha\kappa P_o/4\pi$ results in a maximum chirp swing of approximately 10 GHz for typical CATV modulation signals. This number also corresponds to the equivalent chirp of 10 GHz/(I_{bias}-I_{th})=390 MHz/mA, which is approximately equal to the chirp of our laser.

Figure 4.6.a shows the output CATV spectrum of the simulation after 37 Km of fiber for m=0.04. As can be seen in the figure, the nonlinear distortion build up is more severe at higher frequency than at lower frequency owing to the larger contribution from the sum (ω_1+ω_2) terms than that of the difference (ω_1-ω_2) terms. The CSO is measured at 1.25 MHz below the video carriers for Channel 2, Channel 11, and Channel 42. An example of the CSO of Channel 42 at 336.0 MHz is shown in Figure 4.6.b. The simulation results for fiber length from 1 Km - 37 Km are shown in Figure 4.7.a. As predicted, Channel 42 gives the poorest CSO performance and Channel 2 gives the best CSO performance. Furthermore, as demonstrated by experiments the CSO sharply increases within 5 Km for all channels. For the purpose of comparison, both the CSO of Channel 42 from experiments and simulations are plotted on the same graph in Figure 4.7.b. There is good agreement for long fiber length, but for short fiber there is substantial difference. The reason for higher CSO in the experiment for short fiber length is due to the intrinsic CSO of the laser diode. Low CSO produced by the fiber dispersion and laser chirp for these length is masked by the intrinsic CSO of the laser diode.

The chirp of the laser diode can be lowered by using laser diodes with low α. Typical InGaAsP DFB laser diodes for 1550 nm systems have $\alpha\approx$5. However, with multiple-quantum-well DFB lasers, the α can

be made as low as $\alpha \approx 2$ - 3 [35, 36]. In order to study how decrease in α can improve the CSO performance, we have arbitrarily varied α from 2 to 5 in the simulation. Results of the CSO measurement for these α are plotted in Figure 4.8. As predicted, the figure illustrates that decrease in α indeed improves the CSO performance. However, the improvement is only 4 dB. This means that even with low chirp multiple-quantum-well laser diodes, only a few dB CSO improvement can be obtained.

4.6 Summary

In this chapter, the nonlinear distortion produced by the combined effect of the laser diode chirp and fiber dispersion is discussed. An analytic expression which describes the second-harmonic and second-order-intermodulation distortion generating mechanism is derived on the basis of small-signal two-tone analysis. Two-tone simulation of the second-harmonic and second-order-intermodulation is also performed to cross-check with the results from the analysis. The simulation results are in good agreement with the analytical results. We have performed multichannel experiments and simulations and studied the CSO degradation due to laser chirp and fiber dispersion. The results indicate that for 1550 nm systems using the standard 1310 nm dispersion-minimized fiber, the maximum link distance is limited by the CSO performance and not by the CNR performance, and multichannel simulations can reasonably predict the CSO performance provided that the actual laser diode physical constants are known.

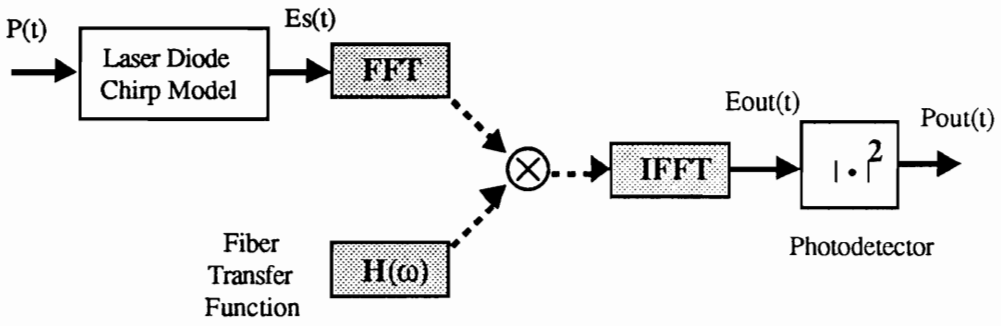

Figure 4.1.a Simulation system block diagram for evaluation of the nonlinear distortion produced by the fiber dispersion and laser chirp

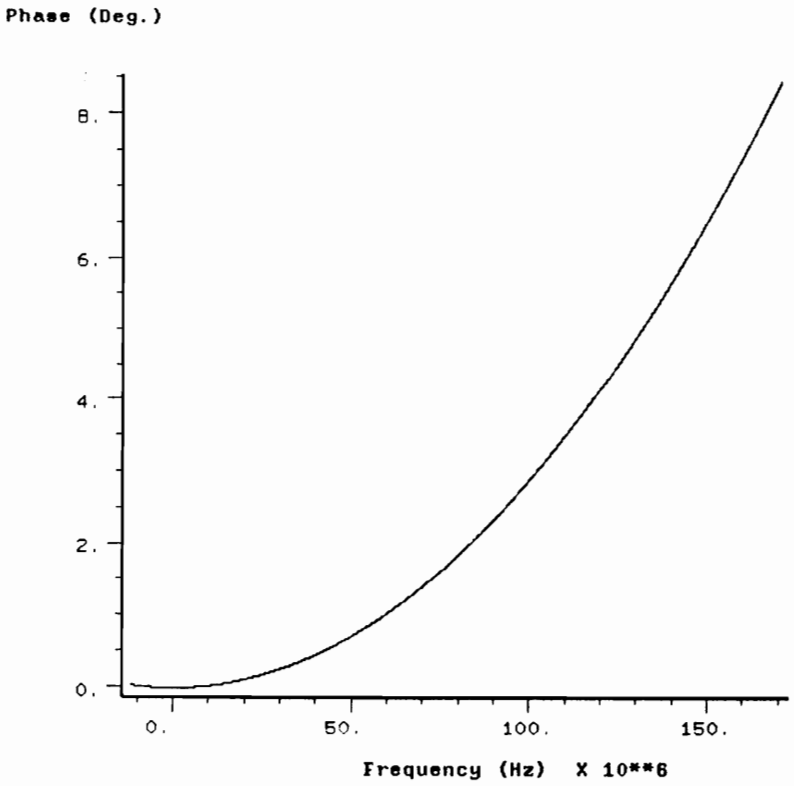

Figure 4.1.b Fiber dispersion induced quadratic phase response of $H(\omega) = e^{-j\ddot{\beta}(\omega - \omega_0)^2 L/2}$.

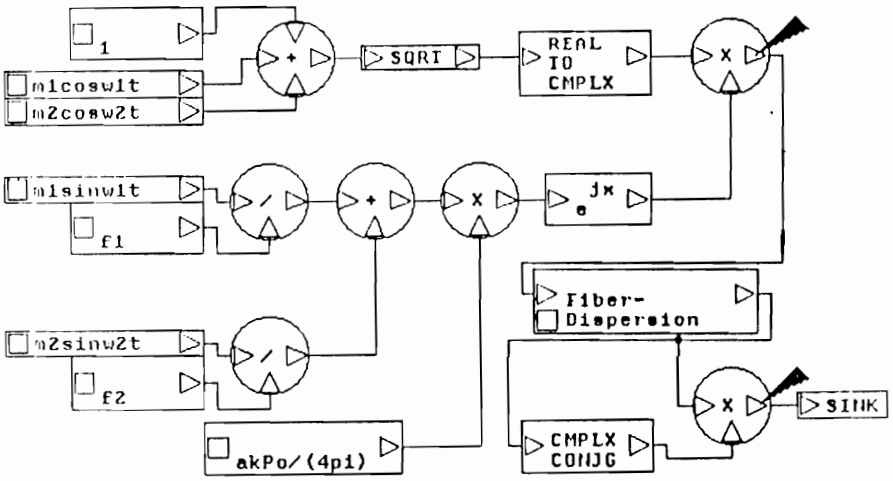

Figure 4.2.a BOSS implementation of the nonlinear distortion induced by fiber dispersion and laser chirp simulation system

Simulation Parameters KB

STOP-TIME	::5.0e-5
DT	::1.0e-9
NUMBER OF POINTS FOR FFT PROCESSING	::8192
TIME DOMAIN XFER OUTPUT FILE	::DUA0:[USERS.CJ]impulse-response;0
FREQ DOMAIN XFER OUTPUT FILE	::DUA0:[USERS.CJ]freq-response;0
PHASE DIST AT BAND EDGE FREQ (DEG)	::1.038
AMPLITUDE DIST AT BAND EDGE FREQ (DB)	::1.0e-5
BAND EDGE FREQUENCY (HZ)	::6.0e7
CARRIER FREQUENCY (HZ)	::0
AKPO/(4PI)	::4.187e8
SIN-PHASE (PI/2)	::1.5708
COS-PHASE (0.0)	::0
M1	::5.0E-3
M1	::5.0E-3
M2	::5.0E-3
F2	::6.0e7
F1	::1.0e8
EXIT	

Figure 4.2.b BOSS simulation parameters

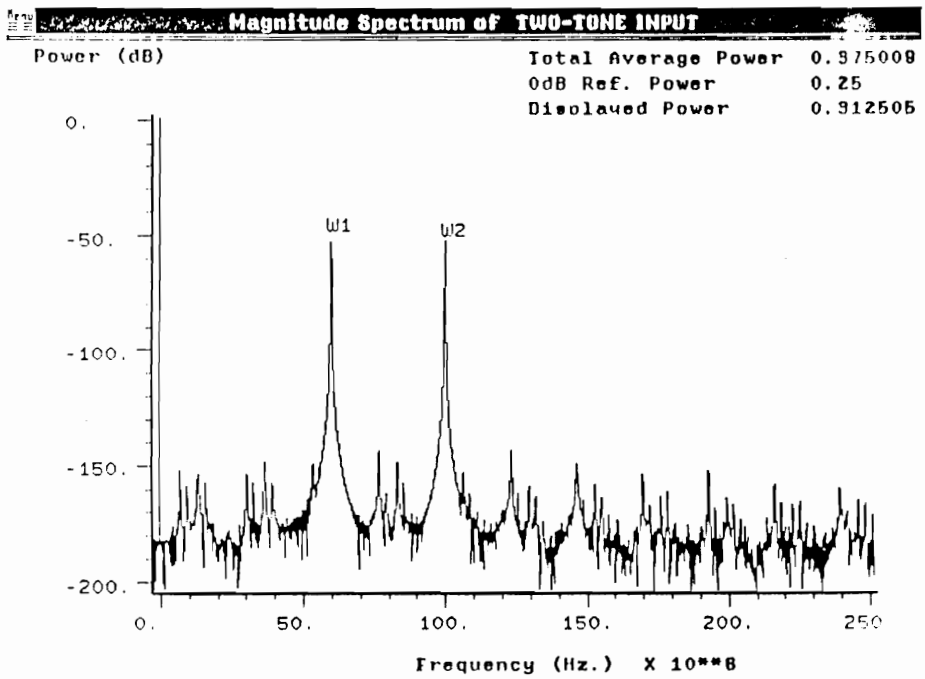

Figure 4.3.a BOSS simulation input showing two frequency components at 60 MH and 100 MHz.

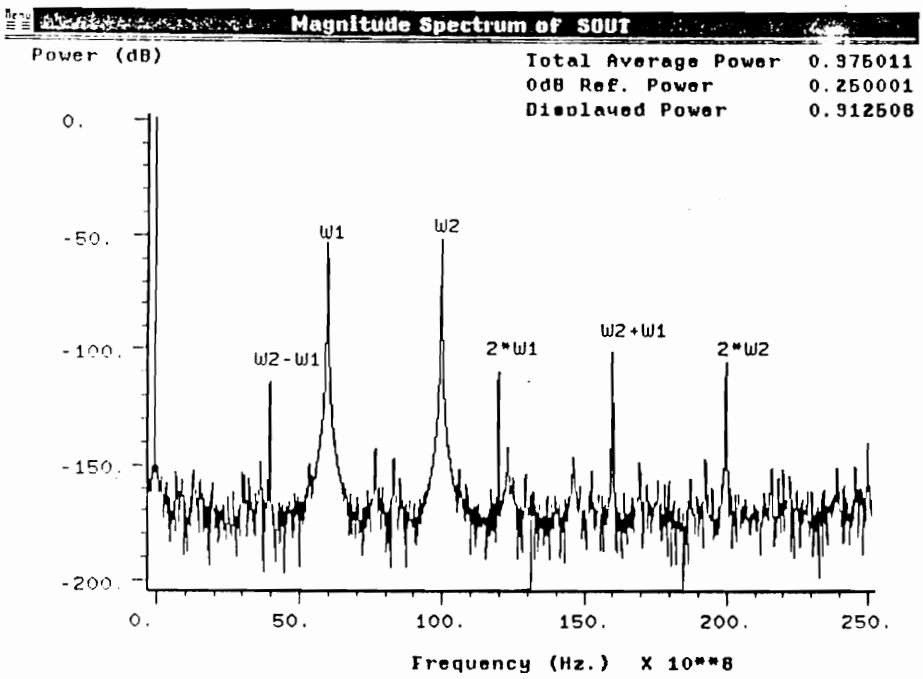

Figure 4.3.b Two-tone simulation output showing the harminic distortion at 120 MHz and 200 MHz and the intermodulation distortion at 40 MHz and 160 MHz

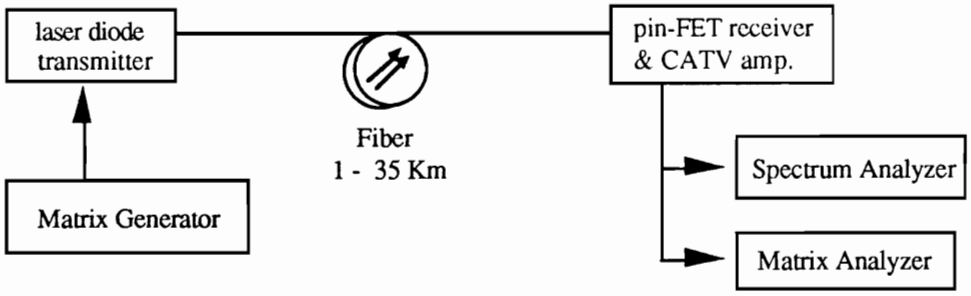

Figure 4.4 Experimental setup to measure CSO degradation due to fiber dispersion and laser chirp

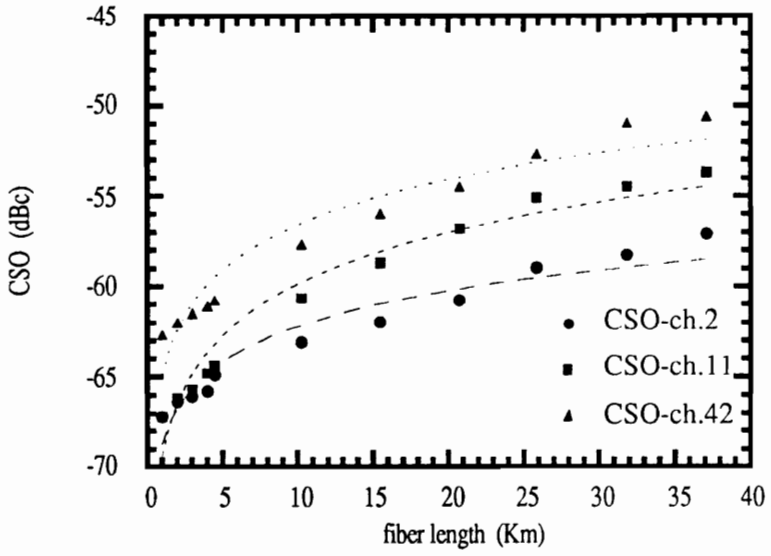

(a)

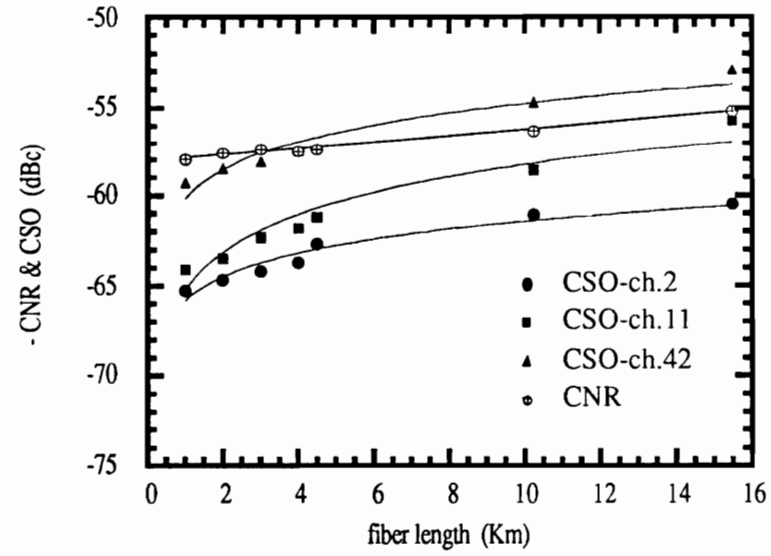

(b)

Figure 4.5 Experimentally measured CSO results versus the fiber length for Channel 2, Channel 11, and Channel 42 for (a) m=0.04 and (b) m=0.058.

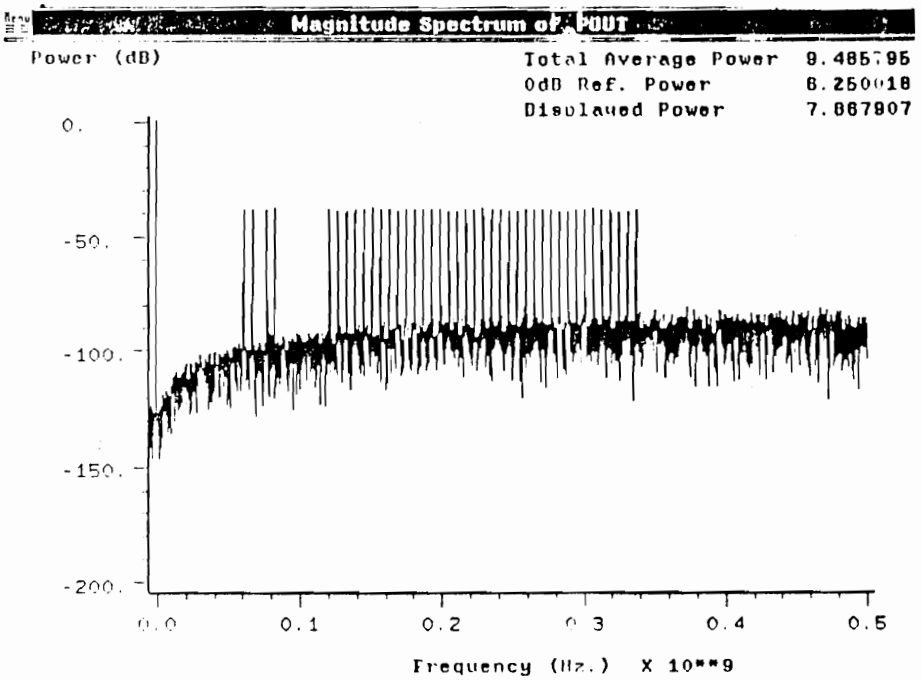

Figure 4.6.a Output spectrum of the simulation showing the nonlinear distortion build-up across the CATV frequency band

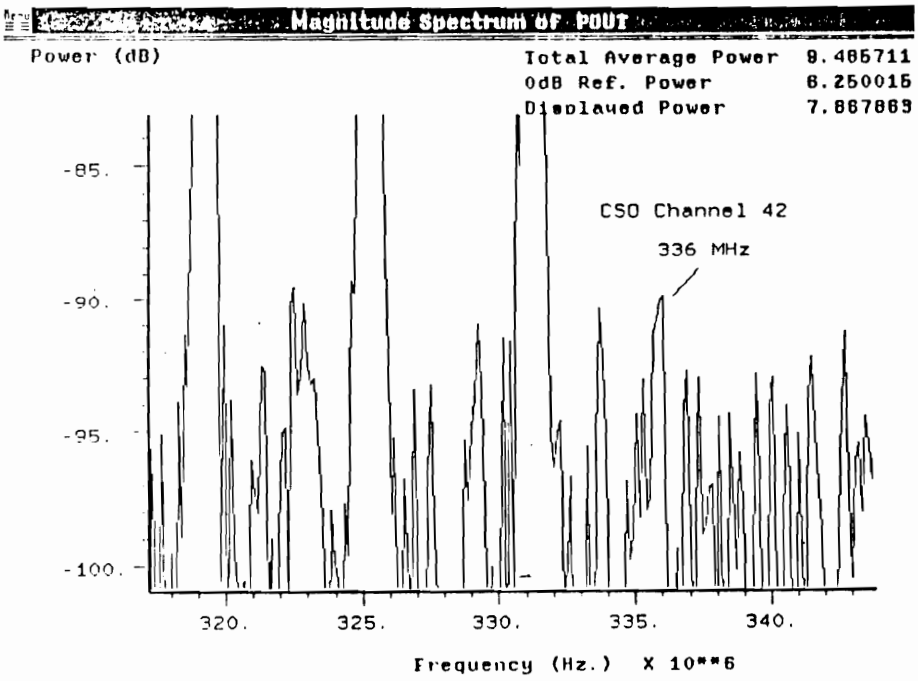

Figure 4.6.b Output spectrum of the simulation results showing the CSO of Channel 42 at 336.0 MHz

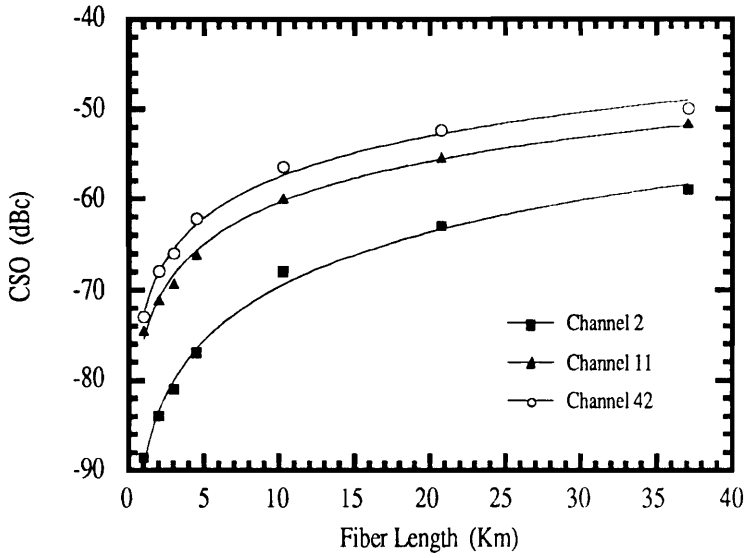

Figure 4.7.a Simulation results of the CSO versus the fiber length for Channel 2, Channel 11, and Channel 42

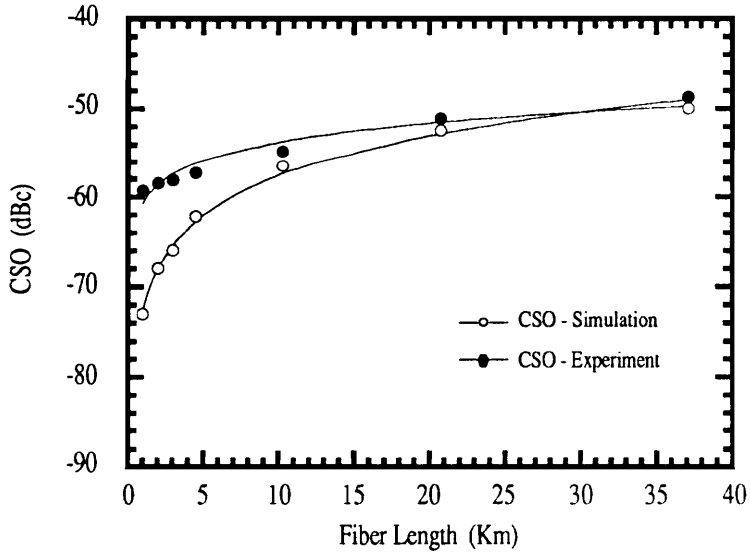

Figure 4.7.b. Comparison between simulation and experimental CSO measurements at Channel 42

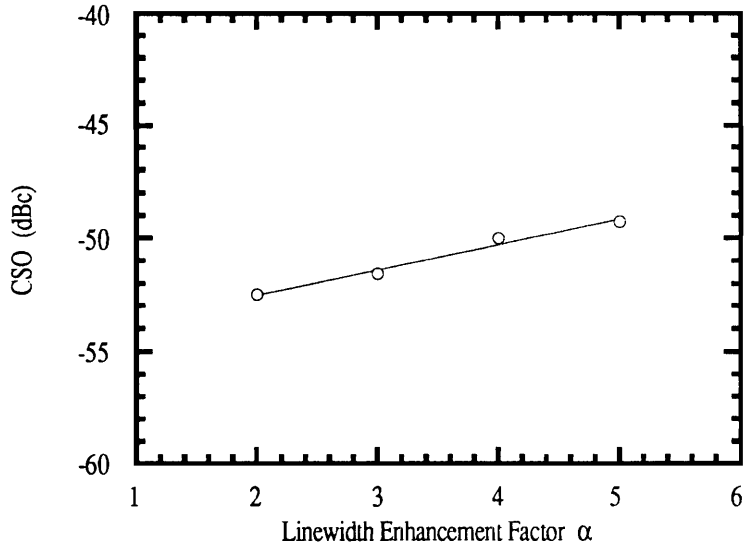

Figure 4.8 The Channel 42 CSO dependence on linewidth enhancement factor at fiber length of 20 Km.

CHAPTER 5.

PRACTICAL PERFORMANCE LIMITS AND SYSTEM CAPACITY

In Chapter 3, channel capacity limited by the nonlinear distortion produced by the laser threshold characteristic was evaluated. It was also noted that the channel capacity is inversely related to the received optical power, thus, system power margins. In this chapter, overall system capacity, which collectively refers to the channel capacity and system power margin, is studied for practical systems. First, basic system performance, and the sensitivity and limits of this performance are discussed. Second, overall system capacity is described showing the inverse relationship between the channel capacity and power margins. Third, analysis of practical channel capacity limits is also presented to provide assessment of the achievable channel capacity as the device technology advances. Finally, improvements in system power margins and limitations associated with use of erbium-doped fiber amplifiers in AM SCM systems are described.

5.1 Review of System Performance

As studied Chapter 2 and 3, system performance is given in terms of the nonlinear distortion (CSO and CTB) and noise (CNR). Figures 5.1 and 5.2 summarize the nonlinear distortion and CNR performance of fiber optic multichannel AM SCM systems. Figure 5.1 illustrates typical CSO and CTB performance

degradation due to over-modulation. When laser diodes are over-modulated, higher channel capacity or system power margins (due to higher CNR) can be obtained. However, as shown in Figure 5.1 that over-modulation introduces additional CSO and CTB due to the laser threshold characteristic. Therefore, the increase in channel capacity or power margin is fundamentally limited by the laser threshold nonlinear characteristic.

For the system noise performance, as mentioned in Chapter 2, there are three main noise degrading mechanisms. They are laser RIN, photodetector shot noise, and receiver thermal noise. Their contribution to system noise is plotted in Figure 5.2 together with the overall system CNR. As can be seen in the figure, the relative contributions from these are different in magnitude at different power levels. Therefore, systems operate in different noise limited regimes at different power levels. For example, for supertrunking systems which typically require a CNR of 55 dB, $P_0 \approx 0$ dBm, photodetector shot noise is the dominant noise. For local distribution systems which require a CNR of 48 dB, $P_0 \approx -8$ dBm, receiver thermal noise is the dominant noise. It should also be noted from Figure 5.2 that the maximum attainable CNR is limited by the laser RIN performance. Thus, to achieve high power margin systems laser diodes with low RIN are needed.

5.2 Sensitivity Analysis

5.2.1 Laser Threshold Limited Channel Capacity

On the basis of the nonlinear distortion requirements, namely the CSO and CTB, we can determine the maximum rms modulation index μ. For example, if both the CSO and CTB requirements are chosen to be less than -65 dBc, then $\mu < 0.295$ as can be seen in Figure 5.1. Since the maximum allowable μ is now fixed, we can then calculate the number of channels N and the modulation index per channel m by using

$\mu=m\sqrt{(N/2)}$. The result of this calculation is shown in Figure 5.3 where N is plotted as a function of m for μ ranging from 0.28 to 0.33, which corresponds to the CSO requirements from -55 dBc to -67 dBc, according to Figure 5.1. It follows that for fixed μ, the number of channels is inversely proportional to m^2. This then limits the number of channels for a fixed modulation index per channel, or conversely, as illustrated in Figure 5.3. This also indicates that the channel capacity is inversely related to the system power margin because the CNR is directly related to m^2, as will be discussed in the next section. It should also be noted that the relationship between N and m assumes that the CSO and CTB is not significantly affected when the number of channels is increased. This assumption is supported by our experimental observations and simulations and prior theory [10].

5.2.2 System Carrier-to-Noise Ratio

The CNR in Figure 5.2 is for a fixed value of per-channel modulation index m. In this section how the CNR performance is affected by changes in m and by changes in the other system noise components is studied and the consequence of these changes to the overall system capacity and performance is discussed.

To study the CNR dependence on m, the CNR is calculated as a function of the received optical power for various values of m (0.04 - 0.06), and the results are plotted in Figure 5.4. RIN=-155 dB/Hz and $\sqrt{<i_{th}^2>}$=7 pA/$\sqrt{\text{Hz}}$ are used for this calculation. As can be seen in Figure 5.4, increasing m increases the CNR thereby increasing the overall optical power margin. However, as discussed in Section 5.2.1, as m is increased the maximum N must be decreased to maintain CSO and CTB at acceptable levels. Therefore, for a fixed number of channels, there is a maximum permissible m if the CSO and CTB requirements are to be met. Conversely, there is a maximum permissible number of channels for a fixed m. Therefore, we see that the number of channels and available optical power margin are inversely related to each other via m.

It is interesting to note from Figure 5.4 that the relative increase in the optical power margins due to an increase in m from 0.04 to 0.06 is larger for a high CNR requirement than for a low CNR requirement. For example, at a CNR requirement of 55 dB the relative gain in available optical power margin is approximately 5 dB where as at a CNR requirement of 48 dB it is only approximately 2.5 dB. This implies that the relationship between the modulation index per channel and the number of channels is more sensitive for supertrunking systems, which typically require a high CNR, than for local distribution systems which require a relatively lower CNR. This also means that the trade-off between the number of channels and the optical power margin is more sensitive for supertrunking systems than for local distribution systems.

Another way of increasing the optical power margin is by decreasing the receiver thermal noise. To illustrate this, the CNR is calculated as a function of the received optical power for various values of the receiver thermal current i_{th} (5 pA/$\sqrt{Hz}$ - 9 pA/$\sqrt{Hz}$), and the results are plotted in Figure 5.5. RIN=-155 dB/Hz, and m=0.04 are used for this calculation. As can be seen in Figure 5.5, decreasing i_{th} generally increases the CNR thereby increasing the overall system power margin. The increase in the CNR is particularly large for low received optical power levels. For relatively large received optical power levels, the decrease in i_{th} has little effect since the CNR is determined primarily by the shot noise and RIN. For example, at P_O=-10 dBm the CNR improves by 3 dB by decreasing the $\sqrt{\langle i_{th}^2 \rangle}$ from 9 pA/$\sqrt{Hz}$ to 5 pA/$\sqrt{Hz}$, whereas at P_O=0 dBm the corresponding CNR improvement is less than 1 dB. This indicates that the use of a low thermal noise receiver is more critical for local distribution systems than for supertrunking systems.

We have indicated in Section 5.1 that the maximum attainable CNR is limited by the laser diode RIN. Although the RIN performance has no effect on overall system power margin as long as it provides a sufficiently high CNR, it is of importance for systems employing cascaded optical amplifiers which require

a high CNR at the transmitter. For this reason, the CNR dependence on RIN performance is studied by calculating the CNR for different laser diode RIN values (-152 dB/Hz - 156 dB/Hz). The results are shown in Figure 5.6. $\sqrt{<i_{th}^2>}$ of 7 pA/$\sqrt{Hz}$ and m=0.04 are used for the calculation. -152 dB/Hz to -156 dB/Hz represents nominal RIN of typical low noise DFB lasers. RIN=-160 dB/Hz represents a practical performance limit of RIN for current semiconductor laser technology. As can be seen in Figure 5.6, decreasing RIN improves the CNR particularly at high power levels. At low optical power levels, the CNR improvements due to decrease in RIN is almost negligible. This indicates that the use of a low RIN laser diode is more critical for supertrunking systems than for local distribution systems.

5.3 System Capacity

In this section, a study of system capacity is presented. It has been suggested in Chapter 3 that because channel capacity is a function of the received optical power, it must be specified together with the available system power margin to properly describe the system capacity. Accordingly, the system capacity in this chapter collectively refers to the channel capacity and power margin. As discussed in Section 5.2.2, the channel capacity is inversely proportional to m^2, whereas the CNR is proportional to m^2. These dependences give an inverse relationship between the channel capacity and the available system power margin.

According to Figure 5.2, typical supertrunking systems having RIN=-155 dB/Hz and $\sqrt{<i_{th}^2>}$=7 pA/$\sqrt{Hz}$ with a 55 dB CNR requirement operate in the shot noise limited regime. Similarly, typical local distribution systems with a 48 dB CNR requirement operate in the thermal noise limited regime. When these shot and thermal noise limits are considered, the calculation for optical power margin becomes simple because the equation for received optical power can be expressed in terms of m, and correspondingly, the

dependence of the optical power margin on m can be obtained. The optical power margin is determined by assuming a finite output power at the transmitter and by specifying the minimum CNR requirement at the receiver.

From Eq. (2.1) the received optical power P_r for the shot noise limit, ignoring laser RIN and receiver thermal noise, can be written as

$$P_r = \frac{4qB\,(CNR)}{m^2 \Re} \quad . \tag{5.1}$$

Similarly for the thermal noise limit, ignoring laser RIN and photodetector shot noise, P_r can be written as

$$P_r = \sqrt{\frac{2\langle i_{th}^2 \rangle B\,(CNR)}{m^2 \Re^2}} \quad . \tag{5.2}$$

Once the minimum received optical power levels P_r are calculated with given CNR requirements, the optical power margins can be obtained from the difference of the light output power (in dBm) at the transmitter P_t and P_r. The calculated power margins for supertrunking systems with CNR=55 dB and for local distributions system with CNR=48 dB are plotted in the right ordinates of Figures 5.7.a and 5.7.b. P_t of 5 dBm (~3 mwatt) is assumed for the calculations. To illustrate the inverse relationship between the channel capacity and the system power margin, the number of channels N is also plotted as a function of m using the left ordinates of the same figures. μ=0.295 (CSO and CTB < -65 dBc) and μ=0.31 (CSO and CTB < -60 dBc) are used for nonlinear distortion requirements of supertrunking and local distribution systems, respectively. As can be seen from these figures, while the optical power margin increases for larger m, the maximum N decreases, thus, demonstrating their inverse relationship.

It should be noted that the calculated channel capacity and power margin are based on the shot and thermal noise limits. As can be seen from Figure 5.2, at a CNR=48 dB although the system with RIN of -155 dB/Hz and $\sqrt{<i_{th}^2>}$=7 pA/$\sqrt{Hz}$ operates in the thermal noise limited regime, it is also influenced by the photodetector shot noise. Similarly, at a CNR=55 dB although the system operates in the shot noise limited regime, it is also influenced by the laser RIN and receiver thermal noise. Observations of the CNR and individual noise contributions in Figure 5.2 shows that typically there is a few decibels difference between the measured or calculated CNR and that caused by the limiting noise source alone. Accordingly, the calculated power margins in this section are a few dB larger and the channel capacity is somewhat higher than those of actual systems. Calculations of the channel capacity of practical systems which take into consideration of the RIN and thermal noise are presented in the next section.

5.4 Channel Capacity of Practical Systems

In Section 5.3, the channel capacity and power margin based on theoretical shot and thermal noise limits are discussed. In this section, channel capacity of practical systems limited by the laser diode RIN, the receiver thermal noise, and the photodetector shot noise are calculated. It should be noted that since the channel capacity is calculated as a function of the received optical power, the available optical power margin can be deduced if the output optical power at the transmitter is known.

Channel capacities are calculated with respect to the received optical power for the system performance requirements of CATV supertrunking and distribution systems using Eq. (5.3), which is obtained by combining $\mu^2=m^2(N/2)$ and the system CNR equation of Eq. (2.1),

$$N = \frac{\Re^2 P_O^2}{CNR \bullet (RIN \bullet B \bullet \Re^2 P_O^2 + 2q \bullet B \bullet \Re P_O + \langle i_{th}^2 \rangle \bullet B)} \mu^2 \qquad (5.3)$$

Figure 5.8.a shows N as a function of P_O for typical supertrunking system requirements of CNR=55 dB, CSO=-65 dBc, and CTB=-65 dBc (μ=0.295). Figure 5.8.b shows N as a function of P_O for typical distribution system requirements of CNR=48 dB, CSO=-60 dBc, and CTB=-60 dBc (μ=0.31). Results are given for a range of values of the laser diode RIN and receiver thermal noise. A RIN=-160 dB/Hz and $\sqrt{\langle i_{th}^2 \rangle}$=5 pA/$\sqrt{\text{Hz}}$ represent the performance limit of current device technology. A RIN=-155 dB/Hz and $\sqrt{\langle i_{th}^2 \rangle}$=7 pA/$\sqrt{\text{Hz}}$ represent noise performance of high quality devices such as those of the analog DFB laser and CATV *pin* photodiode receiver module that are used in our experiments. Comparison with previous studies [37, 38] shows that our analysis gives higher estimates of channel capacity. For example, as can be seen in Figure 5.8.a for P_O=0 dBm approximately 95 channels can be transmitted for RIN=-155 dB/Hz and $\sqrt{\langle i_{th}^2 \rangle}$= 7 pA/$\sqrt{\text{Hz}}$ with a CNR requirement of 55 dB. This is about 10 channels higher than previously reported [38] theoretical limits. Thus, the calculation based on practical system performance considered here gives higher channel capacity than previous estimates based on a theoretical performance limit. The reason for this seeming discrepancy is that previous theoretical limits [37, 38] treated NLD as a system noise component, which is not consistent with normal CATV practice [14].

Present "fiber backbone" CATV networks [74] require 80 channels for trunking applications and plan 150 channels for local distribution for near future systems. Results of calculations shown in Figure 5.8.b indicate that 150 channels can be accommodated with RIN=-155 dB/Hz and $\sqrt{\langle i_{th}^2 \rangle}$= 7 pA/$\sqrt{\text{Hz}}$ at P_O=-6 dBm. If we assume 5 dBm of output optical power at the transmitter, the system can provide 150 channels with an optical power margin of 11 dB. Assuming a 0.5 dB/km fiber loss, the link distance can be as large as 20 km, which is more than adequate for typical local distribution. However, as can be seen in Figure 5.8.a with the supertrunking system requirements and the same output optical power, RIN, and receiver

thermal noise, the system can only accommodate 80 channels with 6 dB of power margin, which translates to 12 km of link distance. This is not an adequate distance for most supertrunking applications. Improvement in RIN to -160 dB/Hz provides only 2 dB gain in the system power margin. Therefore, lightwave AM SCM systems can provide sufficient system capacity for typical CATV distribution networks, but for supertrunking systems it is limited both in the number of channels and system power margins that may be obtained.

5.5 Erbium-Doped Fiber Amplified AM SCM Systems

As has been discussed in Section 5.4, supertrunking systems have limited power margins for today's DFB lasers, whose typical output power is limited to about 5 mwatt. Also, for the currently envisioned passive star fiber-in-the-loop architecture of telecommunication networks, where the signal power from the local distribution center is shared among the subscribers, the signal power at the subscribers are maintained by in-line amplifiers. In either system, erbium-doped fiber amplifiers (EDFAs) can provide additional power margins through optical amplification. EDFAs have low amplification noise figure (typically in the order of 5 dB), low coupling loss (typically less than 0.5 dB) due to the same physical dimension of fibers, and can provide high saturation power, in the order of tens of mwatt, without significantly distorting the signal.

EDFAs have already been used successfully as in-line or post amplifiers in fiber optic AM SCM systems to obtain the additional power margins [39-41]. We have performed a similar experiment with an EDFA from BT&D (model EFA6000). Figure 5.9.a shows the experimental setup for multichannel AM SCM video systems with an EDFA, and Figure 5.9.b shows the configuration of the BT&D model EFA6000. The experimental setup shown in Figure 5.9.a is basically the same as previous setups in

Chapter 2 and Chapter 3 except for the EDFA and optical isolator. In this experiment, the EDFA is used as a high power post-amplifier, where the intensity modulated multichannel AM SCM signal is amplified. An optical isolator is placed in front of the EDFA to suppress optical reflections from fiber ends.

In the BT&D EDFA unit, as shown in Figure 5.9.b, the 1550 nm AM SCM signal from the Port 1 is multiplexed together with 1480 nm optical pump signal and fed into the fiber amplifier section. Within this section, the pump signal is absorbed which gives the population inversion necessary for stimulated emission of photons having the same wavelength of the signal to be amplified. Photons emitted by the EDFA is proportional to the signal, thus, effectively amplifying the signal. The pump lasers shown in Figure 5.9.b are 1480 nm multiple-quantum-well lasers. Each of these lasers launches 30 mwatt of optical power. As can be seen in Figure 5.9.b, the EDFA is a symmetrical device meaning that the input and output ports can be exchanged. Another thing to note is that pumping can be provided from either co- and counter-propagating directions or from both directions. To obtain the maximum output power, the EDFA is operated in a gain-saturated region. The gain profile of the BT&D EDFA is shown in Figure 5.10. The figure shows the gain profile for both pumping directions, namely counter- and co-propagating schemes. As can be seen in the plot, maximum output power of 13 - 14 dBm can be obtained under gain compression operation at which point the EDFA provides 13 dB of signal gain.

Figure 5.11 shows the CNR measurement results with an EDFA in the system versus the optical power at the receiver. The EDFA gives a larger transmitter power, and since it does not significantly degrade the minimum required receiver power, this results in an increase in the power margin. As can be seen in the figure, with the EDFA the output power 10 dBm was measured with the CNR of 53 dB for either co-directional or two-directional pumping. It appears that several additional decibels of output power is possible, but not measured because the photodetector might be damaged at such power levels. When the EDFA is pumped in counter-propagation direction, the CNR is decreased approximately by 5 dB.

Comparing the CNR measurement for systems with and without EDFA shows that EDFA in the system increases the relative noise floor by 5 dB. At such high output power levels, this increase in noise is mainly due to the beating of amplified spontaneous emission noise with the signal [39, 41]. Therefore, the accumulated noise build-up in cascaded EDFAs limits the total number of subscribers that may be served by passive star-networks whose power budgets are maintained by in-line EDFAs. For supertrunking systems, 10 dB gain of the EDFA translates to 20 Km link distances in addition to the original power margins, which provides an additional 20 Km link distance assuming 0.5 dB/Km fiber loss. However, due to the CSO degradation as discussed in Chapter 4, the dispersion-shifted fiber, whose minimum dispersion wavelength is at 1550 nm source wavelength, must be used.

5.6 Summary

Practical lightwave AM SCM system capacity for multichannel video supertrunking and local distribution systems is studied based on conventional CATV performance requirements. Unlike previous studies of channel capacity based on a theoretical performance limit, practical system performance including the laser diode RIN and the receiver thermal noise in addition to photodetector shot noise and laser diode threshold limited performance is considered. It is shown that the channel capacity alone does not provide a meaningful measure of the overall system capacity. Rather, channel capacity and the available system power margin should be specified together. For example, the calculations show that CATV local distribution systems can accommodate 150 channels with 11 dB power margins, and supertrunking systems can accommodate 80 channels with 6 dB power margins with a laser output power of 3 mwatt and a RIN of -155 dB/Hz and a receiver thermal noise of 7 pA/$\sqrt{\text{Hz}}$. For supertrunking system requirements, it is about 80 channels with 6 dB power margin. The analysis also shows that the trade-off between number of channels and the system power margin is more sensitive for supertrunking systems than local distribution

systems. Also studied is 1550 nm optically amplified systems operating on the 1310 nm single-mode platform of telecommunication networks. It is shown that the accumulated noise from cascaded EDFAs limits total subscribers where star-network power budgets are maintained by in-line EDFAs.

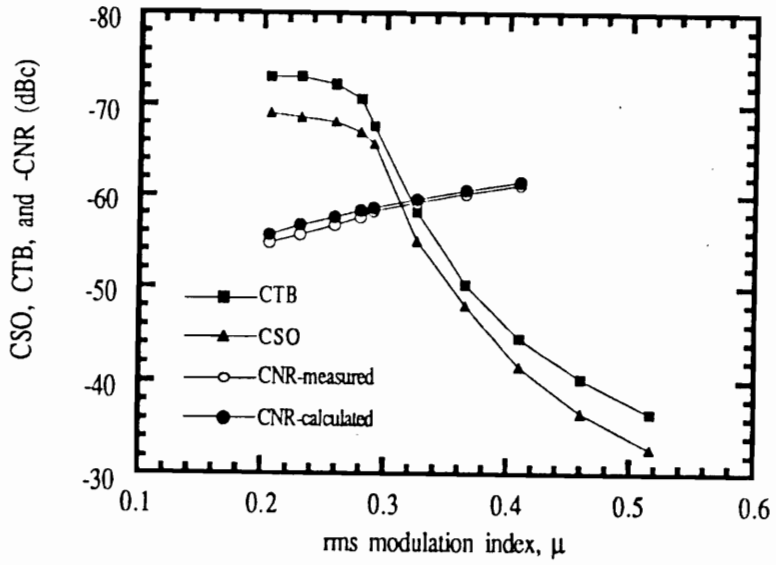

Figure 5.1 Measured CNR, CSO, and CTB and calculated CNR versus rms modulation index μ with N=42 channels, P_O=0 dBm, RIN=-155 dB/Hz, $\sqrt{\langle i_{th}^2 \rangle}$=7 pA/$\sqrt{\text{Hz}}$, and $\Re$=0.93 A/W.

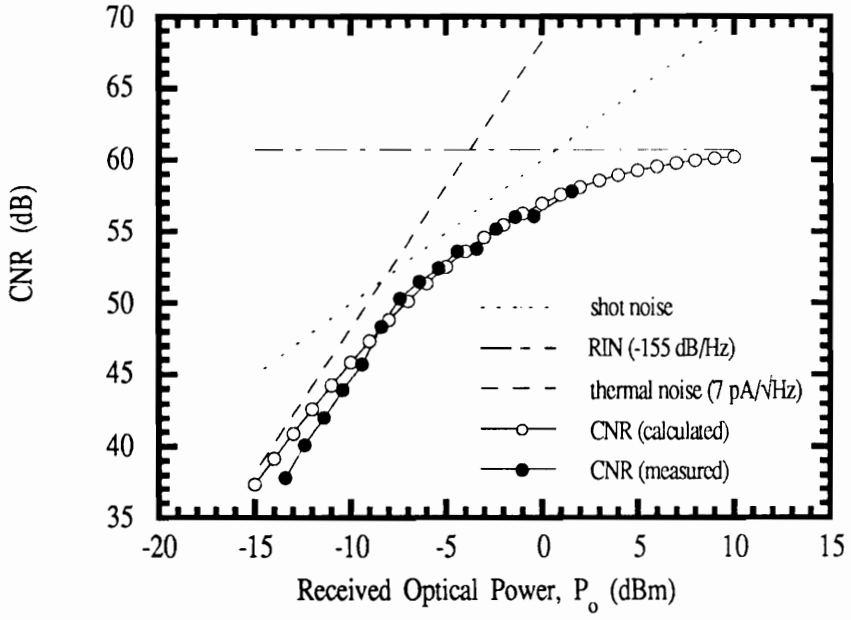

Figure 5.2 CNR as a function of the received optical power with RIN=-155 dB/Hz, $\sqrt{\langle i_{th}^2 \rangle}$= 7 pA/√Hz, and $\Re$=0.93 A/W.

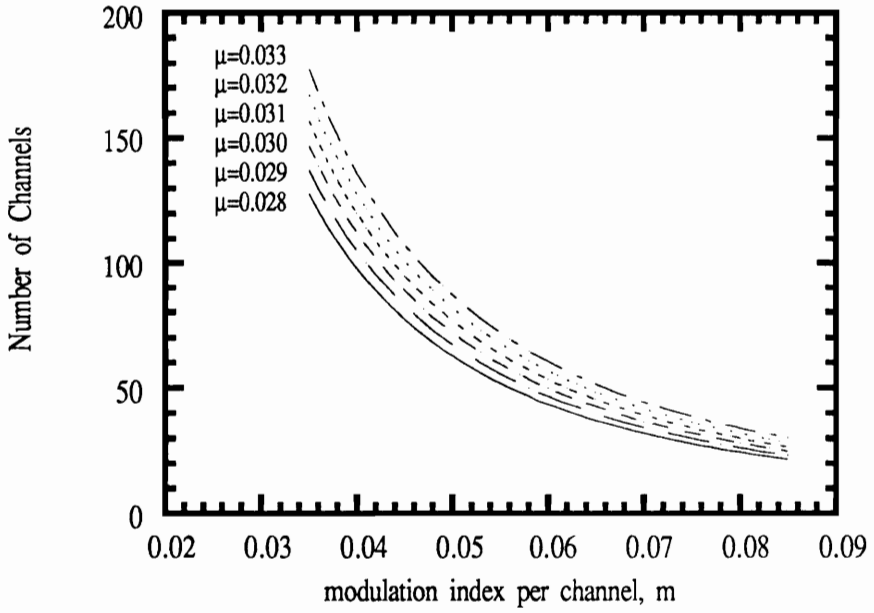

Figure 5.3 Number of channels N versus modulation index per channel m for μ=0.28 to 0.33.

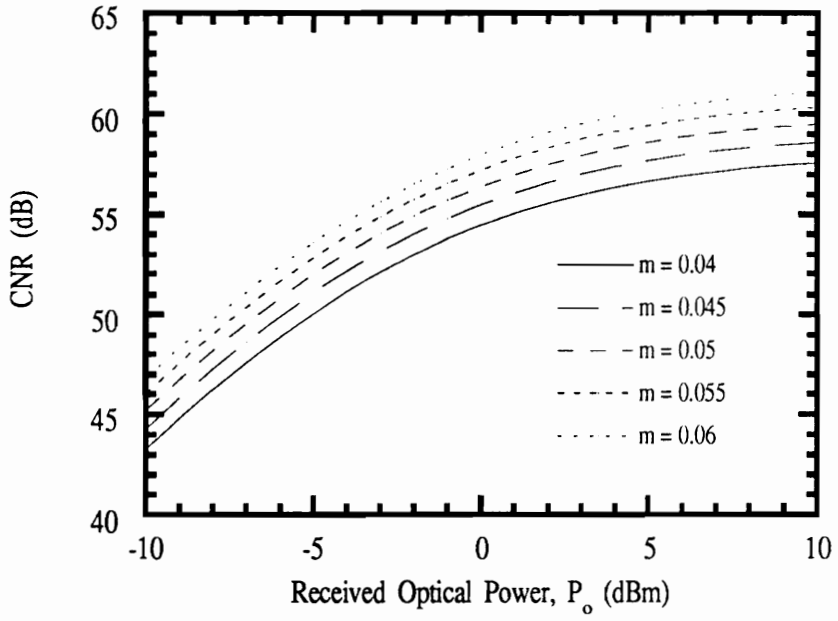

Figure 5.4 CNR as a function of the received optical power for m=0.04, 0.045, 0.05, 0.055, and 0.06 with $\sqrt{\langle i_{th}^2 \rangle}$=7 pA/$\sqrt{\text{Hz}}$, RIN=-155 dB/Hz, and $\Re$=0.93 A/W.

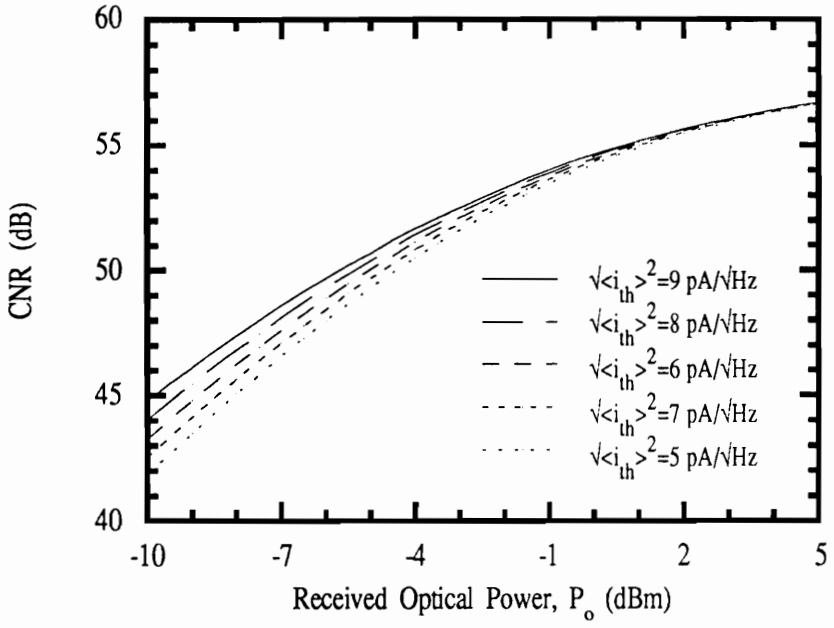

Figure 5.5 CNR as a function of the received optical power for $\sqrt{<i_{th}^2>}$=5,6,7,8 and 9 pA/√Hz, with m=0.04, RIN=-155 dB/Hz, and $\Re$=0.93 A/W.

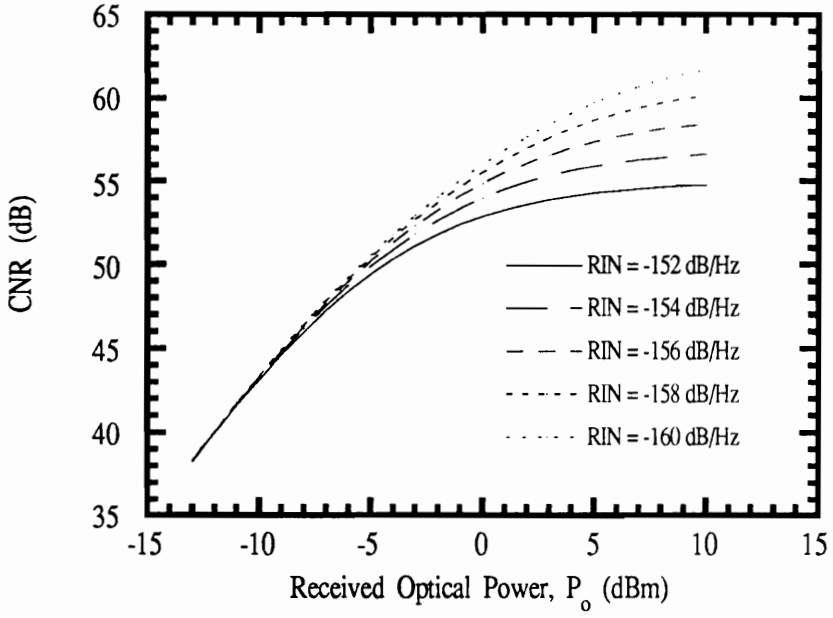

Figure 5.6 CNR as a function of the received optical power for RIN=-152, -154, -156, -158, and -160 dB/Hz, with m=0.04, $\sqrt{\langle i_{th}^2 \rangle}$=7 pA/$\sqrt{\text{Hz}}$ and $\Re$=0.93 A/W.

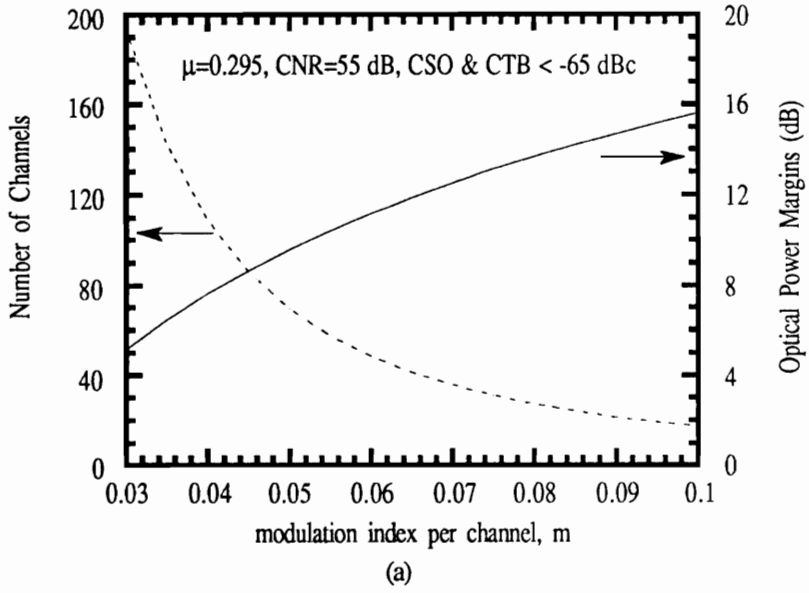

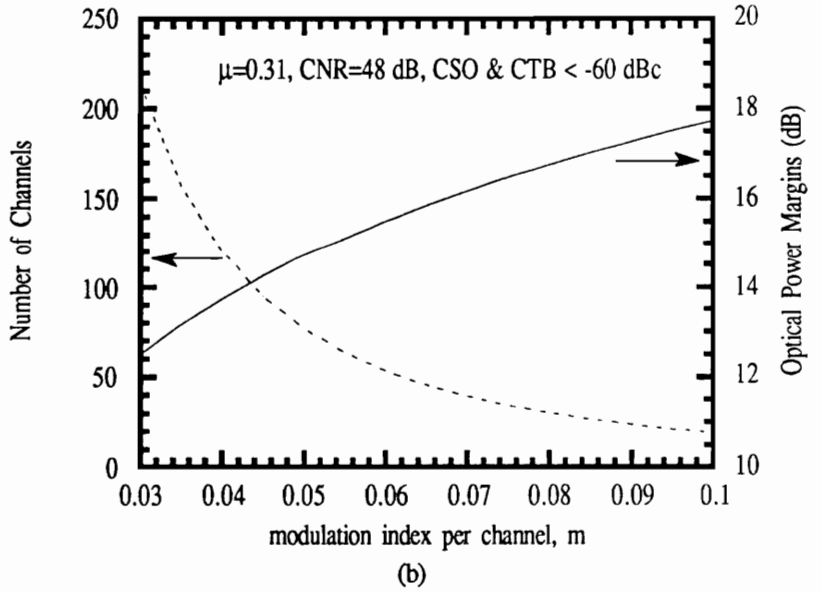

Figure 5.7 Optical power margin and number of channels as a function of m for (a) shot noise limited supertrunking systems (CNR=55 dB, CSO and CTB < -65 dBc) and (b) thermal noise limited local distribution systems (CNR=48 dB, CSO and CTB < -60 dBc) assuming 5 dBm of transmitted power and RIN=-155 dB/Hz, $\sqrt{\langle i_{th}^2 \rangle}$= 7 pA/$\sqrt{\text{Hz}}$, and $\Re$=0.93 A/W.

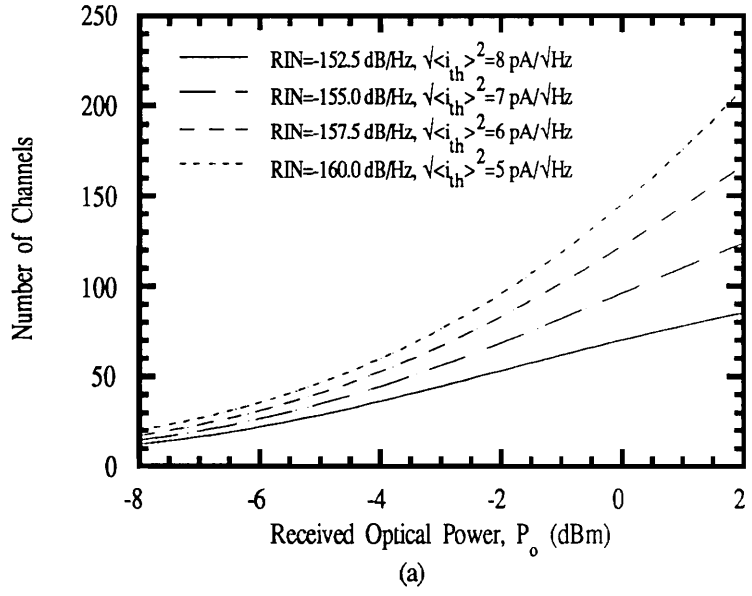

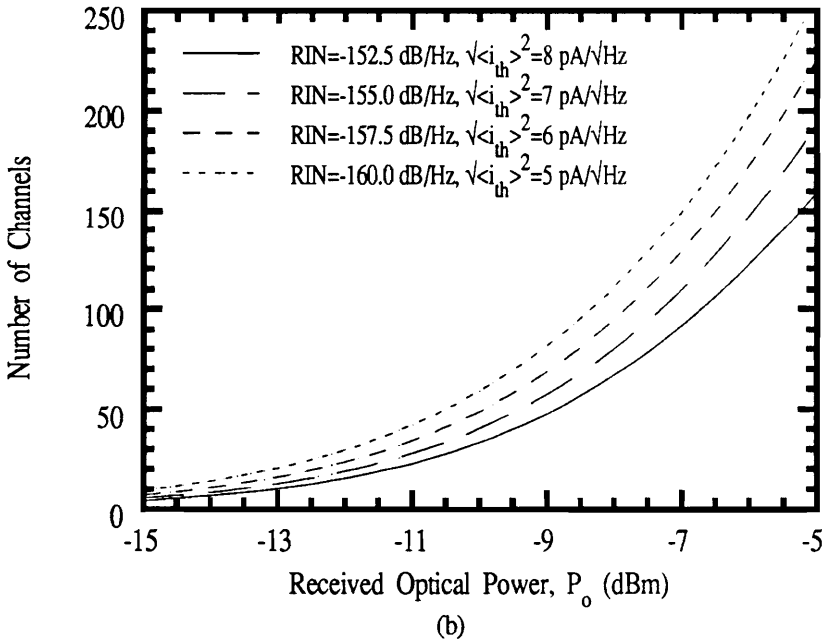

Figure 5.8 Number of channels versus the received optical power for (a) supertrunking system requirements with CNR=55 dB and CSO and CTB < -65 dBc (μ=0.295) and (b) local distribution system requirements with CNR=48 dB and CSO and CTB < -60 dBc (μ=0.31).

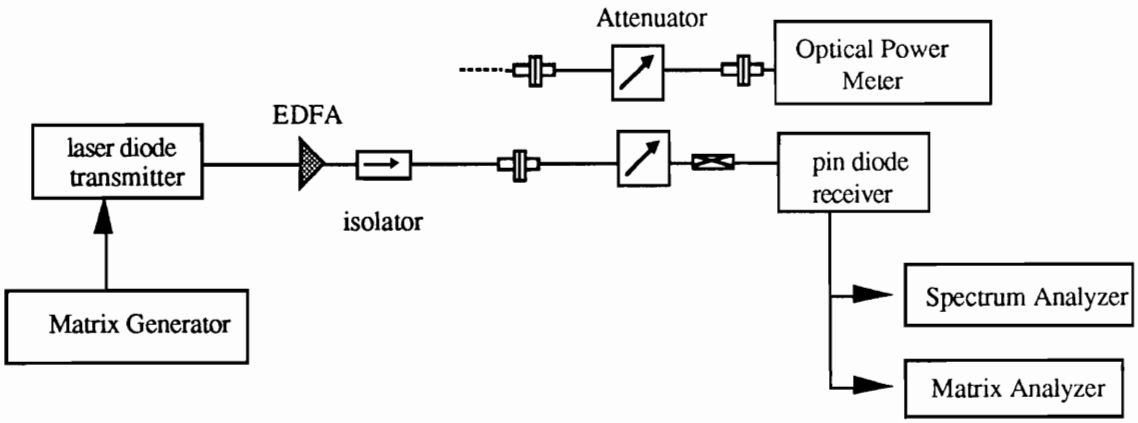

Figure 5.9.a Experimental setup of the EDFA amplified AM SCM system

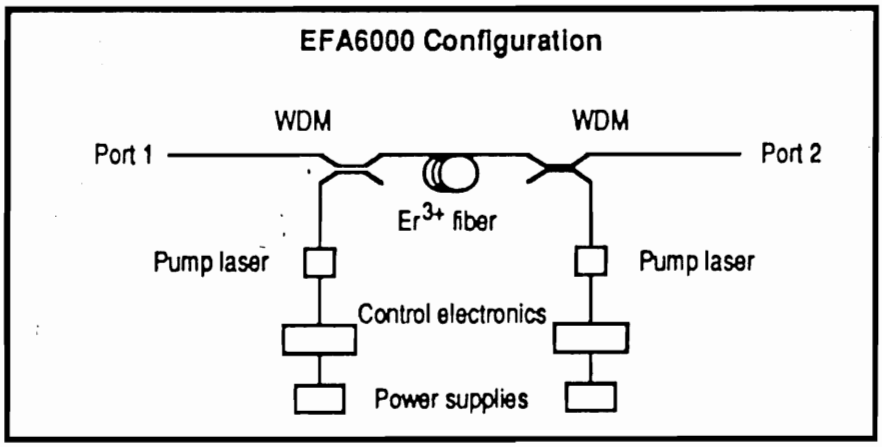

Figure 5.9.b Configuration of BT&D's EDFA model EFA6000
(Taken from the EFA6000 device specification)

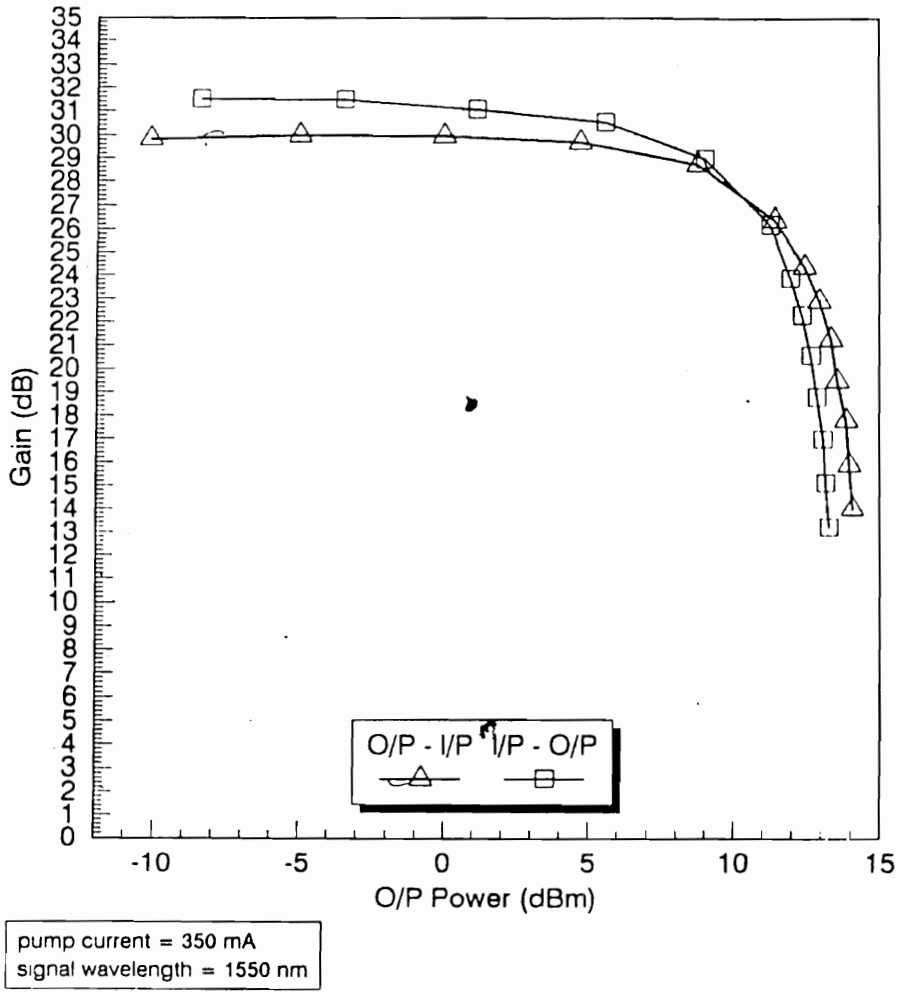

Figure 5.10 The gain profile of the BT&D's EDFA model EFA6000 (Taken from the EFA6000 device specification)

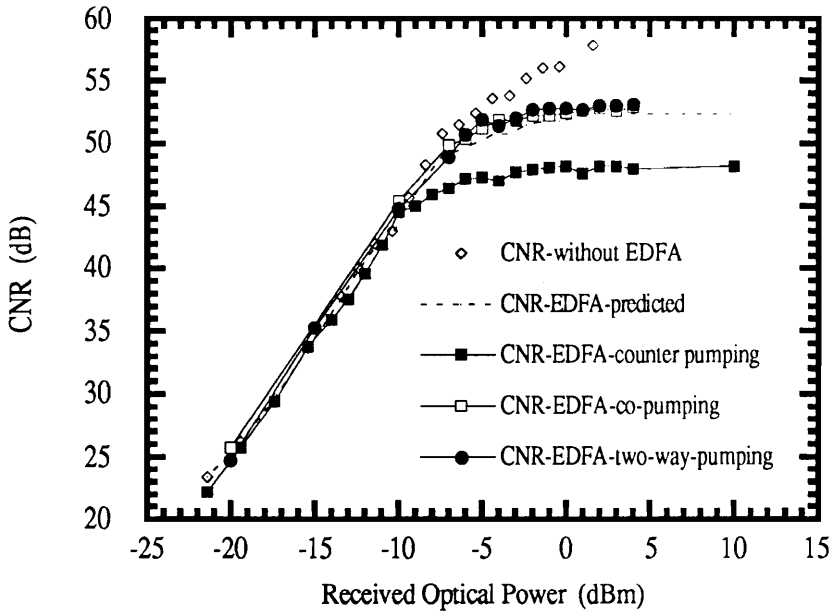

Figure 5.11 CNR measurement versus received optical power for systems with and without the EDFA.

CHAPTER 6.

SUMMARY AND CONCLUSION

In this dissertation, the nonlinear distortion produced by (1) laser threshold nonlinearity and (2) fiber dispersion and laser chirp is studied. On the basis of the results obtained from the nonlinear distortion study, overall system performance limitations and capacity are investigated.

From the nonlinear distortion study of fiber optic multichannel AM SCM video systems, the following is concluded: (1) the nonlinear distortion produced by laser threshold nonlinearity limits both channel capacity and system power margins, thus limiting overall system capacity, and (2) the nonlinear distortion produced by fiber dispersion and laser chirp limits the maximum link distance of standard (dispersion minimum at 1300 nm) single-mode fiber platform when the systems operate with 1550 nm sources.

To study the overall performance limits and system capacity of lightwave multichannel AM SCM video systems, the laser diode threshold nonlinearity and relative intensity noise (RIN), the photodiode shot noise, and the receiver thermal noise are considered. The channel capacity and optical power margin are calculated based on conventional CATV performance requirements. The analysis shows higher channel capacity than previous estimates based on a theoretical limit, but more importantly shows that the channel

capacity and the optical power margins should be specified together to describe the overall system capacity. For example, the calculations indicate that CATV local distribution systems can accommodate 150 channels with 11 dB power margins, and supertrunking systems can accommodate 80 channels with 6 dB power margins with a laser output power of 3 mwatt and a RIN of -155 dB/Hz and a receiver thermal noise of 7 pA/$\sqrt{Hz}$. The system capacity for typical supertrunking systems is shown to be limited by the laser diode threshold characteristic and the RIN performance and the photodiode shot noise. For typical local distribution systems, the capacity is limited by the laser diode threshold characteristic and the receiver thermal noise.

For 1550 nm optically amplified systems operating on the 1310 nm single-mode fiber platform, as planned for Fiber-in-the-Loop applications, the accumulated noise from cascaded erbium-doped fiber amplifiers (EDFAs) limits total number of subscribers served by passive star-network whose power budgets are maintained by in-line EDFAs. However, the maximum link distance for distribution is limited by the CSO degradation from fiber dispersion and laser chirp and not by the available power margin of the system.

The following contributions to general knowledge in fiber optic multichannel AM SCM video systems have been made as an outcome of the research involved in this dissertation : (1) on the basis of the results obtained from simulations and experiments, previously reported estimates of the nonlinear distortion produced by laser threshold characteristics are shown to be overly conservative [75, 76], (2) a proper method of interpreting of TV channel capacity as limited by the system noise and nonlinear distortion is proposed [75, 77], (3) a comparative study of the practical and theoretical performance limit of the system is investigated [75,78, 79], (4) a closed analytical form for the second order nonlinear distortion produced by fiber dispersion and laser chirp which explains the distortion generating mechanism is obtained [80], and (5) multichannel systems simulations to evaluate the CSO degradation due to fiber dispersion and laser chirp is investigated [80].

In addition to the specific contributions mentioned above, this dissertation demonstrates that fiber optic multichannel AM SCM systems are capable of providing sufficient channel capacity and system power margins for the most of today's CATV system applications [79]. This may provide further impetus to deploy optical fibers in the loop distribution plant of both CATV and telecommunication networks, thus, accelerating fiber optic network infrastructures for future broadband services.

REFERENCES

[1] C.K. Kao and G. A. Hockham, "Dielectric-fiber surface waveguides for optical frequencies," *Proc. of IEE*, vol. 113, pp. 1151-1158, July 1966

[2] F.P. Kapron, D.B. Keck and R.D. Maurer, "Radiation losses in glass optical waveguides," *Appl. Phys. Lett.*, vol. 17, pp. 423-425, November 1970

[3] Ira Jacobs, et al., "Atlanta Fiber System Experiment," *Bell System Tech. J.*, vol. 57, pt. 1, July-August 1978

[4] J.S. Cook and O.I. Szentisi, "North American field trials and early applications in telephony," *IEEE J. Sel. Areas in Comm.*, vol. SAC-1, no. 3, pp. 393-397, April 1983

[5] G.R. Boyer, "A perspective on fiber in the loop systems," *IEEE Lightwave Comm. Sys.*, vol. 1, no. 3, pp. 6-11, 1990

[6] E.S. Smith, "The emergence of CATV: A look at the evolution of a revolution," *Proc. of IEEE*, vol. 58, no. 7, pp. 967-982, 1970

[7] K.A. Cox, "A U.S. government view of CATV and its future," *Proc. of IEEE*, vol. 58, no. 7, pp. 963-966, 1970

[8] M. Balmes, John Bourne, and Jung Mar, "Fiber to the home: The technology behind Heathrow," *IEEE Lightwave Comm. Sys.*, vol. 1, no. 3, pp. 25-29, 1990

[9] T.E. Darcie, "Subcarrier multiplexing for lightwave networks and video distribution systems," *IEEE J. Select. Areas in Comm.*, Vol. 8, No. 7, pp. 1229-1239, 1990.

[10] W.I. Way, "Subcarrier multiplexed lightwave system design considerations for subscriber loop applications," *J. Lightwave Tech.*, Vol. LT-7, No. 11, pp. 1806-1818, 1989.

[11] R. Olshansky, E. Eichen and V. Lanzisera, "Subcarrier multiplexed lightwave networks for broadband distribution," *Proc. of ICC '89*, pp. 982-986.

[12] T.E. Darcie, G.E. Bodeep, "Lightwave multichannel analog AM video distribution system," *Proc. of ICC '89*, pp. 1004-1007.

[13] J. A. Chiddix, "Optical fiber super trunking, the time has come: A performance report on a real world system," *IEEE J. On Sel. Areas In Commun.*, vol. SAC-4, no. 5, 1986

[14] J.A. Chiddix, H. Laor, D.M. Pangrac, L.D. Williamson, and R.W. Wolfe, "AM video on fiber in CATV systems: Need and Implementation," *IEEE J. Select. Areas in Comm.*, Vol. 8, No. 7, pp. 1229-1239, 1990.

[15] G.M. Hart and N.F. Hamilton-Piercy, "A brodband urban hybrid coaxial/fiber telecommunication network," *IEEE Lightwave Comm. Sys.*, vol. 1, no. 1, pp. 38-45, 1990

[16] D.R. Huber, "40-channel VSB-AM CATV link utilizing a high-power erbium amplifier," *Technical Digest of Optical Fiber Communication Conference*, vol. 4, paper TuC3, 1991.

[17] J.A. Chiddix, "Fiber technology in CATV networks," *Technical Digest of Optical Fiber Communication Conference*, vol. 4, paper TuC1, 1991.

[18] D. Chan and T.M. Yuen, "System analysis and design of a fiber optic VSB-FDM system for video trunking," *IEEE Trans. Commun.*, vol. COM-25, no. 8, pp.680-686, 1977

[19] E.H. Hara and T. Ozeki, "Optical video transmission by FDM analog modulation," *IEEE Trans. Cable Television, vol. CATV-2*, no. 1, pp. 18-34, 1977

[20] A.U. Tenne-sens and D.C. Johnson, "Optical-fiber video transmission using analog baseband modulation," *IEEE Trans. Cable Television*, vol. CATV-3, no. 4, pp. 145-149, 1978

[21] T.D. Michaelis, "Laser diode evaluation for optical analog link," *IEEE Trans. Cable Television, vol. CATV-4*, no. 1, pp. 30-42, 1979

[22] J.C. Daly, "Fiber optic intermodulation distortion," *IEEE Trans. Commun.*, vol. COM-30, no. 8, pp.1954-1958, 1982

[23] J. Lipson, L. Upadhyayula, S-Y. Huang, C.B. Roxlo, E.J. Flynn, P.M. Nitzsche, C.J. McGrath, G.L. Fenderson, and M.S. Schaefer, "High-fidelity lightwave transmission of multiple AM-VSB NTSC signals," *IEEE Trans. on Microwave Theory and Tech.*, vol. 38, no. 5, pp. 483-493, 1990.

[24] T.E. Darcie, "Lightwave subcarrier CATV trasnmission systems," *IEEE Trans. on Microwave Theory and Tech.*, vol. 38, no. 5, pp. 524-533, 1990.

[25] M. Tanabe, T. Uno, K. Kaida, H. Nakata, K. Fujito, and T. Ichida, "80 ch. AM-FDM signals optical transmission," *LEOS Summer Topical Conf. Dig.*, BAM6, pp. 18-19, Monterey, Calf., July, 1990.

[26] T.E. Darcie, M.E. Dixon, B.L. Kasper, and C.A. Burrus, "Lightwave systems using microwave subcarrier multiplexing," *Electron. Lett.*, vol. 22, pp. 774-775, 1986.

[27] R. Olshansky, V.A. Lanzisera, "60-channel FM video subcarrier multiplexed optical communication system," *Electron. Lett.*, vol. 23, p. 1196, 1987.

[28] W.I. Way, R.S. Wolff, and M. Krain, "A 1.3-mm 35 -km fiber-optic microwave multicarrier transmission system for satellite earth stations," *J. Lightwave Tech.*, Vol. LT-5, No. 9, pp. 1325-1332, 1987.

[29] M. Yamagouchi, M. Ktamuar, I. Mito,, S. Murata, and K. Kobayashi, "Highly efficient single-longitudinal-mode operation of antireflection-coated 1.3 μm DFB-DC-PBH LD," *Electron. Lett.*, vol. 20, pp. 233-235, 1984.

[30] R. Olshansky, P. Hill, V. Lanzisera, W. Powazinik, "Frequency response of 1.3 mm InGaAsP high speed semiconductor lasers," *IEEE J. Quantum Electron.*, vol QE-23, no. 9, pp 1410-1418, 1987.

[31] K. Fujito, T. Uno, T. Ichida, H. Serizawa, "Low-noise wideband analog optical link using a DFB laser diode," Techinical Digest, *Optical Fiber Comm. Conf.*, 1988, paper TH01.

[32] J.J. Gimlett, "Low-noise 8-GHz p-i-n/FET optical receiver," *Electron. Lett.*, vol. 23, pp. 281-283, 1987

[33] T.E. Darcie, B.L. Kasper, J.R. Talman, and C.A. Burrus, Jr., "Resonant p-i-n-FET receivers for lightwave subcarrier systems," *J. Lightwave Tech.*, Vol. LT-6, pp. 582-586, 1988.

[34] S.R. Cochran, "Low-noise receivers for fiber-optic microwave signal transmission," *J. Lightwave Tech.*, Vol. LT-6, pp. 1328-1337, 1988.

[35] W. Susaki, "Recent progress in superlinear InGaAsP laser diodes," *Technical Digest, Optical Fiber Comm. Conf.*, 1991, San Diego, California, paper WG5.

[36] M. Ishino, K. Fujihara, N. Ohtsuka, N. Takenaka, T. Uno, and Y. Matsui, "High-performance analog-transmission characteristics of 1.3-μm-wavelength multiple quantum-well distributed-feedback laser," *Technical Digest, Optical Fiber Comm. Conf.*, 1991, San Diego, California, paper WG6.

[37] A.A.M. Saleh, "Fundamental limit on number of channels in SCM lightwave CATV system," *Electron. Lett.*, vol. 25, pp. 776-777, 1989

[38] K. Alameh and R.A. Minasian, "Ultimate limits of subcarrier multiplexed lightwave transmission," *Electron. Lett.*, Vol. 27, No. 14, pp. 1260-1262, 1991.

[39] I.M.I. Habbab, L.J. Cimini, Jr., " Optimized performance of erbium-doped fiber amplifiers in subcarrier multiplexed lightwave AM-VSB CATV systems," *J. Lightwave Technol.*, vol. LT-9, no. 10, pp. 1321-1329, 1991.

[40] P.M. Gabla, "35 AM-VSB TV channel distribution with high signal quality using a 1480 nm diode-pumped Erbium-doped fiber post amplifier," *IEEE Photon. Technol. Lett.*, Vol. 3, No. 1, p. 56, 1991.

[41] W.I. Way, M.M. Choy, A. Yi-Yan, M. Andrejco, M. Saifi, and C. Lin, "Multi-channel AM-VSB television signal transmission using an erbium-doped optical fiber power amplifier," *IEEE Photon. Technol. Lett.*, vol. 1, p. 343, 1989

[42] M. Shigematsu, K. Nakazato, T. Okita, Y. Tagami, and K. Nawata, *First Topical Meeting on Optical Amplifiers*, paper WB3, Monterey, CA, 1990.

[43] M.R. Philips, T.E. Darcie, D. Marcuse, G.E. Bodeep, and N.J. Frigo, "Nonlinear distortion from fiber dispersion of chirped intensity modulated signals," *Techn. Digest OFC'91*, paper TuC4, 1991

[44] E.E. Bergmann, C.Y. Kuo, and S.Y. Huang, "Dispersion-Induced Composite Second-Order Distortion at 1.5 mm," *IEEE Photon. Technol. Lett.*, vol. 3, no. 1, p. 59, 1991

[45] Block Oriented Systems Simulator User's Manual, COMDISCO Systems, Inc., 1990.

[46] V.R. Borelli and H. Gysel, "Fiber optic supertrunking: A comparision of parameters and topologies using analog and/or digital techniques," *NCTA Technical Digest*, pp. 147-155, 1990.

[47] D.M. Pangrac and L.D. Williamson, "Fiber trunk and feeder - The continued evolution," *NCTA Technical Digest*, pp. 87-91, 1990.

[48] William Grant, Cable Television, Prentice-Hall Publishing Company, Inc., Reston, Va., 1983.

[49] Bobby Harrel, The Cable Television Technical Handbook, Artech House Publishing, Inc., Dedham, Ma, 1985.

[50] R.W. Tkack and A.R. Chraplyvy, "Phase Noise and Linewidth in an InGaAsP DFB laser," *J. Lightwave Technol.*, vol. 4, no. 11, pp. 1711-1716, 1986.

[51] T.E. Darcie, G.E.Bodeep, and A.A.M, Saleh, "Fiber-Reflection-Induced Impairments in Lightwave AM-VSB CATV Systems," *J. Lightwave Technol.*, vol. 9, no. 8, pp. 991-995, 1991.

[52] Ken-Ichi Sato, "Intensity Noise of Semiconductor Laser Diodes in Fiber Optic Analog Video Transmission," *IEEE J. Quantum Electron.*, vol. QE-19, no. 9, pp. 1380-1391, 1983.

[53] T. Hong and Y. Suematsu, "Harmonic distortion in direct modulation of injection lasers," *Trans. IECE Japan*, pp. 142-147, 1979.

[54] K.Y. Lau and A. Yariv, "Intermodulation distortion in a directly modulated semiconductor injection laser," *Appl. Phys. Lett.*, vol. 21, pp. 665-666, 1985.

[55] T.E. Darcie, R.S. Tucker, and G.J. Sullivan, "Intermodulation and Harmonic Distortion in InGaAsP lasers," *Electron. Lett.*, vol. 21, pp. 665-666, 1985; erratum vol. 22, p.619, 1986.

[56] W.I. Way, "Large signal nonlinear distortion prediction for a single-mode laser diode under microwave intensity modulation," *J. Lightwave Technol.*, vol. 5, pp. 305-315, 1987.

[57] J. Helms, "Intermodulation and Harmonic Distortions of Laser Diodes with Optical Feedback," *J. Lightwave Technol.*, vol. 9, no. 11, pp. 1567-1575, 1991.

[58] M. Slack, "The probability distrtibutions of sinusoidal oscillations combined in random phase," *J. Inst. Elect. Eng.*, vol. 93, no. 3, pp. 76-86, 1946.

[59] W.R. Bennett, "Interchannel Interference in FM and PM system under noise loading conditions," *Bell System. Tech. J.*, vol. 34, pp. 601-636, 1955.

[60] IEEE Standards Coordinating Committee Recomendation, *Fiber Optics (SCC-26) Analog Fiber Optic Transmission Systems*, Issue 1, May, 1991.

[61] J.H. Angenent, "Simple Model for Calculation of Distortion in an Optical Analogue Subcarrier Multiplexed CATV System," *Electron. Lett.*, Vol. 26, No. 24, pp. 2049-2050, 1990.

[62] Bell Communications Research Special Report, SR-TSY-00168, "Bellcore Fiber in the Loop (FITL) Architecture Summary Report," *Bellcore*, Issue 1, June, 1990.

[63] Bell Communications Research Special Report, SR-NWT-001851, "Preliminary Study of Multichannel NTSC Video Transport on Fiber in the Loop," *Bellcore*, Issue 1, Decempter, 1990.

[64] G.J. Meslener, "Chromatic dispersion induced distortion of modulated monochromatic light employing direct detection," *IEEE J. Quantum. Electron.*, vol. QE-20, no. 10, pp. 1208-1216, 1984.

[65] F. Koyama and Y. Suematsu, "Analysis of dynamic spectral width of dynamic-single-mode (DSM) lasers and related transmission bandwidth of single-mode fibers," *IEEE J. Quantum. Electron.*, vol. QE-21, no. 4, pp. 292-297, 1985.

[66] C.H. Ih and Wanyi Gu, "Fiber induced distortions in a subcarrier multiplexed lightwave system," *IEEE J. Selec. Areas Commum.*, vol. 8, no. 7, pp. 1296-1304, 1990.

[67] R.S. Tucker, "High-spedd modulation of semiconductor lasers," *J. of Lightwave Technol.*, vol. 3, no. 6, pp. 1180-1192, 1985.

[68] H. Kressel and J.K. Butler, *Semiconductor Lasers and Heterojunction LED's*, New York: Academic Press, 1977.

[69] C.H. Henry, "Theory of the linewidth of semiconductor lasers," *IEEE J. Quantum Electron.*, vol. QE-18, pp. 259-264, Feb. 1982.

[70] R.S. Vodhanel, A.F. Elrefaie, R.E. Wagner, M.Z. Iqbal, J.L. Gimlett, and S. Tsuji, "Ten-to-Twenty gigabit-per-second modulation performance of 1550 nm distributed feedback lasers for frequency shifted-keying systems, *J. of Lightwave Technol.*, vol. 7, no. 10, pp. 1454-1460, 1989.

[71] P.J. Corvini and T.L. Koch, "Computer simulation of high-bit-rate optical fiber transmission using single-frequency lasers," *J. of Lightwave Technol.*, vol. 5, no. 11, pp. 1591-1595, 1989.

[72] J.C. Cartledge, and G.S. Burley, "The effect of laser chirping on lightwave system performance," *J. of Lightwave Technol.*, vol. 7, no. 3, pp. 568-573, 1989.

[73] L.J. Cimini, Jr., L.J. Greenstein, A.A.M. Saleh, "Optical equalization to combat the effects of laser chirp and fiber dispersion," *J. of Lightwave Technol.*, vol. 8, no. 5, pp. 649-659, 1990.

[74] J.A. Chiddix, "Fiber Backbone Trunking in Cable Television Networks: An Evolutionary Adoption of New Technology," *IEEE Lightwave Commun. Systems Mag.*, vol. 1, no. 1, pp. 32-37, 1990.

[75] C.J. Chung and Ira Jacobs, "Practical TV Channel Capacity of the Lightwave multichannel AM SCM System Limited by the Threshold Nonlinearity of Laser Diodes," *IEEE Photonics Technol. Lett.*, vol. 4, no. 3, pp. 289-292, 1992.

[76] C.J. Chung and Ira Jacobs, "Simulation of the Effects of Laser Clipping on the Performance of AM SCM Lightwave Systems," *IEEE Photonics Technol. Lett.*, vol. 3, no. 11, pp.1034-1036, 1991.

[77] C.J. Chung and Ira Jacobs, "TV channel capacity of lightwave multichannel AM SCM systems as limited by laser threshold non-linearity," *Optical Fiber Communication Conference Technical Digest*, vol. 5, pp. 18-19, February 1992, San Jose, California.

[78] C.J. Chung and Ira Jacobs, "Practical TV Channel Capacity of the Lightwave AM SCM System For Multichannel CATV Signal Transmission," *The 2nd International Workshop on Photonic Networks, Components and Applications*, Montebello, Que., Canada, March. 1992.

[79] C.J. Chung and Ira Jacobs, "System Capacity and Practical Performance Limits of Lightwave Multichannel AM SCM Video Systems," submitted to the special issue of the *IEEE/OSA Journal of Lightwave Technology* on Broadband Lightwave Video Transmission, December, 1991.

[80] C.J. Chung and Ira Jacobs, "1550 nm Erbium Fiber Amplified Lightwave Multichannel AM SCM Video System Capacity and Performance Evaluation Limited by Laser Chirp, Fiber Dispersion and Fiber Amplifier Noise," manuscript in preparation for submission to the *IEEE/OSA Journal of Lightwave Technology*.

Appendix

Block Oriented System Simulator (BOSS™)

The Block Oriented Systems Simulator (BOSS™) is an icon-oriented interactive tool for modeling system response to a set of input signals. It can perform time-domain waveform level simulations of communication links that are represented by sets of functional blocks. The time and effort to model a complete system response is substantially less than conventional simulation approaches because of BOSS's built-in graphical interface.

To facilitate implementation of the simulated system, BOSS already includes most of the functional modules used in communication systems such as filters, modulators, signal generators, etc. It also contains a limited set of functional modules for fiber optic communication systems. If the desired functional module is not in the module-library, it is possible to build such a module using basic building blocks which have basic arithmetical, logical, and conditional functional operations. In the event that the desired model is too complicated to be built with existing basic modules, it is possible to create new modules by adding a new corresponding FORTRAN subroutine to the module database. BOSS also provides variety of plots (such as amplitude and phase spectrum plots, eye diagrams histograms and correlation plots) for analysis of the waveforms obtained from the simulations. Currently BOSS is running at Virginia Tech with a "VAXStation3200" workstation computer from Digital Equipment Corporation. In the event that more computing power is required, the compiled execution program can be run under more powerful VAX computers. Also a UNIX version of BOSS is now available.

The signal-clipping simulation to generate Figure 3.5 for 2^{15} samples took approximately 5 minutes. If calculations involve operators such as Fast Fourier Transforms (FFT) and convolutions, the run-time of programs increase drastically. For example, convolution of 2^{14} samples to calculate the fiber dispersion induced nonlinear distortion due to laser chirp takes approximately 10 minutes. The maximum data length BOSS allows is limited to 2^{15} samples.

BOSS™ (Block Oriented Systems Simulator) is a Registered Trademark of *Comdisco Systems*, Inc.

Glossary

1550 nm AM SCM systems: fiber optic AM SCM systems with optical source whose center wavelength is at 1550 nm.

1300 nm single-mode-fiber: a cylindrical optical waveguide designed for the propagation of only single optical mode and having zero chromatic dispersion for a 1300 nm source wavelength.

amplitude modulated subcarrier multiplexing (AM SCM): a signal multiplexing technique where individual amplitude modulated channel signals are frequency division multiplexed, and the resulting VHF signal is used to intensity modulate the laser diode.

amplitude modulated vestigial sideband (AM-VSB): a transmission format used in television signal transmission where most of the lower sideband of the amplitude modulated spectrum is filtered out to save the spectrum. The remaining lower, or vestigial, sidebands (approximately 0.75 MHz) are kept to avoid impairment of the television signal.

broadband services: represents a service that requires a wide electronic bandwidth signal as opposed to a narrow band voice service offered by telephone operating companies. Its purpose is to provide the integrated network which offers video, voice, and, high speed data services.

carrier-to-noise ratio (CNR): the ratio of the power of the carrier to the power of the noise in the bandwidth of the specific system being measured.

chirp of laser diode: an instantaneous phase (or optical frequency) variation of laser diode light output under intensity modulation. This results in a dynamic wavelength excursion from the central wavelength.

composite-second-order (CSO) distortion: second order nonlinear distortion products produced by beating of two frequency components.

composite-triple-beat (CSO) distortion: third order nonlinear distortion products produced by beating of three frequency components.

connector (fiber optic): a device that provides a demountable connection between two fibers.

dispersion of optical fibers: temporal spreading of a light signal caused by different light velocity of different wavelength components in the fibers either because of chromatic or modal effects. The chromatic dispersion is the relevant quantity in this dissertation since only single-mode fibers are considered.

distributed feedback (DFB) laser diode: a semiconductor laser diode with the controlled mode characteristics which is designed to yield a single spectral line output with very low intensity noise.

distribution plant: a portion of the subscriber-outside-plant that connects the subscribers with a local remote switch or a feeder plant.

erbium-doped fiber amplifiers (EDFA): optical amplifiers made by doping erbium ions in the silica glass fibers which have same dimensional characteristics of typical single mode fibers and allows the in-line amplification of optical signal in fibers.

fiber-induced-dispersion: see **dispersion of optical fibers**

Fiber In The Loop (FITL): a project planned by telephone operating companies which brings optical fibers into the subscriber loop distribution plant of the network.

Fiber To The Home (FTTH): a project planned by telephone operating companies which brings optical fiber connection to the residential subscribers.

headend: CATV system starting location where the regional CATV programs are distributed to local distribution centers.

hubs: local distribution center of the CATV network where the regional CATV programs received from the headend is distributed to subscribers.

laser diode-chirp: see **chirp of laser diode**

laser diode threshold-nonlinearity: a characteristic of laser diode which generates no light output when injection current falls below the laser threshold. This produces signal clipping in AM SCM systems which in turn produces clipping induced nonlinear distortion products.

loop distribution: part of telecommunication/CATV networks that links the central-office to the homes or businesses served.

National Television Systems Committee Amplitude Modulated Vestigial Sideband (NTSC AM-VSB): North American standard TV signal format. See **Amplitude Modulated Vestigial Sideband**

nonlinear distortion: distortion of original signal due to nonlinear response of system components.

optical isolator: an optical device that allows the transmission of light in a single direction and suppresses the transmission of light in the opposite direction.

pay-per-view: a service offered by a cable TV company where the viewing of a particular program (or a movie) is charged on a program basis.

photodiode shot noise: noise created by statistical photon-to-electrical-carrier conversion process

receiver thermal noise: noise mainly contributed by the first stage of the electrical amplifier following the photodetector in the receiver..

relative intensity noise of laser: a normalize quantity for describing the the intensity fluctuations of the laser diode light output due to spontaneous emission process. (expressed as a power per unit bandwidth)

splice (optical fiber): a permanent joining of two fibers using either mechanical or fusion technique.

subscriber loop: a part of the telecommunication network that links the central office to the homes or businesses served.

subcarrier multiplexing (SCM): a signal multiplexing technique where individual baseband signals are first frequency division multiplexed by using local oscillators, and then the resulting signal is used to modulate a higher frequency source. The local oscillator frequencies are so-called subcarriers in contrast to the higher frequency carrier source. At the receiver, the desired signal is recovered by tuning the local oscillator to the frequency of the corresponding signal and down converting the RF signal to a baseband signal.

supertrunking: a dedicated link between the remote satellite receiving station to a central location in the CATV serving area.

switched-video-libraries: A feature that may be provided by the future broadband service where the subscribers can choose the video program of interest (from a large video library) dynamically through the switching capability of the network.

system capacity: collectively refers to the system power margin and channel capacity

trunking: A dedicated communication channel between two points in the network. In telecommunications, it refers to links between central offices. In cable TV network it refers to links between the cable programming station and the major cable distribution plant.

wavelength division multiplexing (WDM): sending several signals along one fiber with different wavelengths of light.

VITA

Chul-Jong Chung was born in Seoul, Korea, in 1961. He received the B.Eng and M.Eng degrees from McGill University, Montreal, Canada, 1984 and 1987, respectively. Since 1987, he has been at Virginia Polytechnic Institute and State University, Blacksburg, Va. pursuing a Ph.D degree. His dissertation work involves analysis, simulation, and experiments on the performance evaluation of the lightwave multi-channel AM subcarrier multiplexed system.

From 1986-1987 he worked at National Research Council of Canada, Boucherville, Quebec, on development of ultrasonic measurement systems and acoustic fiber sensors for nondestructive testing applications. In 1989 he worked at Bell-Northern Research, Research Triangle Park, N.C., on development of Optical Line Cards and Network Units for lightwave subscriber loop applications. During the summer of 1991, he worked at Bellcore, Red Bank, N.J., on multi-channel video distribution technology for Fiber-In-The-Loop architecture. His research interests include performance evaluation of subcarrier multiplexed lightwave systems and passive optical components for lightwave subscriber loop applications.